Fermi National Accelerator Laboratory

FERMILAB-Conf-94/410-T
December 9, 1994

QCD at TASI '94

R. K. Ellis
Fermi National Accelerator Laboratory
P. O. Box 500, Batavia, Illinois 60510

December 9, 1994

Abstract

This is the written version of four lectures on perturbative QCD given at the 1994 Theoretical Advanced Summer Institute in Boulder, Colorado in June 1994.

Operated by Universities Research Association Inc. under contract with the United States Department of Energy

Contents

1 QCD and e^+e^- annihilation

1.1 Introduction

The subject of these lectures will be a discussion of the perturbative aspects of Quantum Chromodynamics, and in particular the application of these methods to physics at high energy. Various methods are used in the attempt to make predictions for physical quantities from the QCD Lagrangian. By far the most successful of these is the method of perturbation theory, which exploits the fact that in certain circumstances the coupling constant can be considered to be small. Thus the development of perturbative QCD proceeds in analogy to the perturbative treatment of QED, which is also very successful.

However there are many differences with QED. For example, at acccessible energies the coupling is not so small. In addition, the quarks and gluons are not observed as free particles. So the perturbative treatment of QCD gives us a chance to examine a quantum field theory in a different context. The key ideas in this quest will be the ideas of infrared safety and factorization.

QCD as a theory is now 20 years old. A survey of the present status of the theory including some historical notes can be found in ref.[1]. This is of course not the first year that lectures in perturbative QCD have been given in the TASI series. Lectures from earlier years, which provide a different perspective on the same topic, are given in [2,3,4].

1.2 Lagrangian and Feynman Rules

1.2.1 Why SU(3)?

The motivation for an SU(3) colour gauge theory of the strong interactions was the result of the synthesis of a number of ideas and experimental results. The idea for the quarks themselves was suggested by the need to have a physical manifestation for the $SU(3)_f$ of flavour observed in the spectrum of the low lying mesons and baryons. The quark constituents of the baryons are forced to have half integral spin by the observed spins of the low-lying baryons. The low lying baryons were interpreted in the quark model as symmetric states of space, spin and $SU(3)_f$ degrees of freedom. However Fermi-Dirac statistics require a total anti-symmetry of the wave-function. The resolution of this dilemma was the introduction of the colour degree of freedom. The baryon wavefunctions are totally anti-symmetric in the colour degree of freedom. Of course, the introduction of another degree of freedom would lead to a proliferation of states, so the colour degree of freedom had to be supplemented by a requirement that only colour singlet states can exist in nature. At this point it was clearly important to seek further experimental and theoretical confirmation of colour SU(3).

One early experimental test of the correctness of the three colour idea was provided by the rate for the decay $\pi^0 \to \gamma\gamma$. This decay proceeds by the coupling of the pion to a quark loop as shown in Fig. 1. The rate is determined by the matrix element

$$\langle 0| J(x)J(y)\varphi(0) |0\rangle = \frac{1}{2f_\pi m_\pi^2} \langle 0| J(x)J(y)\partial_\mu A^\mu |0\rangle . \tag{1}$$

The interpolating field for the neutral pion φ can be replaced by by the divergence of the axial current A using the Goldberger-Treiman relation. The parameter $f_\pi \approx$ 93MeV is the decay constant of the pion as measured in pion decay.

$$\langle 0| A^\mu |\pi\rangle = i f_\pi q^\mu \tag{2}$$

Remarkably enough the rate for the decay is exactly calculable using the quark diagram shown in Fig. 1a. This leads to an absolute prediction for the decay rate,

$$\Gamma(\pi^0 \to \gamma\gamma) = \xi^2 \left(\frac{\alpha}{\pi}\right)^2 \frac{1}{64\pi} \frac{m_\pi^3}{f_\pi^2} = 7.6\xi^2\text{eV}. \tag{3}$$

The experimental value is 7.7 ± 0.6 eV. The electric charge and colour factor ξ for three colours of fractionally charged quarks is

$$\xi = 3\left[\left(\frac{2}{3}\right)^2 - \left(\frac{1}{3}\right)^2\right] = 1 \tag{4}$$

where the overall factor 3 represents the number of colours. Note however that the original calculation of this decay rate, performed before the discovery of quarks, used the proton and neutron as constituents yielding

$$\xi = \left[(1)^2 - (0)^2\right] = 1 \tag{5}$$

So the measured decay rate is suggestive of the existence of three colours of fractionally charged quarks, but not conclusive.

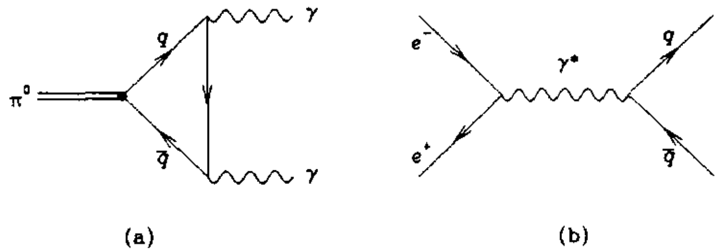

Figure 1: (a) π^0 decay. (b) e^+e^- annihilation to quarks

Another test of the number of charged fundamental constituents is provided by the ratio of the e^+e^- hadronic total cross-section to the cross section for the production of a point-like object such as a muon pair. The virtual photon emitted by the annihilating electron and positron will excite all electrically charged constituent–anti-constituent pairs from the vacuum. Thus the contribution from the u, d and s quarks each of which occurs in three colours is

$$R = 3\left[\left(\frac{2}{3}\right)^2 + \left(-\frac{1}{3}\right)^2 + \left(-\frac{1}{3}\right)^2\right] = 2 \tag{6}$$

The experimental data are shown in Fig. 2. Below charm threshold they are in approximate agreement with Eq. (6).

The existence of approximately point-like constituents inside a hadron was demonstrated by the classic electron deep inelastic scattering experiments performed at SLAC. The surprising result was that the measured structure functions did not fall off as the inelasticity of the reaction increased. Rather the structure functions had the property of scaling which was indicative of point-like structure inside the target nucleons. This gave rise to the 'parton' model, where the constituents of hadrons were identified with partons. The partons are now known to be the coloured quarks and gluons.

The final step in this chain of argument was provided by the discovery of asymptotic freedom. Before the discovery of asymptotic freedom the outstanding question was why quarks appeared to be free particles when probed by a deep inelastic photon. Since quarks were not observed as free entities they evidently had strong interactions which bound them together to form hadrons. The discovery of asymptotic freedom predicted that the coupling of quarks and gluons could be large at large distances

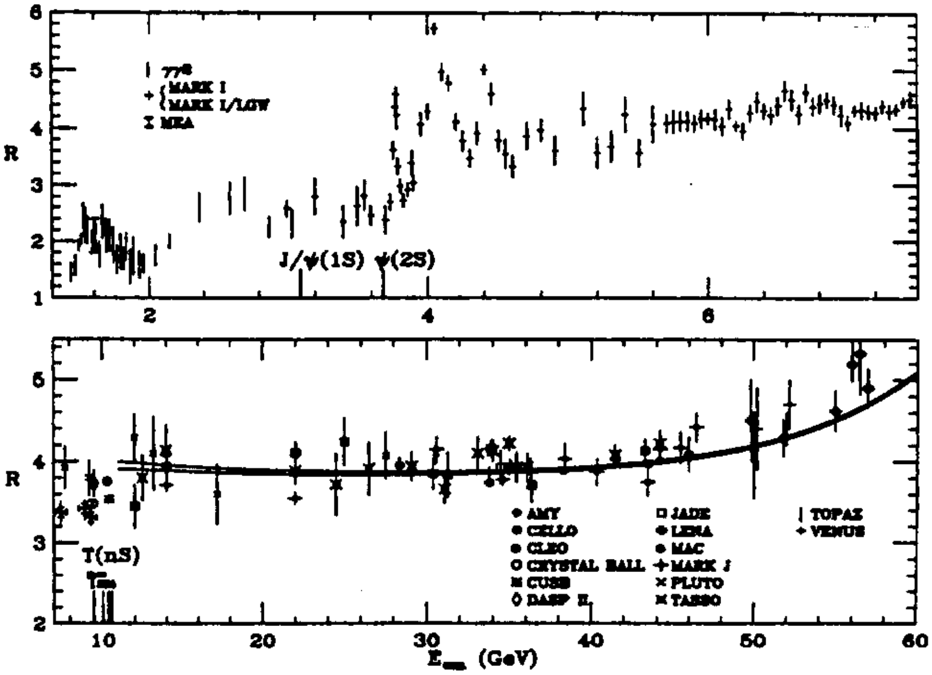

Figure 2: Compilation of values of R

so as to confine quarks; at the same time the coupling was predicted to be small at short distances so that quarks behaved as free particles at asymptotic energies. However the approach to asymptotia is very slow – it is only logarithmic. At any finite energy there are calculable corrections to the free quark result which are unambiguous predictions of the theory. These lectures examine those predictions at collider energies.

1.2.2 QCD Lagrangian

We begin with a brief description of the QCD Lagrangian and the Feynman rules which can be derived from it. This is a practical guide which does little more than introduce notation and certainly does not do justice to the elegant structure of quantum field theory. For more details, the reader is referred to the standard texts [5,6,7]. Introductions to perturbative QCD can be found in refs.[8,9,10,11,12].

Just as in Quantum Electrodynamics, the perturbative calculation of any process requires the use of Feynman rules describing the interactions of quarks and gluons. The Feynman rules required for a perturbative analysis of QCD can be derived from an effective Lagrangian density which is given by

$$\mathcal{L} = -\frac{1}{4} F^A_{\alpha\beta} F^{\alpha\beta}_A + \sum_{\text{flavours}} \bar{q}_a (i\not{D} - m)_{ab} q_b + \mathcal{L}_{\text{gauge-fixing}} + \mathcal{L}_{\text{ghost}}. \tag{7}$$

This Lagrangian density describes the interaction of spin-$\frac{1}{2}$ quarks of mass m and massless spin-1 gluons. $F^A_{\alpha\beta}$ is the field strength tensor derived from the gluon field $\mathcal{A}^A_\alpha$,

$$F^A_{\alpha\beta} = \left[\partial_\alpha \mathcal{A}^A_\beta - \partial_\beta \mathcal{A}^A_\alpha - g f^{ABC} \mathcal{A}^B_\alpha \mathcal{A}^C_\beta\right] \tag{8}$$

and the indices A, B, C run over the eight colour degrees of freedom of the gluon field. It is the third 'non-Abelian' term on the right-hand-side of Eq. (8) which distinguishes QCD from QED, giving rise to triplet and quartic gluon self-interactions and ultimately to the property of asymptotic freedom.

The sum on the flavours runs over the n_f different flavours of quarks, g is the coupling constant which determines the strength of the interaction between coloured quanta, and f^{ABC} $(A, B, C = 1, ..., 8)$ are the structure constants of the SU(3) colour group. The quark fields q_a are in the triplet representation of the colour group, $(a = 1, 2, 3)$ and D is the covariant derivative. Acting on triplet and octet fields the covariant derivative takes the form

$$(D_\alpha)_{ab} = \partial_\alpha \delta_{ab} + ig\left(t^C \mathcal{A}^C_\alpha\right)_{ab}, \quad (D_\alpha)_{AB} = \partial_\alpha \delta_{AB} + ig(T^C \mathcal{A}^C_\alpha)_{AB}, \tag{9}$$

where t and T are matrices in the fundamental and adjoint representations of SU(3) respectively:

$$[t^A, t^B] = i f^{ABC} t^C, \quad [T^A, T^B] = i f^{ABC} T^C, \quad (T^A)_{BC} = -i f^{ABC}. \tag{10}$$

$\not{D}$ in Eq. (7) is a symbolic notation for $\gamma_\mu D^\mu$ and the spinor indices of γ_μ and q_a have been suppressed. We follow the notation of Bjorken and Drell [5] with metric given by $g^{\alpha\beta} = \text{diag}(1,-1,-1,-1)$ and set $\hbar = c = 1$. By convention the normalisation of the SU(N) matrices is chosen to be,

$$\text{Tr}\, t^A t^B = T_R\, \delta^{AB}, \quad T_R = \frac{1}{2}. \tag{11}$$

With this choice the SU(N) colour matrices obey the following relations,

$$\sum_A t^A_{ab} t^A_{bc} = C_F\, \delta_{ac}, \quad C_F = \frac{N^2-1}{2N} = \frac{4}{3}, \quad (N=3) \tag{12}$$

$$\text{Tr}\, T^C T^D = \sum_{A,B} f^{ABC} f^{ABD} = C_A\, \delta^{CD}, \quad C_A = N = 3. \tag{13}$$

1.3 Local gauge invariance

Eq. (7) has the property that it is invariant under local gauge transformations. One can perform a redefinition of the phase of the fields independently at every point in space and time, without changing the physical content of the theory. We redefine the phase of the quark fields,

$$q_a(x) \to q'_a(x) = \exp(it \cdot \theta(x))_{ab} q_b(x) \equiv \Omega(x)_{ab} q_b(x). \tag{14}$$

The covariant derivative is so called because it transforms under a local gauge transformation in the same way as the field itself.

$$D_\alpha q(x) \to D'_\alpha q'(x) \equiv \Omega(x) D_\alpha q(x) \tag{15}$$

In this equation we have dropped the colour labels. We can use this equation to derive the transformation property of the gauge field $\mathcal{A}$

$$\begin{aligned} D'_\alpha q'(x) &= (\partial_\alpha + igt \cdot \mathcal{A}'_\alpha)\Omega(x) q(x) \\ &\equiv (\partial_\alpha \Omega(x)) q(x) + \Omega(x) \partial_\alpha q(x) + igt \cdot \mathcal{A}'_\alpha \Omega(x) q(x) \end{aligned} \tag{16}$$

Thus we find that the transformation property of the gluon field is given by,

$$t \cdot \mathcal{A}'_\alpha = \Omega(x) t \cdot \mathcal{A}_\alpha \Omega^{-1}(x) - \frac{1}{ig}(\partial_\alpha \Omega(x))\Omega^{-1}(x) \tag{17}$$

Using this equation it is straightforward to show that the transformation property of the non-abelian field strength tensor is

$$t \cdot F_{\alpha\beta} \to t \cdot F'_{\alpha\beta} = \Omega(x) F_{\alpha\beta} \Omega^{-1}(x) \tag{18}$$

Alternatively we may use the relation

$$[D_\alpha, D_\beta] = igt \cdot F_{\alpha\beta} \tag{19}$$

to deduce Eq. (18) from Eq. (15). Note that there is no gauge invariant way of including a mass for the gluon. A term such as

$$m^2 \mathcal{A}^\alpha \mathcal{A}_\alpha \tag{20}$$

is not gauge invariant. On the other hand the mass term for the quarks given in Eq. (7) is gauge invariant.

1.3.1 Feynman rules

We cannot perform perturbation theory with the Lagrangian of Eq. (7) without the gauge fixing term. It is impossible to define the propagator for the gluon field without making a choice of gauge. The choice,

$$\mathcal{L}_{\text{gauge-fixing}} = -\frac{1}{2\,\lambda}\left(\partial^\alpha \mathcal{A}^A_\alpha\right)^2, \tag{21}$$

fixes the class of *covariant gauges* and λ is called the gauge parameter. In a non-Abelian theory such as QCD this covariant gauge-fixing term must be supplemented by a ghost Lagrangian, which is given by

$$\mathcal{L}_{\text{ghost}} = \partial_\alpha \eta^{A\,\dagger}\left(D^\alpha_{AB}\eta^B\right). \tag{22}$$

Here η^A is a complex scalar field which obeys Fermi statistics. The derivation of the form of the ghost Lagrangian is best provided by the path integral formalism [13] and the procedures due to Fadeev and Popov [14]. The ghost fields cancel unphysical degrees of freedom which would otherwise propagate in covariant gauges. For an explanation of the physical role played by ghost fields, the reader is referred to ref. [3].

Eqs. (7), (21) and (22) are sufficient to derive the Feynman rules which should be used in weak coupling perturbation theory in a covariant gauge. The Feynman rules are defined from the action operator $S = i\int \mathcal{L}\, d^4x$ rather than from the Lagrangian density. We can separate the effective lagrangian into a free piece $\mathcal{L}_0$, which normally contains all the terms bilinear in the fields, and an interaction piece, $\mathcal{L}_I$, which contains all the rest:

$$\begin{aligned} &S = S_0 + S_I \\ &S_0 = i\int d^4x \mathcal{L}_0(x), \quad S_I = i\int d^4x \mathcal{L}_I(x). \end{aligned} \tag{23}$$

The practical recipe to determine the Feynman rules is that the inverse propagator is derived from $-S_0$, whereas the Feynman rules for the interacting parts of the theory, which are treated as perturbations, are derived from S_I.

This recipe (including the extra minus sign) can be understood [15] by considering the following two different approaches to the quantisation of a theory. For simplicity, consider a theory which contains only a complex scalar field ϕ and an action which contains only bilinear terms, $S = \phi^* (K + K')\, \phi$. In the first approach, both K and K' are included in the free Lagrangian, $S_0 = \phi^* (K + K')\, \phi$. Using the above rule the propagator Δ for the ϕ field is given by

$$\Delta = \frac{-1}{K + K'}. \tag{24}$$

In the second approach K is regarded as the free Lagrangian, $S_0 = \phi^* K \phi$, and K' as the interaction Lagrangian, $S_I = \phi^* K' \phi$. Now S_I is included to all orders in perturbation theory by inserting the interaction term an infinite number of times:

$$\begin{aligned} \Delta &= \frac{-1}{K} + \left(\frac{-1}{K}\right) K' \left(\frac{-1}{K}\right) + \left(\frac{-1}{K}\right) K' \left(\frac{-1}{K}\right) K' \left(\frac{-1}{K}\right) + \cdots \\ &= \frac{-1}{K + K'} \end{aligned} \tag{25}$$

Note that, with the choice of signs described above, the full propagator of the ϕ field is the same in both approaches, demonstrating the internal consistency of the recipe.

Using the free piece $\mathcal{L}_0$ of the QCD Lagrangian given in Eq. (7) one can readily obtain the quark and gluon propagators. Thus, for example, the inverse fermion propagator in momentum space can be obtained by making the identification $\partial^\alpha = -ip^\alpha$ for an incoming field. In momentum space the two point function of the quark field depends on a single momentum p. It is found to be

$$\Gamma^{(2)}_{ab}(p) = -i\delta_{ab}\, (\not{p} - m), \tag{26}$$

which is the inverse of the propagator given in Fig. 3. The $i\varepsilon$ prescription for the pole of the propagator is added to preserve causality, in exactly the same way as in QED[5].

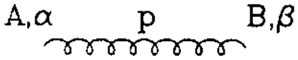

$$\delta^{AB}\left[-g^{\alpha\beta}+(1-\lambda)\frac{p^\alpha p^\beta}{p^2+i\epsilon}\right]\frac{i}{p^2+i\epsilon}$$

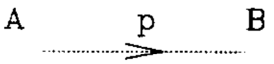

$$\delta^{AB}\frac{i}{(p^2+i\epsilon)}$$

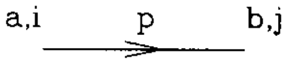

$$\delta^{ab}\frac{i}{(\not{p}-m+i\epsilon)_{ji}}$$

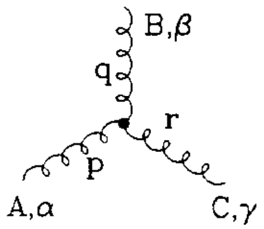

$$-ig\, f^{ABC}[(p-q)^\gamma g^{\alpha\beta}+(q-r)^\alpha g^{\beta\gamma}+(r-p)^\beta g^{\gamma\alpha}]$$

(all momenta incoming)

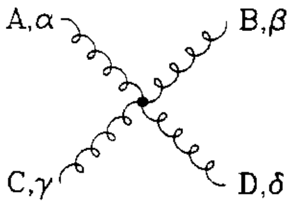

$$\begin{aligned}&-ig^2\, f^{XAC}f^{XBD}\,[g^{\alpha\beta}g^{\gamma\delta}-g^{\alpha\delta}g^{\beta\gamma}]\\&-ig^2\, f^{XAD}f^{XBC}\,[g^{\alpha\beta}g^{\gamma\delta}-g^{\alpha\gamma}g^{\beta\delta}]\\&-ig^2\, f^{XAB}f^{XCD}\,[g^{\alpha\gamma}g^{\beta\delta}-g^{\alpha\delta}g^{\beta\gamma}]\end{aligned}$$

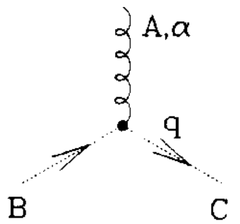

$$g\, f^{ABC}q^\alpha$$

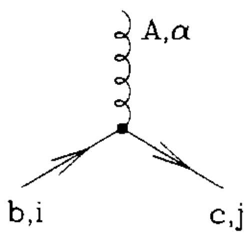

$$-ig\,(t^A)_{cb}\,(\gamma^\alpha)_{ji}$$

Figure 3: Feynman rules for QCD in a covariant gauge

Similarly the inverse propagator of the gluon field is found to be

$$\Gamma^{(2)}_{\{AB,\,\alpha\beta\}}(p) = i\delta_{AB}\ \left[p^2 g_{\alpha\beta} - (1-\frac{1}{\lambda})p_\alpha p_\beta\right]. \tag{27}$$

It is straightforward to check that without the gauge fixing term this function would have no inverse. The result for the gluon propagator Δ is as given in Fig. 3:

$$\Gamma^{(2)}_{\{AB,\,\alpha\beta\}}(p)\ \Delta^{(2)\ \{BC,\,\beta\gamma\}}(p) = \delta^C_A g^\gamma_\alpha \tag{28}$$

$$\Delta^{(2)}_{\{BC,\,\beta\gamma\}}(p) = \delta_{BC}\frac{i}{p^2}\left[-g_{\beta\gamma} + (1-\lambda)\frac{p_\beta p_\gamma}{p^2}\right]. \tag{29}$$

Replacing derivatives with the appropriate momenta, Eqs.(7), (21) and (22) can be used to derive all the rules in Fig. 3.

1.3.2 Axial gauges

The introduction of the gauge fixing explicitly breaks gauge invariance. The form of the breaking depends on the parameter λ. However, in the end, physical results must be independent of λ. Thus it does not really matter which choice one makes for the gauge fixing term, although the calculation may look very different in intermediate stages. An alternative choice of gauge fixing is specified in terms of an auxiliary vector n. Such gauges are called axial gauges and have gauge fixing terms of the form,

$$\mathcal{L}_{\text{gauge-fixing}} = -\frac{1}{2\,\lambda}\left(n^\alpha \mathcal{A}^A_\alpha\right)^2, \tag{30}$$

In this gauge the inverse propagator is given by,

$$\Gamma^{(2)}_{\{AB,\,\alpha\beta\}}(p) = i\delta_{AB}\ \left[p^2 g_{\alpha\beta} - p_\alpha p_\beta + \frac{1}{\lambda}n_\alpha n_\beta\right]. \tag{31}$$

which leads to a propagtor for the gluon field,

$$\Delta^{(2)}_{\{BC,\,\beta\gamma\}}(p) = \delta_{BC}\frac{i}{p^2}\left[-g_{\beta\gamma} + \frac{n_\beta p_\gamma + p_\beta n_\gamma}{n\cdot p} - \frac{(n^2+\lambda p^2)p_\beta p_\gamma}{(n\cdot p)^2}\right]. \tag{32}$$

What are the properties of these gauges which make them interesting? One advantage of this class of gauges is that they require no ghost fields. The price which one pays for this simplicity is the added complication of the propagator in the axial gauge as shown in Eq. (32). Let us specialise to the case $\lambda = 0, n^2 = 0$. This is called the light cone gauge. The propagator becomes

$$\Delta^{(2)}_{\{BC,\,\beta\gamma\}}(p) = \delta_{BC}\frac{i}{p^2}d_{\beta\gamma}(p,n) \tag{33}$$

where

$$d_{\beta\gamma}(p,n) = -g_{\beta\gamma} + \frac{n_\beta p_\gamma + p_\beta n_\gamma}{n \cdot p} \tag{34}$$

In the limit $p^2 \to 0$ we find that

$$n^\beta d_{\beta\gamma}(p,n) = 0,\ p^\beta d_{\beta\gamma}(p,n) = 0 \tag{35}$$

Only two physical polarizations propagate. In fact in the limit $p^2 \to 0$ we may decompose the numerator of the propagator into a sum over two polarizations.

$$d_{\alpha\beta}(p,n) = \sum_i \epsilon_\alpha^{(i)}(p)\epsilon_\beta^{(i)}(p). \tag{36}$$

These polarizations satisfy the constraint $n \cdot \epsilon(p) = 0$ in addition to the Lorentz condition $p \cdot \epsilon(p) = 0$. For this reason these classes of gauges are called physical gauges. The light cone gauge is very tricky. To make practical use of this gauge the gauge-fixing condition has to be supplemented with a regularization of the $n \cdot p$ singularity in Eq. (34). The interest in the light-cone gauge in QCD stems from the fact that the parton model picture is most transparent in this gauge.

1.4 Renormalisation

When the Feynman rules specified above are used to calculate loop diagrams ultraviolet divergences are encountered. Because of the renormalisability of QCD all such divergences can be absorbed order by order in perturbation theory by defining renormalised couplings, masses and fields[19]. The Lagrangian introduced in the previous section is therefore the bare Lagrangian which depends on the bare parameters and fields (which we now denote by the suffix 0).

The renormalised Lagrangian is obtained by rewriting Eq. (7) in terms of renormalized fields,

$$\mathcal{L}(\mathcal{A}_0^\alpha, q_0, \eta_0, m_0, g_0, \lambda_0) = \mathcal{L}(\mathcal{A}^\alpha, q, \eta, m, g\mu^\epsilon, \lambda) + \delta\mathcal{L}(\mathcal{A}^\alpha, q, \eta, m, g\mu^\epsilon, \lambda) \tag{37}$$

Once we specify the relationship between bare and renormalised quantities, Eq. (37) defines the counterterms $\delta\mathcal{L}$. Eq. (37) assumes that the loop integrals are regularised by continuing the dimension of space-time to $d = 4-2\epsilon$ dimensions. More information on this procedure is given below. A mass scale μ has been introduced to keep the coupling constant dimensionless in d dimensions. The advantage of working with renormalised fields is that the Green functions of the theory have a smooth limit as the cut-off is removed in terms of renormalised fields. The bare and renormalised quantities are related by,

$$\mathcal{A}^\alpha = Z_3^{-\frac{1}{2}} \mathcal{A}_0^\alpha,\ \ \lambda = \frac{\lambda_0}{Z_3},\ \ q = Z_2^{-\frac{1}{2}} q_0,\ \ \eta = \tilde{Z}_3^{-\frac{1}{2}} \eta_0,\ \ m_0 = m Z_m$$

$$g_0 = g\mu^\epsilon \frac{Z_1}{Z_3^{\frac{3}{2}}} = g\mu^\epsilon \frac{\tilde{Z}_1}{\tilde{Z}_3 Z_3^{\frac{1}{2}}} = g\mu^\epsilon \frac{Z_1^F}{Z_2 Z_3^{\frac{1}{2}}} = g\mu^\epsilon \frac{Z_4^{\frac{1}{2}}}{Z_3} \equiv g\mu^\epsilon Z_g \tag{38}$$

Note that the renormalisation constants of the theory satisfy the Ward identities,

$$\frac{Z_1}{Z_3} = \frac{\tilde{Z}_1}{\tilde{Z}_3} = \frac{Z_1^F}{Z_2} = \frac{Z_4}{Z_1} \tag{39}$$

which ensure the universality of charge renormalisation. These are the generalisation to non-Abelian theory of the QED relation, $Z_1 = Z_2$. Because of the renormalisability of the theory all matrix elements calculated with $\mathcal{L} + \delta\mathcal{L}$ are finite. We write

$$\begin{aligned}
\mathcal{L} + \delta\mathcal{L} = & -\frac{1}{4} Z_3 \left(\partial_\alpha \mathcal{A}_\beta^B - \partial_\beta \mathcal{A}_\alpha^B\right)^2 - \frac{1}{2\lambda}(\partial_\alpha \mathcal{A}_\beta^B)^2 + Z_2 \bar{q}_a (i\partial\!\!\!/ - Z_m m) q_a \\
& + \tilde{Z}_3 \partial_\alpha \eta_B^\dagger \partial^\alpha \eta_B + \frac{g}{2}\mu^\epsilon Z_1 f^{ABC} (\partial_\alpha \mathcal{A}_\beta^A - \partial_\beta \mathcal{A}_\alpha^A) \mathcal{A}_\alpha^B \mathcal{A}_\beta^C \\
& + \tilde{Z}_1 i g \mu^\epsilon \partial_\alpha \eta_B^\dagger (T \cdot \mathcal{A}^\alpha)_{BC} \eta_C - Z_1^F g \mu^\epsilon \bar{q}_a (t \cdot \mathcal{A}\!\!\!/)_{ab} q_b \\
& - \frac{g^2}{4} \mu^{2\epsilon} Z_4 f^{ABC} f^{ADE} \mathcal{A}_\alpha^B \mathcal{A}_\beta^C \mathcal{A}_\alpha^D \mathcal{A}_\beta^E .
\end{aligned} \tag{40}$$

Thus the counterterms are given by,

$$\begin{aligned}
\delta\mathcal{L} = & -\frac{1}{4}(Z_3 - 1) \left(\partial_\alpha \mathcal{A}_\beta^B - \partial_\beta \mathcal{A}_\alpha^B\right)^2 \\
& + i(Z_2 - 1)\bar{q}_a \partial\!\!\!/ q_a - (Z_2 Z_m - 1)\bar{q}_a m q_a + (\tilde{Z}_3 - 1)\partial_\alpha \eta_B^\dagger \partial^\alpha \eta_B \\
& + \frac{g}{2}\mu^\epsilon (Z_1 - 1) f^{ABC} (\partial_\alpha \mathcal{A}_\beta^A - \partial_\beta \mathcal{A}_\alpha^A) \mathcal{A}_\alpha^B \mathcal{A}_\beta^C \\
& + (\tilde{Z}_1 - 1) i g \mu^\epsilon \partial_\alpha \eta_B^\dagger (T \cdot \mathcal{A}^\alpha)_{BC} \eta_C \\
& - (Z_1^F - 1) g \mu^\epsilon \bar{q}_a (t \cdot \mathcal{A}\!\!\!/)_{ab} q_b - \frac{g^2}{4}\mu^{2\epsilon}(Z_4 - 1) f^{ABC} f^{ADE} \mathcal{A}_\alpha^B \mathcal{A}_\beta^C \mathcal{A}_\alpha^D \mathcal{A}_\beta^E .
\end{aligned} \tag{41}$$

The Z's are defined order by order in perturbation theory to cancel all the ultraviolet divergences.

1.5 Dimensional Regularisation

In the intermediate stages of the calculation we must introduce some regularisation procedure to control these divergences. The most effective regulator is the method of dimensional regularisation which continues the dimension of space-time to $d = 4 - 2\epsilon$ dimensions[21]. This method of regularisation has the advantage that the Ward Identities of the theory are preserved at all stages of the calculation. Integrals over loop momenta are performed in d dimensions with the help of the following formula,

$$\begin{aligned}
& \int \frac{d^d k}{(2\pi)^d} \frac{(-k^2)^r}{\left[-k^2 + C - i\varepsilon\right]^m} = \\
& \frac{i(4\pi)^\epsilon}{16\pi^2} \left[C - i\varepsilon\right]^{2+r-m-\epsilon} \frac{\Gamma(r + d/2)}{\Gamma(d/2)} \frac{\Gamma(m - r - 2 + \epsilon)}{\Gamma(m)} .
\end{aligned} \tag{42}$$

To demonstrate Eq. (42), we first perform a Wick rotation of the k_0 contour anti-

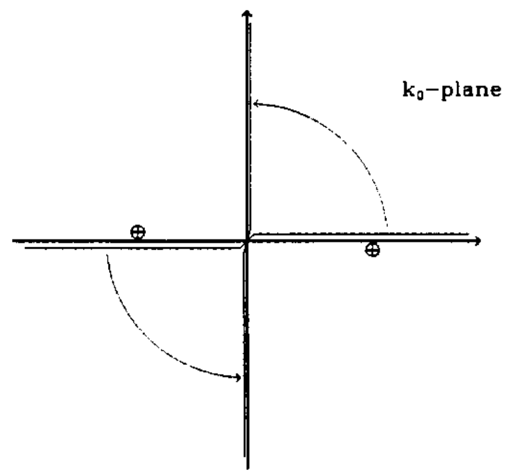

Figure 4: Wick rotation in the complex k_0 plane

clockwise. This is dictated by the $i\varepsilon$ prescription, since for real C the poles coming from the denominator of Eq. (42) lie in the second and fourth quadrant of the k_0 complex plane as shown in Fig. 4. Thus by anti-clockwise rotation we encounter no poles. After rotation by an angle $\pi/2$, the k_0 integral runs along the imaginary axis in the k_0 plane, $(-i\infty < k_0 < i\infty)$. In order to deal only with real quantities we make the substitution $k_0 = i\kappa_d, k_j = \kappa_j$ for all $j \neq 0$ and introduce $|\kappa| = \sqrt{\kappa_1^2 + \kappa_2^2 \ldots + \kappa_d^2}$. We obtain a d-dimensional Euclidean integral which may be written as,

$$\int d^d\kappa\ f(\kappa^2) = \int d|\kappa|\ f(\kappa^2)\ |\kappa|^{d-1} \sin^{d-2}\theta_{d-1} \sin^{d-3}\theta_{d-2} \ldots \times \sin\theta_2\ d\theta_{d-1} d\theta_{d-2} \ldots d\theta_2 d\theta_1. \tag{43}$$

This formula is best proved by induction. The range of the angular integrals is $0 \leq \theta_i \leq \pi$ except for $0 \leq \theta_1 \leq 2\pi$. The angular integrations, which only give an overall factor, can be performed using

$$\int_0^\pi d\theta\ \sin^d\theta = \sqrt{\pi}\frac{\Gamma\left(\frac{(d+1)}{2}\right)}{\Gamma\left(\frac{(d+2)}{2}\right)}. \tag{44}$$

We therefore find that the left hand side of Eq. (42) can be written as,

$$\frac{2i}{(4\pi)^{d/2}\Gamma\left(d/2\right)} \int_0^\infty d|\kappa|\ \frac{|\kappa|^{d+2r-1}}{\left[\kappa^2 + C\right]^m}. \tag{45}$$

This last integral can be reduced to a Beta function, (see Table 2)

$$\int_0^\infty dx \frac{x^s}{\left[x^2 + C\right]^m} = \frac{\Gamma(\frac{(s+1)}{2})}{2} \frac{\Gamma(m - s/2 - 1/2)}{\Gamma(m)} C^{s/2+1/2-m} \tag{46}$$

$\gamma^\mu\gamma^\nu + \gamma^\nu\gamma^\mu = 2\, g^{\mu\nu}\mathrm{I}$ $\gamma^\mu\gamma_\mu = g^\mu_\mu\, \mathrm{I} = d\, \mathrm{I}$ $\gamma^\mu\gamma^\alpha\gamma_\mu = -2\,(1-\epsilon)\,\gamma^\alpha$ $\gamma^\mu\gamma^\alpha\gamma^\beta\gamma_\mu = 4\, g^{\alpha\beta}\mathrm{I} - 2\epsilon\, \gamma^\alpha\gamma^\beta$ $\gamma^\mu\gamma^\alpha\gamma^\beta\gamma^\rho\gamma_\mu = -2\, \gamma^\rho\gamma^\beta\gamma^\alpha + 2\epsilon\, \gamma^\alpha\gamma^\beta\gamma^\rho$
$\mathrm{Tr}\, \mathrm{I} = 4$ $\mathrm{Tr}\, \gamma^\mu\gamma^\nu = 4\, g^{\mu\nu}$ $\mathrm{Tr}\, \gamma^\mu\gamma^\nu\gamma^\rho\gamma^\sigma = 4(g^{\mu\nu}g^{\rho\sigma} + g^{\nu\rho}g^{\mu\sigma} - g^{\mu\rho}g^{\nu\sigma})$

Table 1: Gamma matrix identities in $d = 4 - 2\epsilon$ dimensions.

which demonstrates Eq. (42). When calculating the two, three and four point functions of the quark, gluon and ghost fields the ultraviolet divergences of the theory appear as poles in ϵ. In the mimimal subtraction (MS) renormalisation scheme[15] one chooses the various Z's of the theory in such a way that the poles are all cancelled. In one loop this leads to the renormalisation constants given in Table 3.

Note that the renormalisation constants depend on the gauge parameter. The scheme is called minimal because the renormalisation constants of the theory contain only the pole parts.

1.5.1 One loop renormalisation

We shall now describe a simple technique for calculating one loop diagrams involving self energy corrections. The technique is easily generalised for vertex corrections and box diagrams although the algebra rapidly becomes cumbersome.

Define the one loop self-energy and tadpole integrals,

$$\begin{aligned} B_0; B_1^\mu; B_2^{\mu\nu}(q, m_1, m_2) &\equiv \int \frac{d^n l}{(2\pi)^n} \frac{\{1; l^\mu; l^\mu l^\nu\}}{(l^2 - m_1^2 + i\varepsilon)((l+q)^2 - m_2^2 + i\varepsilon)} \\ A_0(m) &\equiv \int \frac{d^n l}{(2\pi)^n} \frac{1}{(l^2 - m^2 + i\varepsilon)} \end{aligned} \quad (47)$$

By Lorentz invariance the tensor integrals can be expanded in form-factors.

$$\begin{aligned} B_2^{\mu\nu} &= q^\mu q^\nu B_{21} + g^{\mu\nu} B_{22} \\ B_1^\mu &= q^\mu B_1 \end{aligned} \quad (48)$$

The scalar functions B_{21}, B_{22} and B_1 can be expressed in terms of simpler functions by cancelling denominators[20].

$$2l \cdot q = \left[(l+q)^2 - m_2^2\right] - \left[l^2 - m_1^2\right] + \left[m_2^2 - m_1^2 - q^2\right] \quad (49)$$

$\Gamma(z) = \int_0^\infty dt\; e^{-t} t^{z-1}$
$z\Gamma(z) = \Gamma(z+1)$
$\Gamma(2z) = \frac{2^{2z-1}}{\sqrt{\pi}}\Gamma(z)\Gamma(z+\frac{1}{2})$
$\Gamma(n+1) = n!$ for n a positive integer
$\Gamma(1) = 1, \;\; \Gamma(\frac{1}{2}) = \sqrt{\pi}$
$\Gamma'(1) = -\gamma_E, \;\; \gamma_E \approx 0.577215$
$\Gamma''(1) = \gamma_E^2 + \frac{\pi^2}{6}$
$B(a,b) = \int_0^1 dx\; x^a (1-x)^b$
$B(a,b) = \int_0^\infty dt\; \frac{t^{a-1}}{(1+t)^{a+b}}$ for Re $a, b > 0$
$B(a,b) = \frac{\Gamma(a)\Gamma(b)}{\Gamma(a+b)}$

Table 2: Useful properties of the Γ and related functions

By simple algebra we can derive the relations,

$$\begin{aligned} B_{22}(q,m_1,m_2) &= \frac{1}{3-2\epsilon}\Bigg[m_1^2 B_0(q,m_1,m_2) + \tfrac{1}{2}A_0(m_2) \\ &- \tfrac{1}{2}f(q,m_1,m_2)B_1(q,m_1,m_2)\Bigg] \\ B_{21}(q,m_1,m_2) &= \frac{1}{(3-2\epsilon)q^2}\Bigg[(1-\epsilon)A_0(m_2) - m_1^2 B_0(q,m_1,m_2) \\ &\quad +(2-\epsilon)f(q,m_1,m_2)B_1(q,m_1,m_2)\Bigg] \\ B_1(q,m_1,m_2) &= \frac{1}{2q^2}\Bigg[A_0(m_1) - A_0(m_2) + f(q,m_1,m_2)B_0(q,m_1,m_2)\Bigg] \end{aligned} \quad (50)$$

where $f(q,m_1,m_2) = m_2^2 - m_1^2 - q^2$ and $d = 4 - 2\epsilon$.

As an example we shall consider the fermionic contribution to the gluonic self energy which is given by, (see Fig. 5a)

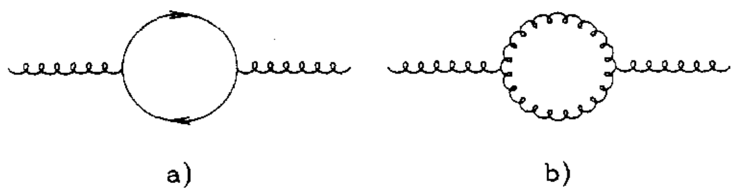

Figure 5: Graphs which contribute to the β function in the one loop approximation

$$\pi^{\mu\nu} = -(-ig)^2 \int \frac{d^n l}{(2\pi)^n} \mathrm{Tr}\{t^A t^B\} \mathrm{Tr}\Big\{\gamma^\mu \frac{i}{\not l - m + i\varepsilon} \gamma^\nu \frac{i}{\not l + \not q - m + i\varepsilon}\Big\} \tag{51}$$

The overall minus sign comes from the fermion loop. Performing the traces we obtain,

$$\pi^{\mu\nu} = -4g^2 T_R \delta^{AB} \int \frac{d^n l}{(2\pi)^n} \frac{\Big(l^\mu (l+q)^\nu + l^\nu (l+q)^\mu - g^{\mu\nu}(l \cdot (l+q) - m^2)\Big)}{(l^2 - m^2 + i\varepsilon)((l+q)^2 - m^2 + i\varepsilon)} \tag{52}$$

Because of current conservation $\pi^{\mu\nu}$ has the form,

$$\pi^{\mu\nu} = (g^{\mu\nu} q^2 - q^\mu q^\nu)\pi(q^2) \tag{53}$$

Dropping terms of ϵ^2 and higher we find,

$$\pi(q^2) = -\frac{4}{3} g^2 T_R \delta^{AB} \Big[B_0(q,m,m)(1 - \frac{\epsilon}{3} + \frac{2m^2}{q^2}(1 + \frac{2\epsilon}{3})) - 2\frac{A_0(m)}{q^2}(1 - \frac{\epsilon}{3}) \Big] \tag{54}$$

The corresponding result for the gluon self energy, Fig. 5b is given in the Feynman gauge ($\lambda = 1$) by,

$$\pi^{\mu\nu} = \frac{N_c g^2}{36} \delta^{AB} B_0(q,0,0) \Big[g^{\mu\nu} q^2 (57 + 2\epsilon) - q^\mu q^\nu (66 + 2\epsilon) + O(\epsilon^2) \Big] \tag{55}$$

The Ghost contribution is, (diagram not shown)

$$\pi^{\mu\nu} = \frac{N_c g^2}{36} \delta^{AB} B_0(q,0,0) \Big[g^{\mu\nu} q^2 (3 + 2\epsilon) - q^\mu q^\nu (-6 + 2\epsilon) \Big] \tag{56}$$

The sum has the correct tensor structure, *cf.* Eq. (53) and π is given by,

$$\pi(q^2) = \frac{5}{3} \delta^{AB} N_c g^2 B_0(q,0,0) \Big[1 + \frac{\epsilon}{15} \Big] \tag{57}$$

With this method we only have to calculate two integrals explicitly. They are,

$$A_0(m) = \frac{im^2}{16\pi^2}\big(\Delta + 1 - \ln m^2\big) \tag{58}$$

$$B_0(q,m,m) = \frac{i}{16\pi^2}\Big(\Delta - \int_0^1 dx \ln\big(-x(1-x)q^2 + m^2 - i\varepsilon\big)\Big) \tag{59}$$

where $\Delta = \frac{1}{\epsilon} + \ln 4\pi - \gamma$ where γ is the Euler constant. The ubiquitous appearance of the $\ln 4\pi$ and the γ with pole, leads us to define the $\overline{MS}$ scheme. In this scheme we subtract the whole of Δ rather than just the pole in $1/\epsilon$.

Examining the pole pieces we can see that we have reproduced the Feynman gauge result for Z_3 as given in Table 3.

$$Z_3 = 1 + \frac{g^2}{16\pi^2}\frac{1}{\epsilon}\Big[N_c\frac{5}{3} - \frac{4}{3}n_f T_R\Big] \tag{60}$$

1.6 The running coupling constant

In order to introduce the concept of the running coupling, consider as an example a dimensionless physical observable R which depends on a single energy scale Q. By assumption the scale Q is much bigger than all other dimensionful parameters such as masses. We shall therefore set the masses to zero. (This step requires the additional assumption that R has a sensible zero mass limit.) Naive scaling would suggest that because there is a single large scale, R should have a constant value independent of Q. This result is not however true in a renormalizable quantum field theory. When we calculate R as a perturbation series in the coupling $\alpha_S = g^2/4\pi$, (defined in analogy with the fine structure constant of QED), the perturbation series requires renormalization to remove ultra-violet divergences. Because this renormalization procedure introduces a second mass scale μ – the point at which the subtractions which remove the ultra-violet divergences are performed – R depends in general on the ratio Q/μ and is not therefore constant. It follows also that the renormalized coupling α_S depends on the choice made for the subtraction point μ.

However μ is an arbitrary parameter. The Lagrangian of QCD makes no mention of the scale μ, even though a choice of μ is required to define the theory at the quantum level. Therefore, if we hold the bare coupling fixed, physical quantities such as R cannot depend on the choice made for μ. Since R is dimensionless, it can only depend on the ratio Q^2/μ^2 and the renormalized coupling α_S. Mathematically, the μ dependence of R may be quantified by

$$\mu^2\frac{d}{d\mu^2}R(\frac{Q^2}{\mu^2},\alpha_S) \equiv \left[\mu^2\frac{\partial}{\partial\mu^2} + \mu^2\frac{\partial\alpha_S}{\partial\mu^2}\frac{\partial}{\partial\alpha_S}\right]R = 0. \tag{61}$$

To rewrite this equation in a more compact form we introduce the notations

$$t = \ln\left(\frac{Q^2}{\mu^2}\right), \quad \beta(\alpha_S) = \mu^2\frac{\partial\alpha_S}{\partial\mu^2}. \tag{62}$$

The derivative of the coupling in the definition of the β function is performed at fixed bare coupling. We rewrite Eq. (61) as

$$\left[-\frac{\partial}{\partial t}+\beta(\alpha_S)\frac{\partial}{\partial\alpha_S}\right]R=0. \tag{63}$$

This first order partial differential equation is solved by implicitly defining a new function – the running coupling $\alpha_S(Q)$ – as follows:

$$t=\int_{\alpha_S}^{\alpha_S(Q)}\frac{dx}{\beta(x)},\quad \alpha_S(\mu)\equiv\alpha_S. \tag{64}$$

By differentiating Eq. (64) we can show that

$$\frac{\partial\alpha_S(Q)}{\partial t}=\beta(\alpha_S(Q)),\ \frac{\partial\alpha_S(Q)}{\partial\alpha_S}=\frac{\beta(\alpha_S(Q))}{\beta(\alpha_S)}. \tag{65}$$

and hence that

$$R(\frac{Q^2}{\mu^2},\alpha_S)=R(1,\alpha_S(Q)) \tag{66}$$

is a solution of Eq. (63). The above analysis shows that all of the scale dependence in R enters through the running of the coupling constant $\alpha_S(Q)$. It follows that knowledge of the quantity $R(1,\alpha_S)$, calculated in fixed order perturbation theory, allows us to predict the variation of R with Q if we can solve Eq. (64). In the next section, we shall show that QCD is an *asymptotically free* theory. This means that $\alpha_S(Q)$ becomes smaller as the scale Q increases. For sufficiently large Q, therefore, we can always solve Eq. (64) using perturbation theory.

1.7 The beta function and the Λ parameter in QCD

The running of the coupling constant α_S is determined by the renormalization group equation. In QCD, the β function has the perturbative expansion

$$\begin{aligned}&\beta(\alpha_S)=-b\alpha_S^2(1+b'\alpha_S+O(\alpha_S^2))\\&b=\frac{(33-2n_f)}{12\pi},\ b'=\frac{(153-19n_f)}{2\pi(33-2n_f)},\end{aligned} \tag{67}$$

where n_f is the number of active light flavours. Fig. 5 shows some of the diagrams which contribute to beta function of QCD in the one loop approximation. Fig. 6 shows the beta function with three light flavours. An alternative notation which is sometimes used is

$$\begin{aligned}&\beta(\alpha_S)=-\alpha_S\sum_{n=0}^{\infty}\beta_n\left(\frac{\alpha_S}{4\pi}\right)^{(n+1)}\\&\beta_0=4\pi b=11-\frac{2}{3}n_f,\ \beta_1=16\pi^2bb'=102-\frac{38}{3}n_f,\ \ldots\end{aligned} \tag{68}$$

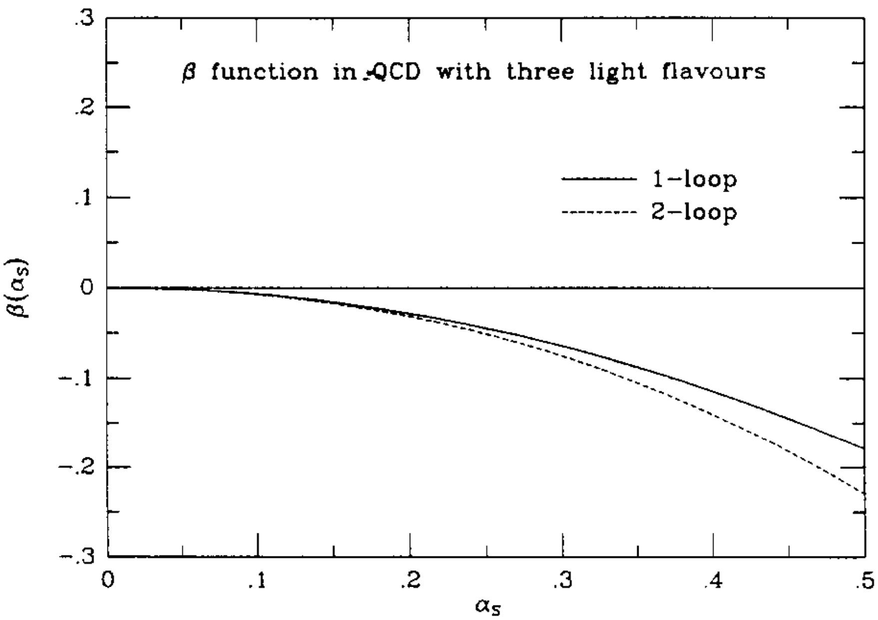

Figure 6: The β function in the one and two loop approximation

The β function coefficients can be extracted from the higher order (loop) corrections to the bare vertices of the theory, as in QED. Here we see for the first time the effect of the non-Abelian interactions in QCD. In QED (with one fermion flavour) the β function is

$$\beta_{QED}(\alpha) = \frac{1}{3\pi}\alpha^2 + \dots \tag{69}$$

and thus the b coefficients in QED and QCD have the opposite sign.

From Eq. (65) we may write,

$$\frac{\partial \alpha_S(Q)}{\partial t} = -b\alpha_S^2(Q)\big[1 + b'\alpha_S(Q) + O(\alpha_S^2(Q))\big]. \tag{70}$$

If both $\alpha_S(\mu)$ and $\alpha_S(Q)$ are in the perturbative region it makes sense to truncate the series on the right-hand-side and solve the resulting differential equation for $\alpha_S(Q)$. For example, neglecting the b' and higher coefficients in Eq. (70) gives the solution

$$\alpha_S(Q) = \frac{\alpha_S(\mu)}{1 + \alpha_S(\mu)bt}, \quad t = \ln\left(\frac{Q^2}{\mu^2}\right). \tag{71}$$

This gives the relation between $\alpha_S(Q)$ and $\alpha_S(\mu)$, if both are in the perturbative region. Evidently as t becomes very large, the running coupling $\alpha_S(Q)$ decreases to zero. This is the property of *asymptotic freedom*. The approach to zero is rather slow since α_S only decreases like an inverse power of $\ln Q^2$. Notice that the sign of b is crucial. With the opposite sign of b the coupling would *increase* at large Q^2, as it does in QED.

It is relatively straightforward to show that including the next-to-leading order coefficient b' yields the solution

$$\frac{1}{\alpha_S(Q)} - \frac{1}{\alpha_S(\mu)} + b' \ln\Big(\frac{\alpha_S(Q)}{1+b'\alpha_S(Q)}\Big) - b' \ln\Big(\frac{\alpha_S(\mu)}{1+b'\alpha_S(\mu)}\Big) = bt. \tag{72}$$

Note that this is now an implicit equation for $\alpha_S(Q)$ as a function of t and $\alpha_S(\mu)$. In practice, given values for these parameters, $\alpha_S(Q)$ can easily be obtained numerically to any desired accuracy.

Returning to the physical quantity R, we can now demonstrate the type of terms which the renormalization group resums. Assume that in perturbation theory R has the expansion

$$R = \alpha_S + \ldots \tag{73}$$

where ... represents terms of order α_S^2 and higher. The solution $R(1, \alpha_S(Q))$ – for the special choice of R given by Eq. (73) – can be re-expressed in terms of $\alpha_S(\mu)$ using Eq. (71):

$$\begin{aligned} R(1, \alpha_S(Q)) &= \alpha_S(\mu) \sum_{j=0}^{\infty} (-1)^j (\alpha_S(\mu) bt)^j \\ &= \alpha_S(\mu) \Big[1 - \alpha_S(\mu) bt + \alpha_S^2(\mu)(bt)^2 + \ldots\Big] \end{aligned} \tag{74}$$

Thus order by order in perturbation theory there are logarithms of Q^2/μ^2 which are automatically resummed by using the running coupling. Higher order terms in R – represented by the dots in Eq. (73) – when expanded give terms with fewer logarithms per power of α_S.

1.7.1 β function with dimensional regularization

The dimensional regularization scheme is very powerful from a calculational point of view, but leads to some loss in intuition. In this scheme the relationship between the bare and renormalized couplings is given by

$$\begin{aligned} g_0^0 &= \mu^\epsilon g Z_g \\ \alpha_S^0 &= (\mu^2)^\epsilon \alpha_S Z_g^2 \end{aligned} \tag{75}$$

The renormalization constant Z_g is calculated in perturbation theory and in the minimal subtraction scheme has the form

$$Z_g = 1 + \sum_{i=1}^{\infty} \frac{Z^{(i)}}{\epsilon^i} \tag{76}$$

For example, the coefficient of the single pole term is given by,

$$Z^{(1)} = -\tfrac{1}{2}b\alpha_S(1 + \tfrac{1}{2}b'\alpha_S + \ldots) \tag{77}$$

The β function determines the scale dependence of the coupling at fixed bare parameters. Thus in $d = 4 - 2\epsilon$ dimensions we have that

$$\beta(\alpha_S, \epsilon) = \left.\frac{d\alpha_S}{d\ln\mu^2}\right|_{\text{fixed } \alpha_S^0} \tag{78}$$

Evaluating this equation using Eq. (75) and exploiting the fact that Z_g depends on μ only through the dependence implicit in the renormalized coupling, we find that

$$\left[\beta(\alpha_S, \epsilon) + \epsilon\alpha_S + 2\alpha_S\beta(\alpha_S, \epsilon)\frac{d}{d\alpha_S}\right] Z_g = 0 \tag{79}$$

The β function, since it depends on the renormalized coupling, contains no poles in ϵ. On the other hand, in dimensionalities different than four it contains extra contributions. We therefore write it in the form

$$\beta(\alpha_S, \epsilon) = \beta(\alpha_S) + \sum_{i=1}^{\infty} \beta^{(i)}(\alpha_S)\, \epsilon^i \tag{80}$$

Inserting this expression into Eq. (79) we find that

$$\beta^{(i)}(\alpha_S) = 0, \quad i > 1 \tag{81}$$

$$\beta^{(1)}(\alpha_S)) = -\alpha_S \tag{82}$$

$$\beta(\alpha_S) = 2\alpha_S^2 \frac{d}{d\alpha_S} \ln Z^{(1)} \tag{83}$$

and hence that

$$\beta(\alpha_S, \epsilon) = -\epsilon\alpha_S + \beta(\alpha_S) \tag{84}$$

We see that the beta function in the MS scheme is determined directly from the single pole terms in the charge renormalization.

1.8 Asymptotic freedom

An unappealing feature of QCD is the absence of a really simple explanation of the property of Asymptotic Freedom. This is in contrast to QED, where the idea that the observed charge of the electron is smaller at large distances because of screening of the electric charge by vacuum polarization is quite intuitive. It would be nice to be able to extend this argument to QCD. The new features in QCD are that the gluons themselves carry charge and that they have spin one.

There are a two types of arguments which purport to give a simple explanation of asymptotic freedom[16,17]. They explain asymptotic freedom either as a dielectric or a paramagnetic effect. The first line of argument[16] calculates the dielectric properties of the vacuum and ascribes the asymptotic freedom of the theory to the self interaction of the gluon field. I shall sketch an argument of the second type [17] which describes asymptotic freedom as a paramagnetic effect due to the spin of the gluons. I refer the reader to the literature for more detailed information.

I start by reviewing the situation in QED. In QED the effective charge grows at small distances (large momenta) as one probes more of the unshielded central charge. This can be thought of as a scale dependent dielectric constant. One can define a running charge at scale q in terms of the charge at the ultraviolet cut-off scale $\Lambda \gg q$ as

$$\alpha(q) = \frac{\alpha(\lambda)}{\varepsilon(q)} \tag{85}$$

where

$$\frac{1}{\varepsilon(q)} = 1 - \frac{\beta(\alpha)}{\alpha} \ln \frac{\Lambda^2}{q^2} \tag{86}$$

and the running charge satisfies the equation

$$\frac{d\alpha(q)}{d\ln q^2} = \beta(\alpha) \tag{87}$$

If the β function is positive then $\varepsilon(q) > 1$, which corresponds to a screening of the central charge.

We now assume that the vacuum of a relativistic quantum field theory can be treated as a polarizable medium. For this special medium the dielectric constant $\varepsilon(q)$ and the magnetic permeability $\mu(q)$ are inversely related,

$$\mu(q) = \frac{1}{\varepsilon(q)} \tag{88}$$

in units in which $c = 1$. This is a consequence of the Lorentz invariance of the vacuum. We are therfore free to exploit this freedom by considering the properties of the QCD vacuum in a backgound magnetic field, rather than an background electric field, if it is simpler to do so. We choose to consider the behaviour of the magnetic susceptibility, χ related to the permeability by the relation $\mu = 1 + \chi$.

$$\chi(q) = -\frac{\beta(\alpha)}{\alpha} \ln \frac{\Lambda^2}{q^2} \tag{89}$$

The relationship between the electric and magnetic explanations is shown in Table 4.

Before going on to describe the paramagnetic properties of the vacuum, a brief reminder of the magnetic properties of a free electron quantum gas may be useful[18]. It is usual when discussing the magnetic properties of a free electron gas to divide the problem into two parts. The first term, known as Pauli paramagnetism, calculates the effect of electrons coupling to the magnetic field only through their spin magnetic

Z_3	$1+\frac{g^2}{16\pi^2}\frac{1}{\epsilon}\left[N_c(\frac{13}{6}-\frac{\lambda}{2})-\frac{4}{3}n_fT_R\right]$
Z_1	$1+\frac{g^2}{16\pi^2}\frac{1}{\epsilon}\left[N_c(\frac{17}{12}-\frac{3\lambda}{4})-\frac{4}{3}n_fT_R\right]$
Z_4	$1+\frac{g^2}{16\pi^2}\frac{1}{\epsilon}\left[N_c(\frac{2}{3}-\lambda)-\frac{4}{3}n_fT_R\right]$
$\tilde{Z}_3$	$1+\frac{g^2}{16\pi^2}\frac{1}{\epsilon}\left[N_c(\frac{3}{4}-\frac{\lambda}{4})\right]$
$\tilde{Z}_1$	$1-\frac{g^2}{16\pi^2}\frac{1}{\epsilon}\left[N_c\frac{\lambda}{2}\right]$
Z_2^F	$1-\frac{g^2}{16\pi^2}\frac{1}{\epsilon}\left[C_F\lambda\right]$
Z_1^F	$1-\frac{g^2}{16\pi^2}\frac{1}{\epsilon}\left[N_c(\frac{3}{4}+\frac{\lambda}{4})+C_F\lambda\right]$
Z_m	$1-\frac{g^2}{16\pi^2}\frac{1}{\epsilon}\left[C_F3\right]$
Z_g	$1-\frac{g^2}{16\pi^2}\frac{1}{\epsilon}\left[N_c\frac{11}{6}-n_fT_R\frac{2}{3}\right]$

Table 3: Minimal subtraction renormalisation constants in a general covariant gauge at one loop order.

Electric		Magnetic		
Screening	$\varepsilon > 1$	$\mu < 1$	$\chi < 0$	diamagnetism
Anti-screening	$\varepsilon < 1$	$\mu > 1$	$\chi > 0$	paramagnetism

Table 4: Relationship between the dielectric and paramagnetic explanation of asymptotic freedom

moments. It therefore describes a gas of particles with magnetic moments but no charges. The second term, known as Landau diamagnetism, describes the coupling of the field to the orbital motion of the electrons. It can be shown that for a free electron gas [18] the two contributions are related by,

$$\chi_{\text{Landau}} = -\tfrac{1}{3}\chi_{\text{Pauli}} \tag{90}$$

A free electron gas will be paramagnetic because the Pauli paramagnetism is larger in magnitude than the Landau diamagnetism.

Returning to the case of the vacuum of a relativistic field theory, we find that both paramagnetic and diamagnetic contributions are present. The Pauli paramagnetic has to be generalized slightly to take into account spins different from one half. The final result is given by Eq. (89) where

$$\beta(\alpha) = -b\alpha^2 \tag{91}$$

and the contribution of particles of spin S to b is,

$$b = \frac{(-1)^{2S}}{2\pi}\left[(2S)^2 - \tfrac{1}{3}\right] \tag{92}$$

The Pauli paramagnetic term is now proportional to S^2. For spins $0, \frac{1}{2}$ and 1 the result from Eq. (92) is,

$$\begin{array}{rccc} S = 0: & \frac{1}{2}: & 1 \\ b = -\dfrac{1}{6\pi}: & -\frac{1}{3\pi}: & \dfrac{11}{6\pi} \end{array} \tag{93}$$

We see that Eq. (92) can be considered as a generalization of Eq (90) to arbitrary spin. As expected the Pauli paramagnetism term grows with the spin of the particle. The overall sign $(-1)^{2S}$ is due to the fact that the perturbative vacuum of charged fields has one particle present in each positive energy mode for Bose fields and one particle present in each negative energy mode for Fermi fields. Because of this overall sign spin-$\frac{1}{2}$ particles give a diamagnetic contribution to the β function, (unlike the case of the free electron gas).

Adding a colour factor of $C_A/2$ for $S = 1$ and $N_F/2$ for $S = \frac{1}{2}$ we obtain the traditional asymptotic freedom result.

$$b = \frac{1}{12\pi}(33 - 2N_f) \tag{94}$$

1.9 The total hadronic cross section

The production of a muon pair in electron-positron annihilation, $e^+e^- \to \mu^+\mu^-$, is one of the fundamental processes of QED. The same annihilation process can also produce hadrons in the final state. The formation of these hadrons is not governed by perturbation theory. Why then would one expect a perturbative approach to give an accurate description of the hadronic cross section? The answer can be understood by visualizing the event in space-time. The electron and positron form a photon (or Z), of virtuality Q equal to the collision energy $\sqrt{s}$, which then fluctuates into a quark and an antiquark. By the uncertainty principle, this fluctuation occurs in a space-time volume $1/Q$, and if Q is large the production rate for this short-distance process should be predicted by perturbation theory. Subsequently, the quarks and gluons form themselves into hadrons. However, this happens at a much later time scale characterized by $1/\Lambda$, where Λ is the scale in α_S, i.e. the scale at which the coupling becomes strong. The interactions which change quarks and gluons into hadrons certainly modify the outgoing state, but they occur too late to modify the original probability for the event to happen. It is this latter quantity which can therefore be calculated in perturbation theory.

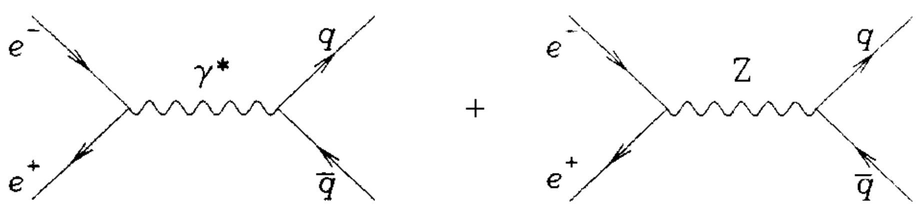

Figure 7: Feynman diagrams for the process $e^+e^- \to f\bar{f}$.

In lowest order, therefore, the total hadronic cross section is obtained by simply summing over all kinematically accessible flavours and colours of quark-antiquark pairs, $e^+e^- \to \sum q\bar{q}$. Real and virtual gluon corrections to this basic process will generate higher-order contributions to the perturbation series.. Since it is convenient to compare the hadronic cross section to that for $\mu^+\mu^-$, and to include the possibility of both photon and Z exchange, we begin by considering the general high-energy $2 \to 2$ process $e^+e^- \to f\bar{f}$, with f a light charged fermion, $f \neq e$. In lowest order, this is mediated by either a virtual photon or a Z in the s-channel, Fig. 7. With θ the centre-of-mass scattering angle of the final state fermion, the differential cross section is

$$\begin{aligned}\frac{d\sigma}{d\cos\theta} &= \frac{\pi\alpha^2}{2s}\Big[(1+\cos^2\theta)\Big\{Q_f^2 - 2Q_f v_e v_f \chi_1(s) + (a_e^2+v_e^2)(a_f^2+v_f^2)\chi_2(s)\Big\} \\ &\quad +4\cos\theta\Big\{2a_e v_e a_f v_f \chi_2(s) - Q_f a_e a_f \chi_1(s)\Big\}\Big]\,, \qquad (95)\end{aligned}$$

where

$$\begin{aligned} \chi_1(s) &= \kappa \frac{s(s-M_Z^2)}{(s-M_Z^2)^2+\Gamma_Z^2 M_Z^2} \\ \chi_2(s) &= \kappa^2 \frac{s^2}{(s-M_Z^2)^2+\Gamma_Z^2 M_Z^2} \\ \kappa &= \left(\frac{\sqrt{2}G_F M_Z^2}{4\pi\alpha}\right) \end{aligned} \tag{96}$$

Here G_F is the Fermi constant, α is the electromagnetic coupling, M_Z and Γ_Z are the mass and total decay width of the Z boson respectively. The vector and axial couplings of the fermions to the Z are

$$v_f = I_{3f} - 2Q_f \sin^2\theta_W, \quad a_f = I_{3f} \ , \tag{97}$$

with $I_{3f} = +\frac{1}{2}$ for $f = \nu,\ u,\ \ldots$ and $I_{3f} = -\frac{1}{2}$ for $f = e,\ d,\ \ldots$. The χ_2 term comes from the square of the Z-exchange amplitude and the χ_1 term from the photon-Z interference. At centre-of-mass scattering energies ($\sqrt{s}$) far below the Z peak, the ratio s/M_Z^2 is small and so $1 \gg \chi_1 \gg \chi_2$. This means that the weak effects — manifest in the terms involving the vector and axial couplings — are small and can be neglected. Eq. (95) then reduces to

$$\frac{d\sigma}{d\cos\theta} = \frac{\pi\alpha^2 Q_f^2}{2s}(1+\cos^2\theta). \tag{98}$$

Integrating over θ gives the total cross section,

$$\sigma_0 = \frac{4\pi\alpha^2}{3s}\, Q_f^2 \ . \tag{99}$$

On the Z pole, $\sqrt{s} = M_Z$, the χ_2 term in (95) dominates and the corresponding (peak) cross section is

$$\sigma_0 = \frac{128\pi\alpha^2\kappa^2}{3\Gamma_Z^2}(a_e^2+v_e^2)(a_f^2+v_f^2) \ . \tag{100}$$

We next introduce the ratio R of the the total e^+e^- hadronic cross section to the muon pair production cross section. As we have seen, the former is obtained at leading order simply by counting the possible $q\bar{q}$ final states. Thus, at energies far below the Z pole, we have

$$R = \frac{\sigma(e^+e^- \to \text{hadrons})}{\sigma(e^+e^- \to \mu^+\mu^-)} = \frac{\sum_q \sigma(e^+e^- \to q\bar{q})}{\sigma(e^+e^- \to \mu^+\mu^-)} = 3\sum_q Q_q^2 \ . \tag{101}$$

On the Z pole, the corresponding quantity is the ratio of the partial decay widths of the Z to hadrons and to muon pairs:

$$R_Z = \frac{\Gamma(Z \to \text{hadrons})}{\Gamma(Z \to \mu^+\mu^-)} = \frac{\sum_q \Gamma(Z \to q\bar{q})}{\Gamma(Z \to \mu^+\mu^-)} = \frac{3\sum_q (a_q^2+v_q^2)}{a_\mu^2+v_\mu^2} \ . \tag{102}$$

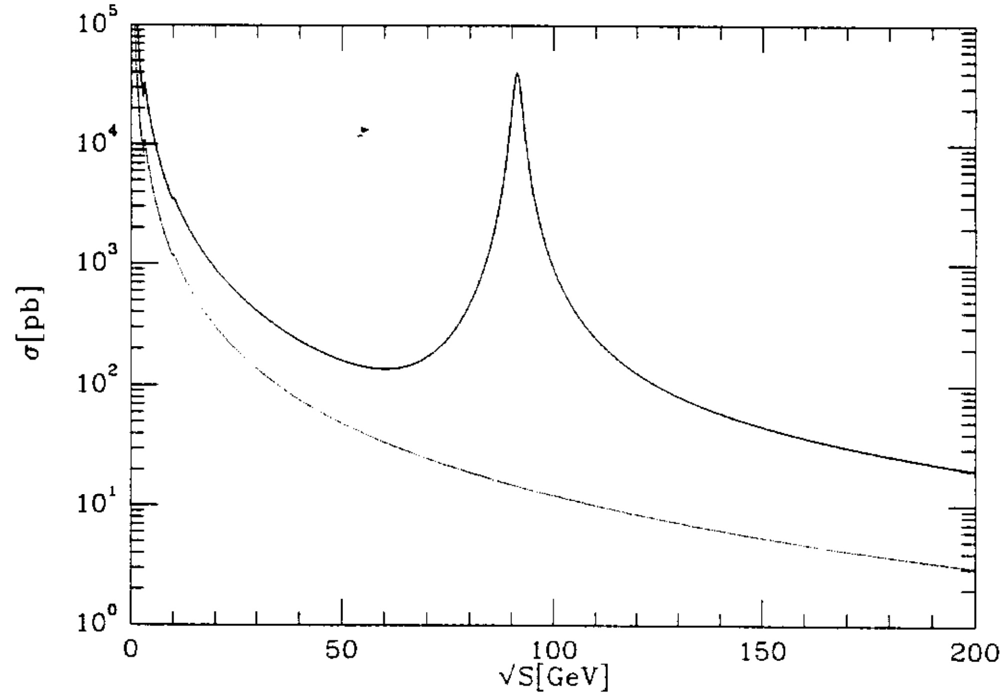

Figure 8: The total cross section as predicted by Eq. (95) and Eq. (99)

These results are valid for massless quarks.

With $q = u, \ldots, b$, Eq. (101) gives $R = 11/3 = 3.67$. From Fig. 2 one can see that at $\sqrt{s} = 34$ GeV the measured value is about 3.9. Even allowing for the Z contribution ($\Delta R_Z \simeq 0.05$ at this energy), the measurement is some 5% higher than the lowest-order prediction. As we shall see, the difference is due to higher-order QCD corrections, and in fact the comparison between theory and experiment gives one of the most precise determinations of the strong coupling constant.

The $O(\alpha_S)$ corrections to the total hadronic cross section are calculated from the real and virtual gluon diagrams shown in Fig. 9. For the former,

$$e^+(q_1) + e^-(q_2) \to q(p_1) + \bar{q}(p_2) + g(k) \tag{103}$$

Fig. 9(b), it is convenient to write the three-body phase space integration as

$$d\Phi_3 = \frac{s}{2^{10}\pi^5} d\alpha\, d\cos\beta\, d\gamma\, dx_1\, dx_2 \tag{104}$$

where α, β, γ are Euler angles, and $x_1 = 2E_q/\sqrt{s}$ and $x_2 = 2E_{\bar{q}}/\sqrt{s}$ are the energy fractions of the final state quark and antiquark. The matrix element is obtained using the Feynman rules.

$$\frac{1}{4}\sum_a \sum_{ij} \sum_{\lambda\lambda'} \mathcal{M} \;=\; 8e^4 Q_q^2 C_F g^2 \frac{[(q_1{\cdot}p_1)^2 + (q_2{\cdot}p_2)^2 + (q_1{\cdot}p_2)^2 + (q_2{\cdot}p_1)^2]}{p_1{\cdot}k\; p_2{\cdot}k\; q_1{\cdot}q_2} \tag{105}$$

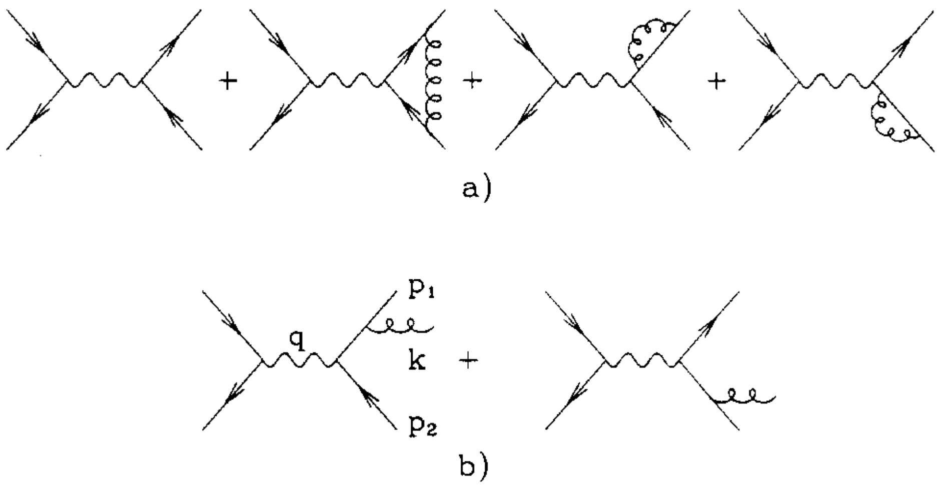

Figure 9: Feynman diagrams for the $O(\alpha_S)$ corrections to the total hadronic cross section in e^+e^- annihilation.

where the sums are over spins and colours. Integrating out the Euler angles gives a matrix element which depends only on x_1 and x_2, and the contribution to the total cross section is

$$\sigma^{q\bar{q}g} = \sigma_0 \, 3 \sum_q Q_q^2 \int dx_1 dx_2 \, \frac{C_F \alpha_S}{2\pi} \, \frac{x_1^2 + x_2^2}{(1-x_1)(1-x_2)} \tag{106}$$

where the integration region is: $0 \leq x_1, x_2 \leq 1$, $x_1 + x_2 \geq 1$. Unfortunately, we see that the integrals are divergent at $x_i = 1$. Since $1 - x_1 = x_2 E_g(1 - \cos\theta_{2g})/\sqrt{s}$ and $1 - x_2 = x_1 E_g(1 - \cos\theta_{1g})/\sqrt{s}$, where E_g is the gluon energy and θ_{ig} the angles between the gluon and the quarks, we see that the singularities come from regions of phase space where the gluon is *collinear* with the quark or antiquark, $\theta_{ig} \to 0$, or where the gluon is *soft*, $E_g \to 0$. These singularities are not of course physical; they simply indicate a breakdown of the perturbative approach. Quarks and gluons are never on-mass-shell particles, as this calculations assumes. When we encounter gluon energies and quark-gluon invariant masses which are of the same order as hadronic mass scales (~ 1 GeV or less) then we cannot ignore the effects of confinement. In the meantime, we can regard the singular behaviour on the boundaries of the phase-space plot at $x_i = 1$ as indicating physics beyond perturbation theory.

The key point is that we have not yet demonstrated that these 'dangerous' regions actually make an important contribution to the total cross section. The way to proceed is to introduce a temporary 'regularization procedure' for making the integrals finite, both for the real and virtual gluon diagrams, and then to see whether we can remove the regulator at the end of the calculation and obtain a finite result. Several methods are suitable. We can give the gluon a small mass, or take the final state quark and antiquark off-mass-shell by a small amount (which one might argue had some physical relevance). With either of these procedures, the singularities are avoided, being manifest instead as logarithms of the regulating mass scale.

A mathematically more elegant regularization procedure is to use dimensional regularization, with the number of space-time dimensions now $d > 4$. Here the method is being extended to *real* gluon emission in addition to loop diagrams. Going to d dimensions affects both the phase space and the traces of the Dirac matrices in the $q\bar{q}g$ cross section calculation. As a result, Eq. (106) becomes

$$\sigma^{q\bar{q}g}(\epsilon) = \sigma_0\, 3\sum_q Q_q^2\, H(\epsilon) \int dx_1 dx_2\, \frac{2\alpha_S}{3\pi}\, \frac{x_1^2 + x_2^2 - \epsilon(2 - x_1 - x_2)}{(1-x_1)^{1+\epsilon}(1-x_2)^{1+\epsilon}} \tag{107}$$

with $\epsilon = \frac{1}{2}(4-d)$, and

$$H(\epsilon) = \frac{3(1-\epsilon)^2}{(3-2\epsilon)\Gamma(2-2\epsilon)} = 1 + O(\epsilon)\,. \tag{108}$$

With the three-body phase space integrals recast in d dimensions, the soft and collinear singularities are regulated, appearing instead as *poles* at $d = 4$. Performing the integrals in Eq. (107) gives

$$\sigma^{q\bar{q}g}(\epsilon) = \sigma_0\, 3\sum_q Q_q^2\, \frac{C_F \alpha_S}{2\pi}\, H(\epsilon) \left[\frac{2}{\epsilon^2} + \frac{3}{\epsilon} + \frac{19}{2} + O(\epsilon)\right]. \tag{109}$$

The virtual gluon contribution can be calculated in a similar fashion, with dimensional regularization again used to control the infra-red divergences in the loops. The result is

$$\sigma^{q\bar{q}(g)}(\epsilon) = \sigma_0\, 3\sum_q Q_q^2\, \frac{C_F \alpha_S}{2\pi}\, H(\epsilon) \left[-\frac{2}{\epsilon^2} - \frac{3}{\epsilon} - 8 + O(\epsilon)\right]. \tag{110}$$

When the two contributions Eqs. (109) and (110) are added together, the poles exactly cancel and the result is *finite* in the limit $\epsilon \to 0$:

$$R = 3\sum_q Q_q^2 \left\{1 + \frac{\alpha_S}{\pi} + O(\alpha_S^2)\right\}. \tag{111}$$

Note that the next-to-leading order correction is positive, and with a value for α_S of about 0.15, can accommodate the experimental measurement at $\sqrt{s} = 34$ GeV. In contrast, the corresponding correction is negative for a scalar gluon.

The cancellation of the soft and collinear singularities between the real and virtual gluon diagrams is not accidental. Indeed, there are theorems — the Bloch, Nordsieck [23] and Kinoshita, Lee, Nauenberg [24] theorems — which state that suitably defined inclusive quantities will be free of singularities in the massless limit. The total hadronic cross section is an example of such a quantity, whereas the cross section for the exclusive $q\bar{q}$ final state, i.e. $\sigma(e^+e^- \to q\bar{q})$, is not.

In the above result, the coupling α_S is understood to be evaluated at a renormalization scale μ. Since the ultra-violet divergences in the loop diagrams in Fig. 9 cancel, the coefficient of the coupling is independent of μ at this order. At $O(\alpha_S^2)$ and higher, we encounter the ultra-violet divergences associated with the renormalization of the strong coupling. The coefficients are therefore renormalization scheme dependent, and we can write,

$$\begin{aligned} R &= K_{QCD}\, 3\sum_q Q_q^2, \\ K_{QCD} &= 1+\frac{\alpha_S(\mu^2)}{\pi}+\sum_{n\geq 2} C_n\left(\frac{s}{\mu^2}\right)\left(\frac{\alpha_S(\mu^2)}{\pi}\right)^n . \end{aligned} \tag{112}$$

The $O(\alpha_S^2)$ and $O(\alpha_S^3)$ corrections have been calculated. In the $\overline{\rm MS}$ scheme with the renormalization scale choice $\mu=\sqrt{s}$, the values are

$$\begin{aligned} C_2(1) &= \left(\frac{2}{3}\zeta(3)-\frac{11}{12}\right)n_f+\left(\frac{365}{24}-11\zeta(3)\right) \\ &\simeq 1.986-0.115 n_f \\ C_3(1) &= \left(\frac{87029}{288}-\frac{1103}{4}\zeta(3)+\frac{275}{6}\zeta(5)\right)-\frac{\pi^2}{48}\beta_0^2+\eta\left(\frac{55}{72}-\frac{5}{3}\zeta(3)\right) \\ &\quad -\left(\frac{7847}{216}-\frac{262}{9}\zeta(3)+\frac{25}{9}\zeta(5)\right)n_f+\left(\frac{151}{162}-\frac{19}{27}\zeta(3)\right)n_f^2 \\ &\simeq -6.637-1.200 n_f-0.005 n_f^2-1.240\eta, \end{aligned} \tag{113}$$

where $\eta=(\sum_q Q_q)^2/3\sum_q Q_q^2$ and and the sum extends over the (n_f) quarks which are effectively massless at the energy scale $\sqrt{s}$. The coefficient β_0 is given by Eq. (68). The expression for C_3 is taken from Ref. [25]. For massless quarks, the QCD corrections to the ratio R_Z of hadronic to leptonic Z decay widths are the same, except that η changes to [1]

$$\eta=\frac{(\sum_q v_q)^2}{3\sum_q(v_q^2+a_q^2)} . \tag{114}$$

The μ^2 dependence of the coefficients C_2, C_3 ... is fixed by the requirement that order-by-order, the series should be independent of the choice of scale:

$$\begin{aligned} C_2\left(\frac{s}{\mu^2}\right) &= C_2(1)-C_1(1)\frac{\beta_0}{4}\log\frac{s}{\mu^2} \\ C_3\left(\frac{s}{\mu^2}\right) &= C_3(1)+C_1(1)\left(\frac{\beta_0}{4}\right)^2\log^2\frac{s}{\mu^2}-\left(C_1(1)\frac{\beta_1}{16}+C_2(1)\frac{\beta_0}{2}\right)\log\frac{s}{\mu^2}\, , \end{aligned} \tag{115}$$

[1] This result assumes complete isodoublets of massless quarks.

where β_0 and β_1 are defined in Eq. (68).

The above result provides an explicit example of how the coefficients of any QCD perturbative expansion depend on the choice made for the renormalization scale μ, in such a way that as μ is varied, the change in the coefficients exactly compensates the change in the coupling $\alpha_S(\mu^2)$. However this μ-independence breaks down whenever the series is *truncated.* One can show by differentiating the above expression for K_{QCD} with respect to μ that the result is $O(\alpha_S^4)$. More generally, changing the scale in a physical quantity which has been calculated to $O(\alpha_S^n)$ induces changes which are $O(\alpha_S^{n+1})$. This is illustrated in Fig. 10, which shows K_{QCD} defined in Eq. (112) as a function of μ, as the higher order terms are added in. As expected, the more terms

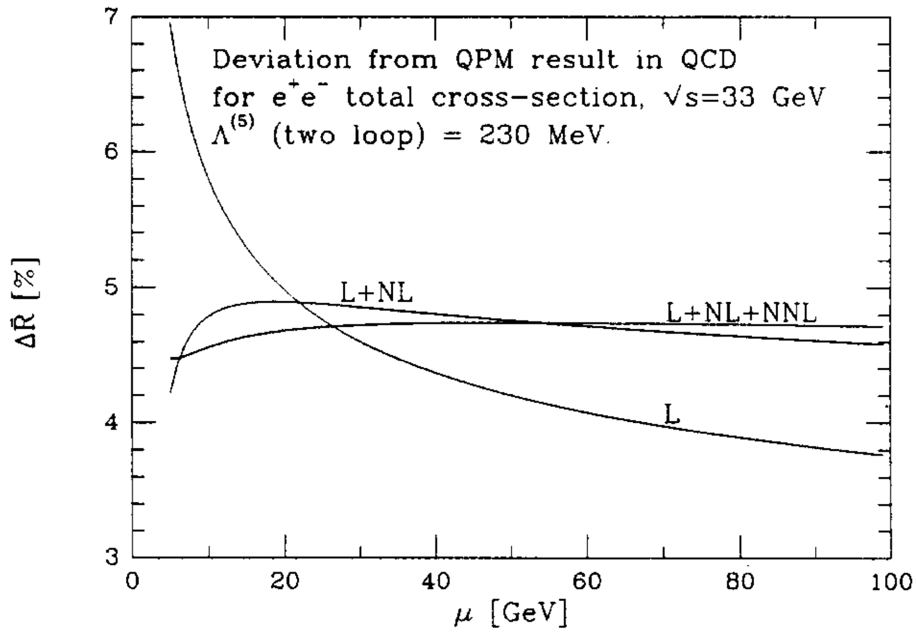

Figure 10: The effect of higher order QCD corrections to R, as a function of the renormalization scale μ.

are added, the more stable the prediction.

In the absence of higher-order corrections, one can try to guess the 'best' choice of scale (more generally, renormalization scheme), defined as the scale which makes the truncated and all-orders predictions equal.[2] In the literature, various particular choices have been advocated. Suppose that the perturbation series for R has been calculated to order α_S^n. In the *fastest apparent convergence* approach, one chooses the scale $\mu = \mu_{FAC}$, where

$$R^{(1)}(\mu_{\rm FAC}) = R^{(n)}(\mu_{\rm FAC}). \tag{116}$$

[2]We do not address here the meaning of an 'all-orders' summation of what is an asymptotic rather than a convergent series.

On the other hand, the *principle of minimal sensitivity* [26] imposes the known renormalization-scheme independence of the all-orders result on the truncated calculation. Within the $\overline{\text{MS}}$ renormalization prescription, this suggests a scale choice $\mu = \mu_{\text{PMS}}$, where

$$\mu \frac{d}{d\mu} R^{(n)}(\mu) \bigg|_{\mu_{\text{PMS}}} = 0 \,. \tag{117}$$

A third approach [27] argues that the n_f dependent terms in the coefficients indicate which parts should be associated with the the QCD β function, and that the appropriate scale is the one which absorbs all these terms into α_S. To $O(\alpha_S^2)$, it is straightforward to calculate these three special scales from Eq. (115):

$$\begin{aligned}
\mu_{\text{FAC}} &= \sqrt{s} \exp\left(-\frac{2C_2(1)}{\beta_0}\right) \simeq 0.692\,\sqrt{s}\,, \\
\mu_{\text{PMS}} &= \sqrt{s} \exp\left(-\frac{\beta_1 + 8\beta_0 C_2(1)}{4\beta_0^2}\right) \simeq 0.587\,\sqrt{s}\,, \\
\mu_{\text{BLM}} &= \sqrt{s} \exp\left(2\zeta(3) - \frac{11}{4}\right) \simeq 0.708\,\sqrt{s}\,,
\end{aligned} \tag{118}$$

where $C_2(1)$ is given in Eq. (113) and five massless flavours have been assumed. In the present context, these three scales are numerically rather close (the first two can be identified directly in Fig. 10), indicating that the scale dependence of R is rather weak, and that the α_S value obtained from fitting the above expressions to the e^+e^- total cross section or the Z hadronic decay width should be reliable. It is, however, important to remember that there are no theorems that *prove* that any of the above scale-fixing schemes are correct. All one can say is that the theoretical error on a quantity calculated to $O(\alpha_S^n)$ is always $O(\alpha_S^{n+1})$. Fixing a special scale does *not* remove this theoretical error on the prediction. One can vary the scale over some 'physically reasonable range' (for example, the range of momentum scales flowing through the Feynman diagrams) to try to quantify this uncertainty, but ultimately there is no substitute for actually performing the higher-order calculations.

1.10 Jet cross sections

The expression given for the total hadronic cross section in the previous section is very concise, but it tells us nothing about the kinematic *distribution* of hadrons in the final state. If the hadronic fragments of a fast moving quark have limited transverse momentum relative to the quark momentum (collinear fragmentation), then the lowest order contribution to the cross section — $e^+e^- \to q\bar{q}$ — can naively be interpreted as the production of two back-to-back jets. Experimentally, it *does* appear to be true that most events are 'two-jet-like', with a smaller fraction containing three jets, an even smaller fraction containing four jets, and so in. At first sight, this seems consistent with our intuition that each jet after the first two should correspond to the emission of a gluon off the quark lines, each emission 'costing' a power of $\alpha_S \ll 1$. However, this simple picture, although essentially correct, masks a much more complicated situation, which involves both perturbative and non-perturbative aspects of the theory. We will now attempt to construct a theory of jets based on the lowest orders in perturbation theory.

We begin by considering the next-to-leading process $e^+e^- \rightarrow q\bar{q}g$. From the previous section (Eq. (106)), we have

$$\frac{1}{\sigma}\frac{d^2\sigma}{dx_1 dx_2} = C_F \frac{\alpha_S}{2\pi}\frac{x_1^2 + x_2^2}{(1-x_1)(1-x_2)}\,. \tag{119}$$

Recall that this cross section becomes (infinitely) large when one or both of the x_i approach 1, which corresponds to the gluon being collinear with one of the quarks, or soft (i.e. its energy is small compared to $\sqrt{s}$) respectively. If we again assume that quarks and gluons fragment collinearly into hadrons, then this preference for the gluon to be soft or collinear means that the two-jet-like structure of the lowest order is maintained at $O(\alpha_S)$. If, on the other hand, the gluon is *required* to be well-separated in phase space from the quarks — a configuration corresponding to a 'three-jet event' — then the singular regions of the matrix element are avoided and the cross section is suppressed relative to lowest order by one power of α_S. In fact, this qualitative result holds to *all* orders of perturbation theory. The amplitudes for multiple gluon emission contain the same type of singularities as those which appear at first order, which leads to a final state which is predominantly 'two-jet-like', with a smaller probability (determined by α_S) for three or more distinguishable jets.

To make all this more quantitative, we need to introduce the concept of a *jet measure*, i.e. a procedure for classifying a final state of hadrons (experimentally) or quarks and gluons (theoretically) according to the number of jets it contains. To be useful, a jet measure should give cross sections which, like the total cross section, are free of soft and collinear singularities when calculated in perturbation theory, and should also be relatively insensitive to the non-perturbative fragmentation of quarks and gluons into hadrons.

One of the first attempts to define jet cross sections in perturbation theory was by Sterman and Weinberg [29]. In their picture, a final state is classified as two-jet-like if all but a fraction ϵ of the total available energy is contained in a pair of cones of half-angle δ. The two-jet cross section is then obtained by integrating the matrix elements for the various quark and gluon final states over the appropriate region of phase space determined by ϵ and δ. At lowest order, the two-jet and total cross sections obviously coincide, for any values of the parameters. At $O(\alpha_S)$, the two-jet cross section is obtained by integrating the right-hand-side of Eq. (119) over the appropriate range of x_1 and x_2. Fig. 11 shows the boundaries (solid lines) for the specific choice of parameters $\epsilon = 0.3$ and $\delta = 30°$. The two-jet region is the narrow band between these boundaries and the edges of the triangle. Note that the δ constraint corresponds to the curved portions of the boundary, while the ϵ constraint gives the straight line segments at the corners.

Rather than calculating the two-jet cross section directly, integrating the $q\bar{q}g$ matrix element (in d dimensions) over this region and adding the contribution from the virtual gluon diagrams, it is easier to use the fact that at this order $\sigma = \sigma_2 + \sigma_3$. The two-jet cross section can therefore be obtained by subtracting the three-jet cross section from the total cross section already obtained in Section 1.9. The advantage of this is that the calculation of σ_3 can be performed in 4 dimensions, since the matrix element singularities are outside the three-jet region at this order. Defining the two- and three-jet fractions[3] by $f_i = \sigma_i/\sigma$ ($i = 2, 3$) we obtain[4]

$$\begin{aligned} f_2 &= 1 - 8C_F\frac{\alpha_S}{2\pi}\left\{\log\frac{1}{\delta}\left[\log\left(\frac{1}{2\epsilon}-1\right)-\frac{3}{4}+3\epsilon\right]\right. \\ &\qquad \left. +\frac{\pi^2}{12}-\frac{7}{16}-\epsilon+\frac{3}{2}\epsilon^2+O(\delta^2\log\epsilon)\right\} , \\ f_3 &= 1 - f_2 . \end{aligned} \tag{120}$$

Notice that when the parameters ϵ and δ are small, the $O(\alpha_S)$ correction becomes logarithmically large. This is simply the vestige of the soft and collinear singularities. There are techniques for resumming terms involving $\alpha_S \log\delta$ to all orders in perturbation theory; when δ is small this should improve on the first order result. On the other hand, as the parameters become large, the three-jet region in Fig. 11 shrinks and the three-jet fraction decreases, as expected.

At higher orders in perturbation theory, we can have events with more than three jets. For example, the $O(\alpha_S^2)$ $q\bar{q}q\bar{q}$ and $q\bar{q}gg$ production processes can give rise to two, three or four jet events, depending on the separation in phase space and energy of the outgoing partons. It turns out that from an experimental and theoretical point of view, the Sterman-Weinberg jet definition based on cones is not well-suited to analysing multijet final states. One of the reasons is that fixed-angle cones give an inefficient 'tiling' of the phase-space 4π solid angle. For this reason, various alternatives have been proposed, the most important of which is the 'minimum invariant mass' or JADE algorithm [30], which we shall now describe.

Consider $q\bar{q}g$ production at $O(\alpha_S)$. A three-jet event is defined as one in which the minimum invariant mass of the parton pairs is larger than some fixed fraction y (sometimes called $y_{\rm cut}$) of the overall centre-of-mass energy:

$$\min\,(p_i+p_j)^2 = \min\,2E_iE_j(1-\cos\theta_{ij}) > ys, \qquad i,j = q,\bar{q},g\ , \tag{121}$$

for massless partons in the e^+e^- centre-of-mass frame. It is easily shown that this region of phase space avoids the soft and collinear singularities of the matrix element. In fact in terms of the energy fractions, Eq. (121) is equivalent to

$$0 < x_1, x_2 < 1 - y, \qquad x_1 + x_2 > 1 + y. \tag{122}$$

[3] The notation R_i is also used for jet fractions in the literature.

[4] We show here only those terms which are important when δ is small. The full expression is rather unwieldy.

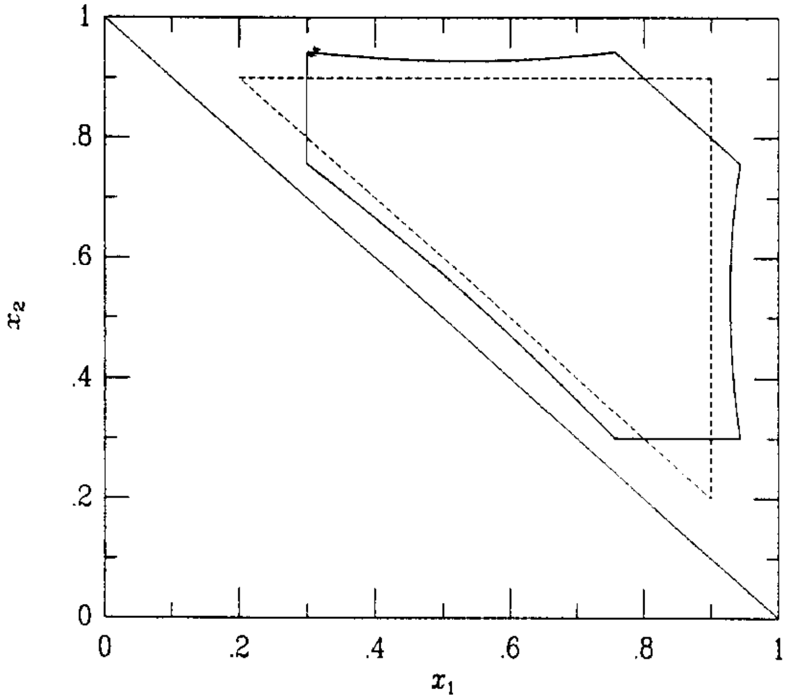

Figure 11: Boundaries between the two- and three-jet regions in the (x_1, x_2) plane for (a) Sterman-Weinberg jets with $(\epsilon, \delta) = (0.3, 30°)$ (solid lines), and (b) JADE algorithm jets with $y = 0.1$ (dashed lines).

The corresponding boundary (for $y = 0.1$) is shown by the dashed lines in Fig. 11. As for the Sterman-Weinberg jets, the two- and three-jet fractions to $O(\alpha_S)$ are obtained by integrating the right-hand side of Eq. (106) over the appropriate region:

$$\begin{aligned} f_3 &= C_F\frac{\alpha_S}{2\pi}\left[(3-6y)\log\left(\frac{y}{1-2y}\right)+2\log^2\left(\frac{y}{1-y}\right)\right. \\ &\left. +\frac{5}{2}-6y-\frac{9}{2}y^2+4\,\mathrm{Li}_2\left(\frac{y}{1-y}\right)-\frac{\pi^2}{3}\right], \\ f_2 &= 1-f_3\,, \end{aligned} \tag{123}$$

where Li_2 is the dilogarithm function,

$$\mathrm{Li}_2(x) = -\int_0^x dy\frac{\log y}{1-y}\,. \tag{124}$$

Eq. (123) is valid for $y < \frac{1}{3}$. Fig. 12 shows the two and three jet ratios from Eq. 123 for $\alpha_S = 0.118$. The soft and collinear singularities again reappear as large logarithms in the limit $y \to 0$. Clearly the result in Eq. (123) only makes sense for y values large enough such that $f_2 \gg f_3$, so that the $O(\alpha_S)$ correction to f_2 is perturbatively small.

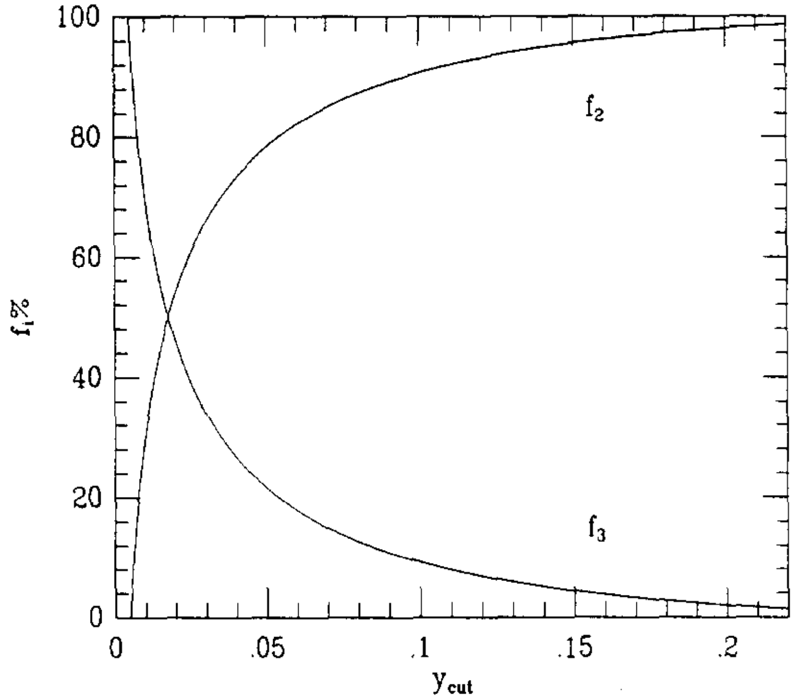

Figure 12: The values of f_3 and f_2 from Eq. (123)

The generalization to multi-jet fractions is straightforward, using the following algorithm. Starting from an n-parton final state, identify the pair with the minimum invariant mass squared. If this is greater then ys then the number of jets is n. If not, combine the minimum pair into a single 'cluster'. Then repeat for the $(n-1)$-parton/cluster final state, and so on until all partons/clusters have a relative invariant mass squared greater than ys. The number of clusters remaining is then the number of jets in the final state. According to this definition, an n-parton final state can give any number of jets between n (all partons well-separated) and 2 (for example, two hard quarks accompanied by soft and collinear gluons).

Since a soft or collinear gluon emitted from a quark line does not change the multiplicity of jets, the cancellation of the corresponding singularities that was evident in the total cross section calculation can still take place, and the jet fractions defined this way are 'infra-red safe', i.e. free of such singularities to all orders in perturbation theory. We shall discuss other examples of infra-red safe jet variables below.

Now in general we have[5]

$$f_{n+2}(\sqrt{s},y) \;=\; \left(\frac{\alpha_S(\mu^2)}{2\pi}\right)^n \sum_{j=0}^{\infty} C_{nj}\left(y,\frac{s}{\mu^2}\right)\left(\frac{\alpha_S(\mu^2)}{2\pi}\right)^j, \quad n \geq 0,$$

[5]We follow the convention in the literature to expand the perturbation series for the total cross section and jet cross sections in powers of (α_S/π) and $(\alpha_S/2\pi)$ respectively.

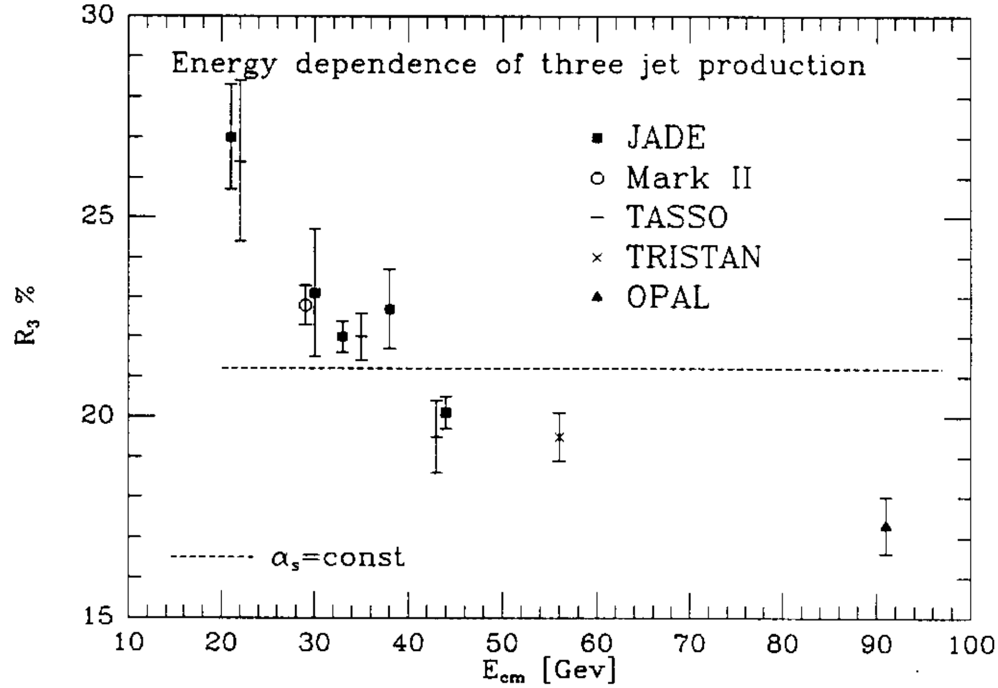

Figure 13: A compilation of three-jet fractions at different e^+e^- annihilation energies, from the OPAL collaboration[33]

$$\sum_{n=2}^{\infty} f_n = 1 . \tag{125}$$

We have assumed here some particular renormalization prescription ($\overline{\text{MS}}$ is almost always used in practice) and introduced μ as the renormalization scale. Since the jet parameter y is dimensionless, with the choice $\mu = \sqrt{s}$ all the energy dependence of the jet fractions is contained in the coupling $\alpha_S(s)$. One can therefore exhibit, at least in principle, the *running* of the strong coupling by measuring, for example, a decrease in f_3 as $\sqrt{s}$ increases, see Fig. 13.

In experiments, the JADE algorithm is applied to final state *hadrons* rather than *partons*.[6] However studies using hadronization models to describe the transition from partons to hadrons have shown that — at least at high energy — the hadronization corrections are small and therefore the QCD parton-level predictions can be reliably compared with the experimental data.

The next-to-leading order corrections to f_3 have been calculated [31]. Because the hadronization corrections to f_3 are small, the three-jet rate provides one of the most precise measurements of α_S at e^+e^- colliders. A typical fit is shown in Fig. 14 [33].

[6]There are in fact several slight variants of the JADE algorithm which are used in practice, see Ref. [32].

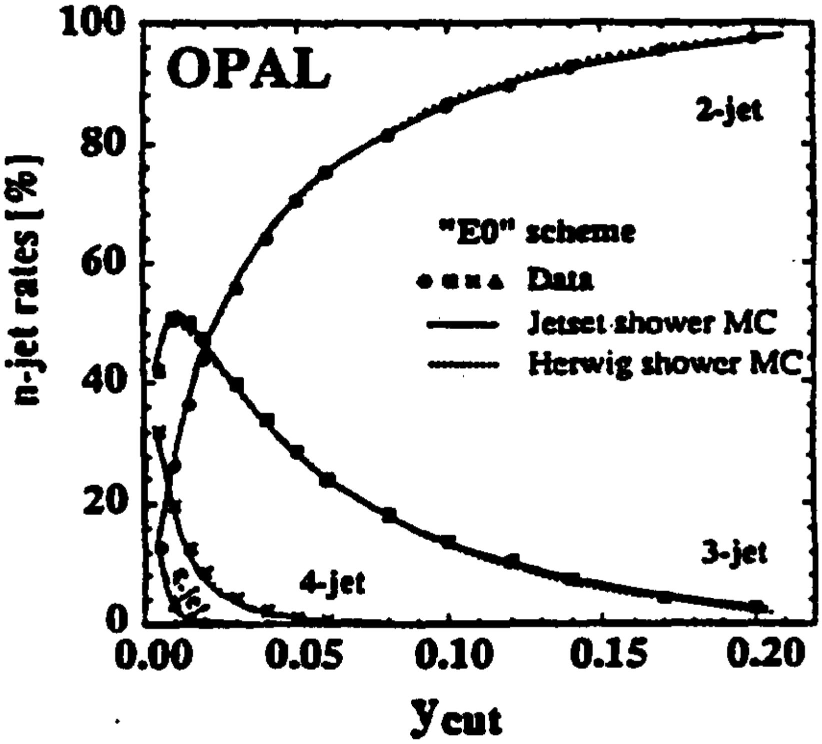

Figure 14: QCD fits to the jet rates at LEP, as measured by the OPAL collaboration.

The curves correspond to the perturbative predictions calculated in the $\overline{\mathrm{MS}}$ prescription with two different choices of scale. At large y, the events are mostly classified as two (broad) jets. As y decreases, and the jets are allowed to be narrower, fewer events are two-jet and the number of multijet events increases. Notice that at medium and large y, where these calculations should be most reliable, both scale choices give equally acceptable fits, *but with different values of* $\Lambda_{\overline{\mathrm{MS}}}$. This is an example of the scale-dependence uncertainty discussed above. At smaller y, there appears to be some preference for the curve corresponding to the smaller scale. However, some care must be taken with this interpretation. We have already seen (Eq. (123) that when y is so small that $\alpha_S \log^2 y \sim 1$, the perturbation series for f_2 breaks down. In fact one can show that all the jet fractions have higher-order corrections which contain terms like $\alpha_S^n \log^{2n} y$ at small y. Before concluding anything about which renormalization scales are preferred, we should make sure that these large corrections are correctly taken into account.

References

1) QCD, 20 year later, World Scientific (1993), (eds. P.M. Zerwas and H.A. Kastrup)

2) George Sterman, Proceedings of 1991 TASI in Elementary Particle Physics, (eds. R.K. Ellis,

C.T. Hill, J.D. Lykken).

3) R.K. Ellis, Proceedings of 1987 TASI in Elementary Particle Physics, (eds. R. Slansky and G. West).

4) A. H. Mueller, Proceedings of 1985 TASI in Elementary Particle Physics, (eds. M.J. Bowick and F. Gürsey).

5) J.D. Bjorken and S.D. Drell, 'Relativistic Quantum Fields', McGraw Hill, New York (1964).

6) G. Sterman, 'Quantum Field Theory', Cambridge University Press, Cambridge (1993).

7) C. Itzykson and J.B. Zuber, 'Quantum Field Theory', McGraw Hill, New York (1980).

8) F. Yndurain, 'Quantum Chromodynamics', Springer-Verlag (1983).

9) T. Muta, 'Foundations of Quantum Chromodynamics', World Scientific (1987).

10) G. Altarelli, *Phys. Rep.* **81** (1982) 1.

11) A.H. Mueller, *Phys. Rep.* **73** (1981) 237.

12) D.W. Duke and R.G. Roberts, *Phys. Rep.* **120** (1985) 275.

13) E. Abers and B.W. Lee, *Phys. Rep.* **9** (1973) 1.

14) L. Faddeev and V.N. Popov, *Phys. Lett.* **258** (1977) 377.

15) G. t'Hooft and M.J.G. Veltman, Diagrammar, CERN Yellow Report 73-9, published in the proceedings of the summer school, 'Particle Interactions At Very High Energies, Part B', Louvain (1973).

16) V.N. Gribov, Lectures at the 12th Winter School of the Leningrad Nuclear Physics Institute, SLAC-TRANS-176 (1977);
S. D. Drell, in a 'Festschrift for Maurice Goldhaber', Trans. NY Acad. Sci., Series II, **40**, 76 (1980).

17) N.K. Nielsen, *Am. J. Phys.* **49** (1981) 1171;
R.J. Hughes, *Phys. Lett.* **97B** (1980) 246; *Nucl. Phys.* **B186** (1981) 376;
K. Johnson, in Asymptotic Realms of Physics, edited by A. Guth, K. Huang and R. L. Jaffe, MIT press, Cambridge, Mass., (1983).

18) R. E. Peierls, 'Quantum Theory of Solids', Oxford, 1955.

19) J.C. Collins, 'Renormalization', Cambridge University Press, Cambridge, (1984).

20) G. Passarino and M.J.G. Veltman, *Nucl. Phys.* **B161** (1979) 151.

21) G. t'Hooft and M.J.G. Veltman, *Nucl. Phys.* **B44** (1972) 189;
G.G. Bollini and J.J. Giambiagi, *Nuovo Cimento* **12B** (1972) 20;
W.J. Marciano, *Phys. Rev.* **D12** (1975) 3861.

22) M. Gell-Mann, in 'QCD, 20 year later', P.M. Zerwas and H. A. Kastrup, (Eds.), World Scientific (1993).

23) F. Bloch and A. Nordsieck, *Phys. Rev.* **52** (1937) 54.

24) T. Kinoshita, *J. Math. Phys.* **3** (1962) 650 ;
T.D. Lee and M. Nauenberg, *Phys. Rev.* **133B** (1964) 1549.

25) M.A. Samuel and L.R. Surguladze, *Phys. Rev. Lett.* **66** (1991) 560.
S.G. Gorishny, A.L. Kataev and S.A Larin, *Phys. Lett.* **B259** (1991) 144.

26) P.M. Stevenson, *Nucl. Phys.* **B150** (1979) 357.

27) S.J. Brodsky, G.P. Lepage and P.B. MacKenzie *Phys. Rev.* **D28** (1983) 228.

28) B.A. Kniehl and J.H. Kuhn, *Nucl. Phys.* **B329** (1990) 547.

29) G. Sterman and S. Weinberg, *Phys. Rev. Lett.* **39** (1977) 1436.

30) JADE collaboration: S. Bethke *et al.*, *Phys. Lett.* **B213** (1988) 235.

31) G. Kramer and B. Lampe, *Fortschr. Phys.* **37** (1989) 161.

32) S. Bethke, Z. Kunszt, D.E. Soper and W.J. Stirling, *Nucl. Phys.* **B370** (1992) 310.

33) OPAL collaboration: *Zeit. Phys.* **C49** (1991) 375.

2 QCD and the parton model

In this lecture we will discuss the parton model and its generalization in QCD. The parton model was originally formulated in the infinite momentum frame using time ordered perturbation theory. We begin with a brief introduction to old-fashioned perturbation theory.

2.1 Time ordered perturbation theory

The Feynman rules for a quantum field theory yield a perturbation series in which Lorentz covariance is preserved at every step of the calculation. The benefits of this approach in streamlining practical calculations are apparent. However this simplification is achieved by sacrificing manifest unitarity, since intermediate states containing different numbers of particles are represented by a single covariant diagram. For this reason there is a continuing interest in the precursor to Lorentz invariant field theory, which goes by the name of old-fashioned or time-ordered perturbation theory. One can recover time-ordered perturbation theory from the covariant formulation by integrating over the energies of the internal lines. The purpose of this section is to illustrate the relationship between the two approaches.

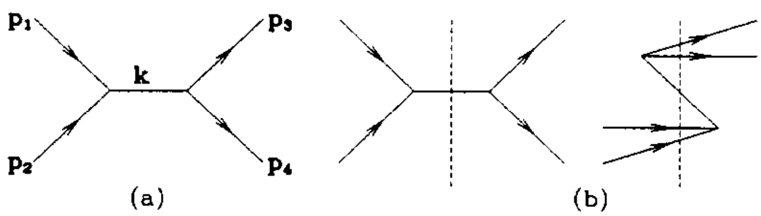

Figure 15: a) Scattering in scalar field theory. b) Representation as pair of time-ordered diagrams

Consider a simple scattering in a scalar field theory which, in the Born approximation, is due to the exchange in the s-channel of a particle of mass m. The appropriate Feynman diagram is shown in Fig. 15a. The contribution to the S-matrix of the covariant amplitude shown in Fig. 15a is given by

$$S = -i(2\pi)^4\delta^3(\mathbf{p}_1 + \mathbf{p}_2 - \mathbf{p}_3 - \mathbf{p}_4)A \tag{126}$$

$$A = \delta(\omega_1 + \omega_2 - \omega_3 - \omega_4)\left[\frac{1}{k^2 - m^2 + i\epsilon}\right] \tag{127}$$

where ω_i is the energy of the state with 3-momentum $\mathbf{p}$.

$$\omega_i = \sqrt{\mathbf{p}_i^2 + m^2},\ \omega_k = \sqrt{\mathbf{k} + m^2},\ \mathbf{k} = \mathbf{p}_1 + \mathbf{p}_2 \tag{128}$$

The 3-momenta of the various lines are indicated by bold-face symbols. The Dirac delta function expressing the conservation of 3-momentum can be ignored because it plays no role in the following discussion. Introducing the integration variable k_0 the amplitude may be re-written as,

$$A = \int_{-\infty}^{\infty} dk_0 \delta(\omega_1 + \omega_2 - k_0)\delta(k_0 - \omega_3 + \omega_4)\frac{1}{k_0^2 - \omega_k^2 + i\epsilon} \tag{129}$$

We now use an exponential representation of the Dirac delta functions to re-write Eq. (129) as

$$\begin{aligned} A &= \frac{1}{(2\pi)^2}\int dt \int dt' \int dk_0 \frac{\exp[-i(\omega_1+\omega_2-k_0)t]\exp[-i(k_0-\omega_3-\omega_4)t']}{k_0^2-\omega_k^2+i\epsilon} \\ &= \frac{1}{(2\pi)^2}\int dt \int dt' \int dk_0 \exp[-i(\omega_1+\omega_2-k_0)t]\exp[-i(k_0-\omega_3-\omega_4)t'] \\ &\quad \times\frac{1}{2\omega_k}\Big[\frac{1}{k_0-\omega_k+i\epsilon}-\frac{1}{k_0+\omega_k-i\epsilon}\Big] \end{aligned} \tag{130}$$

where the integrals over t, t' and k_0 run from $-\infty$ to ∞. The variables t and t' are the times at which the two interactions occur. We now perform the k_0 integral using Cauchy's theorem (closing the contour in the lower half plane for $t - t' < 0$ and in the upper half plane for $t - t' > 0$). The result for A is,

$$\begin{aligned} A = &\frac{-i}{2\pi}\int_{-\infty}^{\infty} dt \int_{-\infty}^{\infty} dt' \,\frac{1}{2\omega_k} \\ &\Big[\theta(t'-t)\exp[-i(\omega_1+\omega_2-\omega_k+i\epsilon)t]\exp[-i(\omega_k-\omega_3-\omega_4-i\epsilon)t'] \\ &+\theta(t-t')\exp[-i(\omega_1+\omega_2+\omega_k-i\epsilon)t]\exp[i(\omega_k+\omega_3+\omega_4-i\epsilon)t']\Big] \end{aligned} \tag{131}$$

The integrals over the times are easily performed to give,

$$A = \delta(\omega_1+\omega_2-\omega_3-\omega_4)\frac{1}{2\omega_k}\Big[\frac{1}{\omega_1+\omega_2-\omega_k+i\epsilon}+\frac{1}{-\omega_1-\omega_2-\omega_k+i\epsilon}\Big] \tag{132}$$

The two terms correspond to the two temporal orderings of the interactions shown in Fig. 15b. Thus we see that one covariant diagram is equal two (time-ordered) old-fashioned perturbation theory diagrams. The denominators are of the energy deficit type, expressing the energy difference between the initial state and the intermediate state and are familiar from non-relativistic quantum mechanics. It is self-evident that

Eq. (132) is equivalent to Eq. (127). The route which we have followed for our simple example illustrates the role of the time-ordering. Our procedure for this simple graph is an example of a more general result. One can recover time-ordered perturbation theory from covariant perturbation theory by performing the energy integrals.

The procedure generalizes to more complicated graphs. Thus for any Green's function the sum over covariant Feynman graphs is equivalent to a sum over a (larger) number of time ordered graphs. We may formulate a series of rules to generate the S-matrix for any transition using time-ordered perturbation theory[1]. This procedure is entirely analogous to the normal prodedure for covariant Feynman diagrams. We want to construct the S-matrix for a transition $\alpha \to \beta$.

$$S_{\beta\alpha} = \delta_{\beta\alpha} - i(2\pi)^4 M_{\beta\alpha}\delta^4(P_\beta - P_\alpha) \tag{133}$$

where $P_\alpha(P_\beta)$ is the 4-momentum of the initial (final) state. The rules for a scalar theory are as follows[1],

1. Draw all possible time-ordered diagrams for the transition in question. In nth order perturbation theory one will need to draw every Feynman diagram $n!$ times corresponding to the $n!$ different time orderings of the vertices. Label each line with a three dimensional momentum $\mathbf{k}_i$.

2. For each internal line include a factor $(2\pi)^{-3}(2\omega_{k_i})^{-1}$ where

$$\omega_{k_i} = \sqrt{\mathbf{k}_i^2 + m^2} \tag{134}$$

3. For every vertex (except the last) include a factor

$$(2\pi)^3\delta^3(\sum \mathbf{k}_i) \tag{135}$$

   to express the conservation of three momentum at every vertex. Energy-momentum conservation for the whole process, Eq. (133), ensures three momentum conservation at the last vertex.

4. For each intermediate state γ include an energy denominator.

$$\frac{1}{E_\alpha - E_\gamma + i\epsilon} \tag{136}$$

   where $E_\gamma = \sum \omega$ is the total energy of the intermediate state and E_α is the total energy of the initial state.

5. Integrate the product of these factors over the internal momenta and sum over all diagrams.

2.1.1 The infinite momentum frame

In our simple example, shown in Fig. 15b, the two diagrams are not separately Lorentz invariant, but their sum is. Since the diagrams are not separately Lorentz invariant it suggests that there might be a reference frame in which the diagrams are particularly simple. The infinite momentum frame is an example of such a frame.

Let us evaluate an arbitrary time-ordered diagram in a frame in which the total momentum is very large in the z direction and equal in magnitude to P. In this frame the momentum of the ith particle can be written

$$\mathbf{p}_i = x_i \mathbf{P} + \mathbf{t}_i \tag{137}$$

where the vectors $\mathbf{t}_i$ are transverse to the large momentum $\mathbf{P}$

$$\mathbf{t}_i \cdot \mathbf{P} = 0 \tag{138}$$

and subject to the constraints

$$\sum_i \mathbf{t}_i = 0, \ \sum_i x_i = 1. \tag{139}$$

We shall show that in the limit $P \to \infty$ the diagrams either have a finite limit or vanish. In order to distinguish the two classes of diagrams we will begin by evaluating the energy denominators. The energies of the individual particles are given by,

$$\begin{aligned} \omega_{k_i} &= \sqrt{\mathbf{p}_i + m^2} = \sqrt{x_i^2 P^2 + \mathbf{t}_i^2 + m^2} \\ &\approx |x_i| P + \frac{\mathbf{t}_i^2 + m^2}{2|x_i| P} + O\left(\frac{1}{P^2}\right) \end{aligned} \tag{140}$$

The total energy of the intermediate state is given by,

$$E_\gamma = \lambda P + \frac{1}{2P} \sum_i \frac{\mathbf{t}_i^2 + m^2}{|x_i|} + O\left(\frac{1}{P^2}\right) \tag{141}$$

where

$$\lambda = \sum_i |x_i| \tag{142}$$

Thus we may write

$$E_\gamma = \lambda P + \frac{s_\gamma}{2\lambda P} \tag{143}$$

$$s_\gamma = \lambda \sum_i \frac{\mathbf{t}_i^2 + m^2}{|x_i|} \tag{144}$$

If all of the x_i are positive then using Eq. (139) we find that $\lambda = 1$ and energy denominator becomes

$$\frac{1}{E_\alpha - E_\gamma + i\epsilon} = \frac{2P}{s_\alpha - s_\gamma + i\epsilon} \tag{145}$$

If on the other hand some of the momentum fractions are negative, the cancellation of the leading term no longer occurs and we find that the contribution is a factor of P^2 smaller.

$$\frac{1}{E_\gamma - E_\alpha} = \frac{1}{P(1-\lambda_\gamma)} \tag{146}$$

Let us consider an Nth order diagram with $N-1$ intermediate states in which all the x_i's are positive. In addition to the $N-1$ energy denominator factors of order P as shown in Eq. (145), we will have $(N-1)$ delta functions expressing the conservation of momentum in the z direction, each of which scales as $1/P$. All other factors are independent of P and the net result for this class of diagrams is finite in the limit $P \to \infty$. Diagrams involving internal or external particles with negative x_i's are zero in this frame, because of the large energy denominators, Eq. (146)

We have shown that in the IMF that any diagram involving intermediate states with particles travelling backward in time are zero. It is this fact which makes the infinite momentum frame an attractive frame in which to formulate the wave function of a hadron. Our treatment has been valid for a scalar theory. For applications of the IMF technique in gauge theories we refer the reader to ref. [2].

2.2 The naive parton model

The naive parton model[3] pre-dates the invention of QCD. It has a special status as a model, because much of the motivation for the model came from field theory but with additional assumptions added from the phenomenonology of hadronic interactions. Later in this lecture we will consider the full QCD description of inelastic interactions. With slight modifications, much of the structure of the naive parton model will survive.

The basic assumption of the naive parton model is that the interactions of hadrons are due to the interactions of partons; in certain types of reactions the structure of the hadrons may be described by an instantaneous distribution of partons present at any time. A necessary condition for such a picture to make sense is that changes in the number and momenta of the partons should be negligible during the time which they are probed. An analogy with diffraction studies of a crystal may be useful here. An X-ray diffracted off a crystal reveals the detailed structure of the crystal, because the atoms in the crystal lattice can be considered to be at rest during the transit time of the X-ray across the crystal. In hadronic systems we ensure that the transit time across the target is less than the interaction time by moving to an infinite momentum frame.

Let us now examine deep inelastic scattering in a frame in which the proton is moving very fast. In this frame the 4-momentum of the target and the incident virtual photon may be written as

$$p = (P + \frac{m^2}{2P}, \vec{0}, P)$$

$$q = (q_0, \vec{q}_T, 0) \tag{147}$$

In this frame the constituents of the proton will have a wave function. Consider the amplitude that a constituent with 3-momentum $(\vec{k}_0, x_0)$ decay into a state of two partons with 3-momenta $(\vec{k}_1, x_1)$ and $(\vec{k}_2, x_2)$. The momenta $\vec{k}_i$ are transverse to the large momentum P. The amplitude for this process to occur in time ordered perturbation theory will contain an energy denominator

$$\frac{1}{\Delta E} = \frac{1}{E_0 - E_1 - E_2} \tag{148}$$

where

$$\begin{aligned} \Delta E &= \sqrt{x_0^2 P^2 + \vec{k}_0^2} - \sqrt{x_1^2 P^2 + \vec{k}_1^2} - \sqrt{x_2^2 P^2 + \vec{k}_2^2} \\ \lim_{P \to \infty} & \frac{1}{2P}\left[\frac{\vec{k}_0^2}{x_0} - \frac{\vec{k}_1^2}{x_1} - \frac{\vec{k}_2^2}{x_2}\right] \end{aligned} \tag{149}$$

The lifetime of the fluctuation is $\Delta T = 1/\Delta E$.

$$\Delta T = 2P\left[\frac{\vec{k}_0^2}{x_0} - \frac{\vec{k}_1^2}{x_1} - \frac{\vec{k}_2^2}{x_2}\right]^{-1} \tag{150}$$

On the assumption that the x's are finite and the $\vec{k}$'s bounded this time scale is very large in the infinite momentum frame. It is Lorentz dilated and so is very much larger than the time scale of the deep inelastic interaction, t.

$$\Delta T \gg t \tag{151}$$

The two assumptions are both important. Reactions in which arbitrarily soft partons play a role cannot be described by the parton model. Large transverse momentum partons cannot be considered free particles during the time of the inelastic scattering.

How does a proton look in the infinite momentum frame? Because of the Lorentz contraction the longitudinal size of the proton is contracted by a factor m/P with respect to its size in the rest frame. Partons with finite values of x and fixed transverse size distributed on this disk as shown in Fig. 16 and the number of partons per unit of rapidity is rather small. Partons with very small values of x, such that $x \sim 1\text{GeV}/P$ are called wee partons. Because of their very small momentum they are not confined to the Lorentz contracted disk. Their spatial extent can be determined using the uncertainty principle.

$$\Delta z = \frac{1}{xP} \tag{152}$$

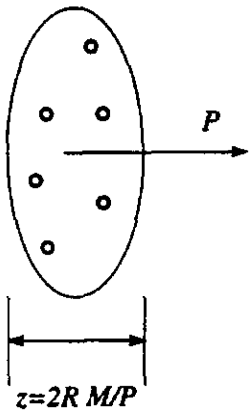

Figure 16: Proton as viewed in the infinite momentum frame

2.3 Deep Inelastic Scattering

2.3.1 Kinematics of deep inelastic scattering

Consider the scattering of a high energy charged lepton off a hadron target. If we label the incoming and outgoing lepton four-momenta by k^μ and k'^μ respectively, the momentum of the target hadron (assumed hereafter to be a proton) by P^μ and the momentum transfer by $q^\mu = k^\mu - k'^\mu$, then the standard deep inelastic variables are defined by:

$$\begin{aligned} Q^2 &= -q^2, \qquad P^2 = M^2 \\ x &= \frac{Q^2}{2P\cdot q} = \frac{Q^2}{2M(E-E')} \\ y &= \frac{q\cdot P}{k\cdot P} = 1 - E'/E\,, \end{aligned} \tag{153}$$

where the energy variables refer to the target rest frame. If the lepton is an electron or muon, then the scattering is mediated by the exchange of a virtual photon, Fig. 17.

The structure of the lepton vertex is assumed to be completely understood. The hadronic tensor contains all the information about the interaction of the electromagnetic current with the target.

$$\begin{aligned} W_{\alpha\beta}(P,q) &= \frac{1}{4\pi}\sum_X \left\langle P\middle|j^\dagger_\beta(0)\middle|X\right\rangle \left\langle X\middle|j_\alpha(0)\middle|P\right\rangle (2\pi)^4\delta^4(q+P-P_X) \\ &= \frac{1}{4\pi}\int d^4z e^{iq\cdot z}\left\langle P\middle|j^\dagger_\beta(z)j_\alpha(0)\middle|P\right\rangle \\ &\equiv \frac{1}{4\pi}\int d^4z e^{iq\cdot z}\left\langle P\middle|\left[j^\dagger_\beta(z),j_\alpha(0)\right]\middle|P\right\rangle \end{aligned} \tag{154}$$

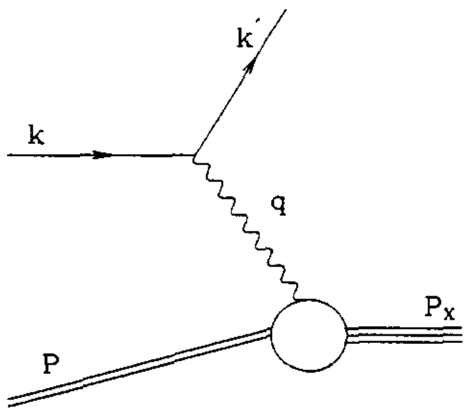

Figure 17: Deep inelastic charged lepton-proton scattering

Because of the conservation of the electromagnetic current we may write

$$W^{\alpha\beta}(P,q) = \left(g^{\alpha\beta} - \frac{q^\alpha q^\beta}{q^2}\right)W_1(x,Q^2) + \left(P^\alpha + \frac{1}{2x}q^\alpha\right)\left(P^\beta + \frac{1}{2x}q^\beta\right)\frac{W_2(x,Q^2)}{M^2} \quad (155)$$

where M is the mass of the struck hadron and $x = -q^2/2\nu \equiv Q^2/2\nu$ where $\nu = P \cdot q$.

The lepton scattering cross section is defined in terms of the structure functions $F_i(x,Q^2)$. For charged lepton scattering, $lp \to lX$, we have

$$\begin{aligned} \frac{d^2\sigma}{dxdy} &= \frac{8\pi\alpha^2 ME}{Q^4}\Big[\Big(\frac{1+(1-y)^2}{2}\Big)2xF_1 \\ &\quad +(1-y)(F_2 - 2xF_1) - (M/2E)xyF_2\Big], \end{aligned} \quad (156)$$

where

$$\begin{aligned} F_1(x,Q^2) &= W_1(x,Q^2) \\ F_2(x,Q^2) &= \frac{\nu W_2(x,Q^2)}{M^2} \end{aligned} \quad (157)$$

2.3.2 DIS in naive parton model

We shall consider the dynamics of DIS in a frame in which the struck proton is moving very fast. In order to specify this frame it is convenient to introduce two light-like vectors p and n which have their 3-momenta directed along the positive and negative z-axis. The vector p can be thought of as the four momentum of the target in the approximation in which we ignore its mass. By convention we choose $n \cdot p = 1$ so that n has the dimensions of an inverse mass. In this frame we have that,

$$p^2 = n^2 = n \cdot k_T = p \cdot k_T = 0 \quad (158)$$

where k_T is any vector in the transverse plane. An explicit representation for the vectors p and n is

$$\begin{aligned} p^\mu &= (P, 0, 0, P) \\ n^\mu &= (\frac{1}{2P}, 0, 0, -\frac{1}{2P}) \end{aligned} \tag{159}$$

The important vectors in DIS can be written as,

$$\begin{aligned} P^\mu &= p^\mu + \frac{M^2}{2} n^\mu \\ q^\mu &= \nu n^\mu + q_T^\mu \end{aligned} \tag{160}$$

For simplicity we will ignore the mass M in the following so that p and P are taken to be identical. In the frame given by Eq. (160) we may project out the components of the hadronic tensor.

$$\nu n^\alpha n^\beta W_{\alpha\beta} = \frac{\nu W_2}{M^2} = F_2 \tag{161}$$

$$\frac{4x^2}{\nu} p^\alpha p^\beta W_{\alpha\beta} = \frac{\nu W_2}{M^2} - 2x W_1 = F_2 - 2x F_1 \tag{162}$$

Now consider the simple handbag diagram shown in Fig. (18) in this frame.

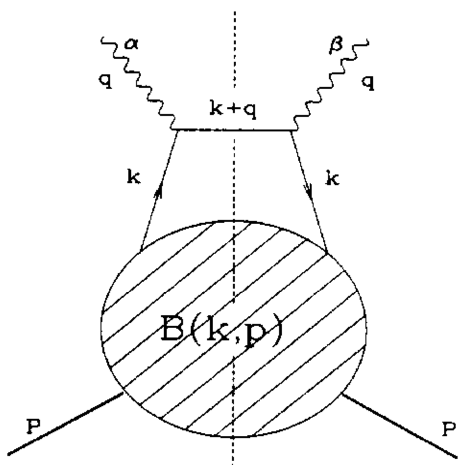

Figure 18: Handbag diagram

$$W^{\alpha\beta}(p,q) = e^2 \int \frac{d^4k}{(2\pi)^4} \left[\gamma^\alpha (\not k + \not q) \gamma^\beta\right]_{ij} \left[B(k,p)\right]_{ji} \delta((k+q)^2) \tag{163}$$

where $B(k,p)$ is the forward hadron-quark amplitude. We now perform a Sudakov decomposition of the momentum of k,

$$k^\mu = \xi p^\mu + \frac{k^2 + {k_T}^2}{2\xi} n^\mu + {k_T}^\mu \tag{164}$$

The assumption of the parton model is that the transverse momentum k_T and the virtuality k^2 are limited, presumably by the behaviour of the function $B(k,p)$. Imposing this constraint the delta function may be simplified to give.

$$\delta((k+q)^2) = \delta(k^2 + 2\xi\nu - 2q_T.k_T + q^2) \approx \delta(2\xi\nu - Q^2) \equiv \frac{1}{2\nu}\delta(\xi - x) \tag{165}$$

Hence we may write the result for W_2 for a single flavour of quark as,

$$\begin{aligned}\frac{\nu W_2}{M^2} &= \frac{e^2}{2}\int \frac{d^4k}{(2\pi)^4}\left[\not{n}(\not{k}+\not{q})\not{n}\right]_{ij} B_{ji}(k,p)\delta(\xi - x)\\ &= e^2 x\int \frac{d^4k}{(2\pi)^4}\left[\not{n}\right]_{ij} B_{ji}(k,p)\delta(\xi - x)\\ &= e^2 x q(x)\end{aligned} \tag{166}$$

where the quark distribution is given by,

$$q(x) = \int \frac{d^4k}{(2\pi)^4}\,[\not{n}B(k,p)]\;\delta(n\cdot k - x) \tag{167}$$

We therefore see that in the naive parton model the structure functions scale, i.e. they depend only on the dimensionless variable x:

$$F_i(x,Q^2) \longrightarrow F_i(x). \tag{168}$$

In addition we find the Callan-Gross relation $F_2 = 2xF_1$ which is indicative of the spin $\frac{1}{2}$ nature of the constituents.

One can give an operator representation for the quark distribution. In the light-cone gauge two quark fields separated by a light-like distance along the n direction defines a gauge invariant operator. The string connecting the two quarks is unnecessary because $n\cdot A = 0$. The quark distribution is given by the Fourier transform of this correlation function.

$$q(x) = \int \frac{d\lambda}{2\pi} e^{i\lambda x}\left\langle P\middle|\bar{\psi}(0)\not{n}\psi(\lambda n)\middle|P\right\rangle \tag{169}$$

The identification of $q(x)$ with a number density is only valid in a particular frame, (the infinite momentum frame). Taking the first moment of the quark density with respect to x we find,

$$\int dx q(x) = \left\langle P\middle|\bar{\psi}(0)\not{n}\psi(0)\middle|P\right\rangle \approx \left\langle P\middle|\bar{\psi}^\dagger(0)\psi(0)\middle|P\right\rangle \tag{170}$$

where the approximate relation is only valid in a fast moving frame when

$$\bar{\psi}\gamma^0\psi \approx \bar{\psi}\gamma^3\psi \tag{171}$$

Thus the first moment of the quark distribution counts the number of quarks.

2.3.3 Experimental results on DIS

The *Bjorken limit* is defined as $Q^2, p \cdot q \to \infty$ with x fixed. In this limit the structure functions are found experimentally to obey an approximate *scaling* law. i.e. they depend only on the dimensionless variable x:

$$F_i(x, Q^2) \longrightarrow F_i(x). \tag{172}$$

This is illustrated in Fig. 19, where data on the electromagnetic structure function F_2, measured with a proton target, are displayed. The data span nearly two decades of experiments, from the original SLAC-MIT measurements [10] to the most recent measurements from the BCDMS collaboration [11]. Only a representative sample of data points is shown. Note that even though the Q^2 values vary by two orders of magnitude, to a good approximation the data lie on a universal curve.

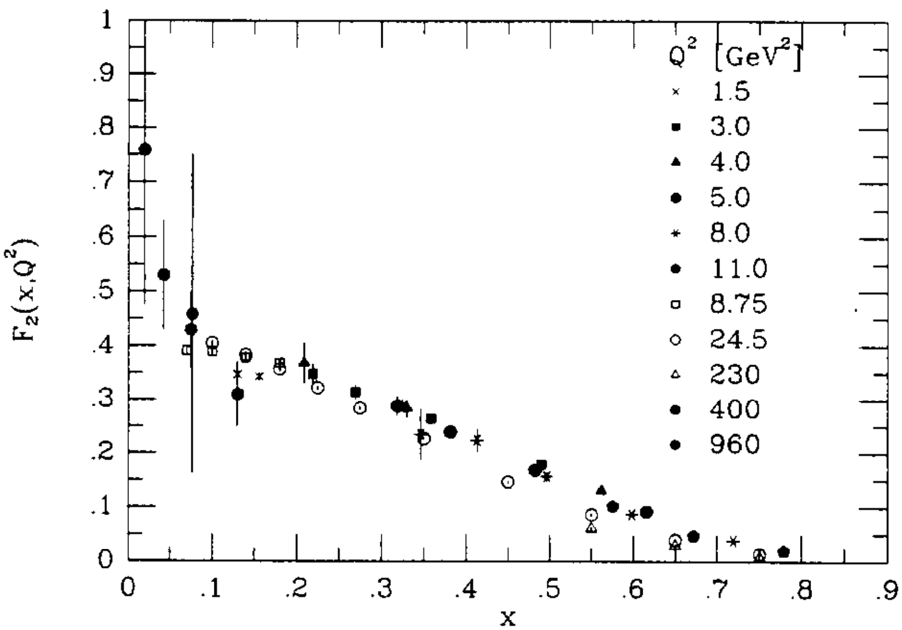

Figure 19: The F_2 structure function from the SLAC-MIT and BCDMS collaborations

Bjorken scaling implies that the virtual photon scatters off *pointlike constituents*, since otherwise the dimensionless structure functions would depend on the ratio Q/Q_0, with $1/Q_0$ some length scale characterizing the size of the constituents. Feynman called these fundamental constituents partons. The above ideas are incorporated in what is now known as the 'naive parton model' [3]:

- $q(\xi)d\xi$ represents the probability that a quark q carries momentum fraction between ξ and $\xi + d\xi$
- the virtual photon scatters incoherently off the quark constituents

Thus

$$\begin{aligned} F_2(x) &= \sum_q \int_0^1 d\xi \; q(\xi) \; x e_q^2 \delta(x-\xi) \\ &= \sum_q e_q^2 x q(x). \end{aligned} \tag{173}$$

and so for the scattering of a charged lepton off a proton target,

$$F_2(x) = x\Big[\frac{4}{9}u(x) + \frac{1}{9}d(x) + \frac{1}{9}s(x) + \frac{4}{9}\bar{u}(x) + \ldots\Big]. \tag{174}$$

For neutrino scattering – $\nu p \to lX$ – the virtual W^+ probe measures the quark distributions weighted by the *weak* charge:

$$F_2^\nu(x) = 2x\Big[d(x) + s(x) + \bar{u}(x) + \bar{c}(x) + \ldots\Big]. \tag{175}$$

A complete list of the most commonly encountered structure functions is given below.

$$\begin{aligned} F_2^\nu &= 2x[d + s + \bar{u} + \bar{c}] \\ xF_3^\nu &= 2x[d + s - \bar{u} - \bar{c}] \\ F_2^{\bar{\nu}} &= 2x[u + c + \bar{d} + \bar{s}] \\ xF_3^{\bar{\nu}} &= 2x[u + c - \bar{d} - \bar{s}] \\ F_2^{em} &= x[\frac{4}{9}(u + u + c + \bar{c}) + \frac{1}{9}(d + \bar{d} + s + \bar{s})] \\ 2xF_1 &= F_2. \end{aligned} \tag{176}$$

This last result follows from the spin-$\frac{1}{2}$ property of the quarks.

With sufficient number of measured structure functions, the above relations can be inverted to give the quark distribution functions themselves. From such an analysis, the following picture emerges. The proton consists of three *valence* quarks (uud) which carry the electric charge and baryon quantum numbers of the proton, and an infinite *sea* of light $q\bar{q}$ pairs. When probed at scale Q, the sea contains all quark flavours with $m_q \ll Q$. Thus at a scale of $O(1\ \mathrm{GeV})$ we have

$$\begin{aligned} u(x) &= u_V(x) + \bar{u}(x) \\ d(x) &= d_V(x) + \bar{d}(x) \end{aligned} \tag{177}$$

with the sum rules

$$\begin{aligned} \int_0^1 dx\, u_V(x) &= 2 \\ \int_0^1 dx\, d_V(x) &= 1 \\ \sum_q \int_0^1 dx\, x(q(x) + \bar{q}(x)) &\simeq 0.5. \end{aligned} \tag{178}$$

The last of these is an experimental result. It indicates that the quarks only carry about 50% of the proton's momentum. The rest is attributed to ***gluon*** constituents. Although the gluons are not directly measured in deep inelastic lepton hadron scattering, their presence is evident in other hard scattering processes such as large transverse momentum jet and prompt photon production. Fig. 20 shows a typical set of quark

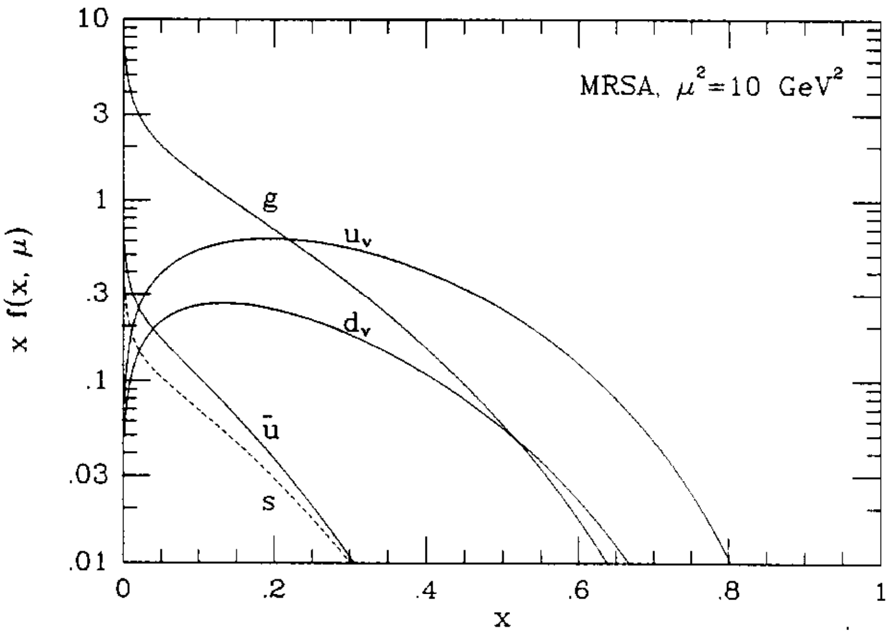

Figure 20: Quark and gluon distribution functions at $Q^2 = 10$ GeV^2

and gluon distributions extracted from fits to deep inelastic data, at $\mu^2 = 10$ GeV^2.

Closer examination of Fig. 19 reveals a systematic deviation from exact Bjorken scaling: the structure function decreases with increasing Q^2 at large x and has the opposite behaviour at small x. In the following section, we discuss how these scaling violations are understood in perturbative QCD.

2.4 The QCD parton model

We shall now consider the case the status of the parton model when we have gluon radiation. We shall find that the transverse momentum of the partons is not bounded. So we do not expect the parton model to be exactly true in perturbation theory. In fact since there is no scale in the problem it is clear that the transverse momentum will extend up to the kinematic limit which is of the order of Q^2.

To establish the normalization we calculate the scattering of a virtual photon off a free quark, Fig. 21a

$$\gamma^*(q) + q(p) \to q(l) \tag{179}$$

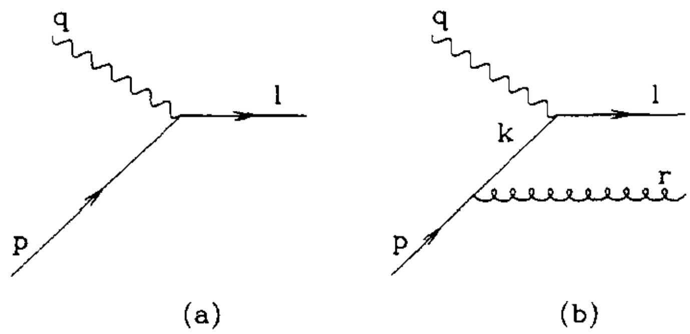

Figure 21: Amplitudes for Deep Inelastic Scattering

The momenta of the lines are shown in brackets. The invariant matrix element is

$$M_\alpha = -ie\bar{u}(l)\gamma^\alpha u(p) \tag{180}$$

leading to a squared matrix element (summed and averaged over spins and colours)

$$n^\alpha n^\beta \overline{\sum} |M|^2_{\alpha\beta} = 4e^2 \tag{181}$$

We have taken the quarks to be massless. The one dimensional phase space is

$$PS_1 = 2\pi\delta((p+q)^2) \tag{182}$$

Inserting a 'flux factor' of $1/4\pi$ from Eq. (154) we obtain the overall result

$$F_2(x) = e^2\delta(1-x) \tag{183}$$

Having established the free result we now investigate the more complicated parton process, Fig. 21b

$$\gamma^*(q) + q(p) \rightarrow g(r) + q(l) \tag{184}$$

The squares of the four diagrams involving real radiation are shown in Fig. 22. We shall start by considering the graph of Fig. 22a in which the hadron quark amplitude of the previous section, $(B(p,k))$, is represented by a particular model, single gluon exchange. The Lorentz invariant phase space for the diagrams with real gluon emission is,

$$PS_2 = \int \frac{d^4r}{(2\pi)^3}\frac{d^4l}{(2\pi)^3}\delta^+(r^2)\delta^+(l^2)(2\pi)^4\delta^4(p+q-r-l). \tag{185}$$

Introducing the momentum k to denote the momentum of the struck parton line we get

$$PS_2 = \frac{1}{4\pi^2}\int d^4k\ \delta^+((p-k)^2)\ \delta^+((k+q)^2) \tag{186}$$

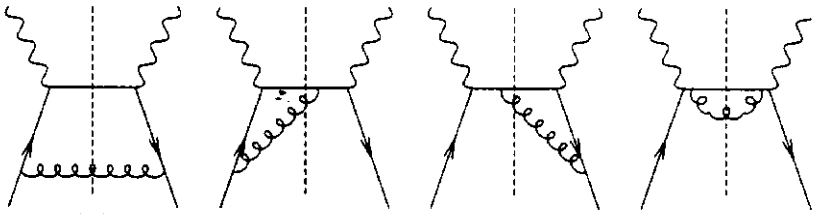

(a) (b) (c) (d)

Figure 22: Real graphs contributing to Deep Inelastic Scattering

Performing a Sudakov decomposition

$$\begin{aligned} k^\mu &= \xi p^\mu + \frac{k_T^2 - |k|^2}{2\xi} n^\mu + k_T^\mu & (187) \\ d^4k &= \frac{d\xi}{2\xi} dk^2 d^2k_T & (188) \end{aligned}$$

we find in the frame specified by Eq. (160)

$$\begin{aligned} (p-k)^2 &= (1-\xi)\frac{|k|^2}{\xi} - \frac{k_T^2}{\xi} & (189) \\ (k+q)^2 &= 2\xi\nu - Q^2 - |k|^2 - 2q_T.k_T & (190) \end{aligned}$$

In this frame the phase space can be written as,

$$PS_2 = \frac{1}{16\nu\pi^2}\int d\xi dk^2 dk_T^2 d\theta\, \delta\left(k_T^2 - (1-\xi)|k|^2\right)\, \delta\left(\xi - x - \frac{|k|^2 + 2q_T\cdot k_T}{2\nu}\right) \quad (191)$$

where the $0 < \theta < \pi$. Now let us consider the matrix element

$$M^\alpha = -ige\bar{u}(l)\gamma^\alpha \frac{1}{\not k}\not\epsilon t^A u(p) \quad (192)$$

Squaring and averaging over colours and spins we obtain

$$\overline{\sum}|M|^2_{\alpha\beta} = \tfrac{1}{2}e^2g^2\sum_{\text{pol}} C_F \mathrm{Tr}\{\gamma^\beta(\not k + \not q)\gamma^\alpha \not k \not\epsilon \not p \not\epsilon^* \not k\}\frac{1}{k^4} \quad (193)$$

where $\sum_A (t^A t^A)_{ij} = C_F\delta_{ij}$.

We will perform the sum over the polarization of the real gluon using the projector

$$\sum_{\text{pol}} \epsilon_\mu(r)\epsilon^*_\nu(r) = -g_{\mu\nu} + \frac{n_\mu r_\nu + n_\nu r_\mu}{n\cdot r} \quad (194)$$

Thus in addition to the Lorentz condition $\epsilon.r = 0$, the gluon satisfies the gauge condition $\epsilon.n = 0$. Thus we have only two physical polarizations propagating. This is important and would not be true if we performed the sum over polarizations using another method, (such as the Feynman trick). An important property of the quark gluon amplitude is that it vanishes in the forward direction. This is easy to see because helicity is conserved in the vector interaction. A positive helicity quark cannot decay to a collinear quark and a transverse gluon and conserve both the helicity of the quark and the component of (spin) angular momentum along the direction of travel. In fact the amplitude vanishes like,

$$A(q \to qg) \sim k_T \tag{195}$$

The argument depends on the spin of the produced gluon, therefore it is only true in a physical gauge in which only physical degrees of freedom propagate.

We can project the virtual photon components out with the vector n to calculate F_2 as shown in Eq. (161). Using the kinematic relations implicit in the phase space we find

$$\frac{1}{4\pi} n^\alpha n^\beta \overline{\sum} |M|^2_{\alpha\beta} = \frac{8e^2 \alpha_S}{|k|^2} \xi P(\xi) \tag{196}$$

where $P(\xi)$ is a property of the qqg vertex known as the known as the Altarelli-Parisi splitting function. The $1/k^4$ factor in Eq. (193) has been cancelled to $1/k^2$ by the two amplitude factors in Eq. (195) and for P we find,

$$P(\xi) = C_F \frac{1+\xi^2}{(1-\xi)} \tag{197}$$

Putting the whole thing together and performing the k_T^2 and θ integrations we obtain.

$$F_2 = e^2 \frac{\alpha_S}{2\pi^2} \int_0^{2\nu} \frac{d|k|^2}{|k|^2} \int_{\xi_-}^{\xi_+} d\xi \frac{\xi P(\xi)}{\sqrt{(\xi_+ - \xi)(\xi - \xi_-)}} \tag{198}$$

where

$$\xi_\pm(y, x) = x + y - 2yx \pm \sqrt{4x(1-x)y(1-y)} \tag{199}$$

In order to simplify the notation we have introduced the variable $y = |k|^2/(2\nu)$. The necessity that we have real roots limits $0 < y < 1$. The first thing to notice is that the transverse momentum is not limited. This was predictable since we have no small scale at which it could be limited, but $|k|^2$ can be as big as 2ν. In addition the $|k|^2$ integral is logarithmically divergent at small $|k|$. Let us isolate the coefficient of the logarithmical divergence. In the limit y tends to zero, $\xi_\pm$ both become identically equal to x and the range of integration vanishes. Thus were it not for the divergence in the denominator of the integrand the integral would vanish. We therefore find that the coefficient of the logarithmical divergence is,

$$F_2 \approx \frac{\alpha_S}{2\pi^2} x P(x) \int_0^{2\nu} \frac{d|k|^2}{|k|^2} \int_{\xi_-}^{\xi_+} d\xi \frac{1}{\sqrt{(\xi_+ - \xi)(\xi - \xi_-)}}$$

$$= \frac{\alpha_S}{2\pi} x P(x) \int_0^{2\nu} \frac{d\,|k|^2}{|k|^2} \tag{200}$$

So in our concrete example we have learnt two things. The first is that the virtuality (transverse momentum) integral is not cut-off at large k. The integral extends all the way to 2ν. If the integral went like

$$\frac{dk^2}{(k^2)^{1+\delta}},\ \delta > 0 \tag{201}$$

the conditions of the parton model would be satisfied. Instead we have found that $\delta = 0$ and since the integral is logarithmic it receives contributions from all values of k^2. The second feature which we have found is the divergence at small virtuality. It is interesting to go back and review this divergence from the standpoint of old-fashioned perturbation theory. Let us calculate the energy denominator in Fig. 23a

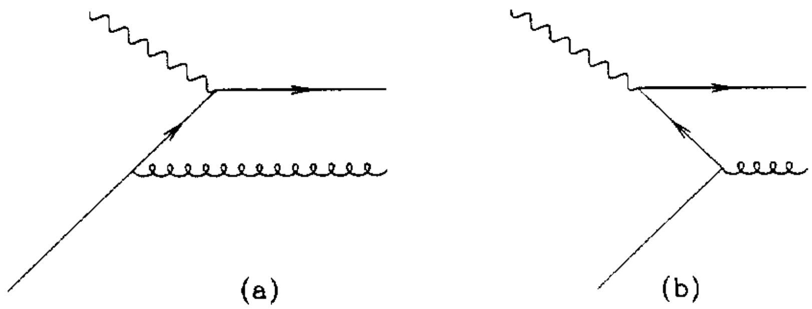

Figure 23: Two time orderings

for the intermediate state

$$\begin{aligned} E_S - E_i &= \omega_l + \omega_k - \omega_p \\ &= \left((1-\xi)P + \frac{k_T^2}{2(1-\xi)P}\right) + \left(\xi P + \frac{k_T^2}{2\xi P}\right) - P \\ &= \frac{k_T^2}{2(1-\xi)\xi P} \end{aligned} \tag{202}$$

The vanishing of the denominator as $k_T \to 0$ leads to an energy degeneracy of the initial and intermediate states. So by the standard uncertainty principle argument this is a fluctuation which has an extremely long life. The other time ordering is of order P and is suppressed as $P \to \infty$.

In the light-cone gauge the crucial role is played by the diagram of Fig 22a. This is reason for using the light cone gauge. The correspondence with the parton model is clear because Fig 22a is a handbag type of diagram. The other diagrams only give finite corrections to the cross-section. Consider for example Fig 22b. Instead of the $1/k^4$ present in Fig 22a, this graph contains only one propagator which can vanish. The other propagator is equal to $(p+q)^2$. Because of Eq. (195) the numerator factors at the gluon emission vertex contribute another factor of $k_T \sim \sqrt{k^2}$, in the light cone gauge. This graph gives only a finite contribution to the deep-inelastic scattering cross-section.

2.4.1 Factorization

QCD overcomes the divergent result found above by a procedure known as factorization. The idea of factorization is that we can separate the short and long distance parts in a multiplicative way. The property of factorization is proved in perturbation theory, although, because the idea of separating low and high frequency parts is rather simple, one hopes that the factorization is more generally true. One example of factorization is the operator product expansion.

$$J_1(x)J_2(0) \lim_{x\to 0} \sum_n C_n(x^2)O_n(0) \tag{203}$$

where J_1 and J_2 are two operators. The C_i are C-number functions which contain all of the physics of the short distances.

The essence of the parton model is the impulse approximation which states that there are two time scales which characterize a high energy scattering. A short time scale of order of the large momenta in the problem, (Q, ν) characterizes the hard scattering. A long time scale of order of the hadron radius characterizes the binding and recombination of the constituents. The short time scale physics depends on the particular process but is calculable. The long time scale physics depends on the complexity of hadronic binding but is independent of the particular process.

Explicitly the required factorization takes the following form. Let $d\sigma(p)$ be an inclusive differential cross section involving an incoming parton of type j. The result for the hard process calculated in perturbation theory is,

$$d\sigma_j(p) = \sum_k \int_0^1 d\xi \tilde{\sigma}_k(\xi p)\Gamma_{kj}(\xi, \epsilon) \tag{204}$$

All of the singularites are contained in the factor Γ which can now be absorbed into distribution function. Note that Γ is a matrix in the space of quarks and gluons. $\tilde{\sigma}(\xi p)$ is an effective cross section in the re-scaled momentum evaluated at $p^2 = 0$. $\tilde{\sigma}$ is normally referred to as the short distance cross section. For an incoming hadron the hadronic cross section is related to the parton cross section by,

$$d\sigma(P) = \sum_j \int \sigma_j(\xi p) f_j(\xi) d\xi \tag{205}$$

where f is some bare quark distribution. Combining Eqs. (204) and Eqs. (205) we get,

$$d\sigma(P) = \sum_k \int \tilde{\sigma}_k(\xi P)\tilde{f}_k(\xi)d\xi \tag{206}$$

where $\tilde{f}$ is a 'renormalized' parton distribution function.

$$\tilde{f}_k(\tilde{\xi}) = \sum_j \int d\beta d\xi \Gamma_{kj}(\beta) f_j(\xi)\delta(\tilde{\xi} - \xi\beta) \tag{207}$$

The factorization assures us that $\tilde{\sigma}$ is finite and calculable perturbatively. Equations of the type shown in Eq. (207) can be simplified by taking moments. If we define the moments of any function f by

$$f(j) = \int_0^1 d\xi \xi^{j-1} f(\xi) \tag{208}$$

we find that Eq. (207) may be written as

$$\tilde{f}_k(j) = \sum_j \Gamma_{kl}(j,\epsilon) f_l(j) \tag{209}$$

2.4.2 Regularization

In calculating the radiative corrections to the matrix element we have encountered a divergence and interpreted that divergence as a part of the long time physics. However in order to calculate this term and factor the divergence we must regulate it so that we have control over the finite parts. The method of preference is the method of dimensional regularization. The use of dimensional regularization for UV divergences is common. In the present context it is also used to control IR divergences. The Lorentz invariant phase space in d dimensions is

$$PS_2 = \int \frac{d^d r}{(2\pi)^{d-1}} \frac{d^d l}{(2\pi)^{d-1}} \delta^+(r^2)\delta^+(l^2)(2\pi)^d \delta^4(p+q-r-l) \tag{210}$$

After performing the integration over irrelevant angles, we find that the generalization of Eq. (191) is,

$$\begin{aligned} PS_2 &= \frac{1}{16\nu\pi^2}\frac{\sqrt{\pi}(4\pi)^\epsilon}{\Gamma(\frac{1}{2}-\epsilon)} \int d\xi dk^2 dk_T^2 d\theta \, (k_T^2 \sin^2\theta)^{-\epsilon} \\ & \quad \delta\left(k_T^2 - (1-\xi)\,|k|^2\right) \, \delta\left(\xi - x - y - \frac{q_T k_T}{\nu}\cos\theta\right) \end{aligned} \tag{211}$$

where the $0 < \theta < \pi$. Performing the θ and k_T integral we obtain

$$PS_2 = \frac{1}{16\nu\pi^2}\frac{\sqrt{\pi}(4\pi)^\epsilon}{\Gamma(\frac{1}{2}-\epsilon)}(\frac{2x}{\nu})^\epsilon \int dk^2 \int_{\xi_-}^{\xi_+} d\xi \, \left[(\xi_+ - \xi)(\xi - \xi_-)\right]^{-\frac{1}{2}-\epsilon} \tag{212}$$

Note that the ξ integral can be performed by making the change of variable $\xi = (\xi_+ - \xi_-)t + \xi_-$,

$$\begin{aligned} I &= \int_{\xi_-}^{\xi_+} d\xi \, \left[(\xi_+ - \xi)(\xi - \xi_-)\right]^{-\frac{1}{2}-\epsilon} \\ &= (\xi_+ - \xi_-)^{-2\epsilon} \int_0^1 dt \, [t(1-t)]^{-\frac{1}{2}-\epsilon} = (\xi_+ - \xi_-)^{-2\epsilon} \frac{\Gamma^2(\frac{1}{2}-\epsilon)}{\Gamma(1-2\epsilon)} \end{aligned} \tag{213}$$

The matrix element in n dimensions is given by Eq. (196) with $P(\xi)$ generalized to

$$P(\xi) = C_F\Big(\frac{1+\xi^2}{(1-\xi)} - \epsilon(1-\xi)\Big) \tag{214}$$

Putting everything together we find that the expression for the singular part in $O(\alpha_S)$ is,

$$F_2 = e^2 \frac{\alpha_S}{2\pi} x P(x) \left(\frac{4\pi}{Q^2}\frac{x}{1-x}\right)^{\epsilon} \frac{1}{\Gamma(1-\epsilon)} \int_0^1 dy \, y^{-1-\epsilon}(1-y)^{-\epsilon} \tag{215}$$

Thus the corrected expression for the quark distribution function due to real radiation is,

$$\tilde{q}(z) = \int dx dy \, \Gamma(x,\epsilon) q(y) \delta(z - xy) \tag{216}$$

$$= \int dx dy \, \left[\delta(1-x) - \frac{\alpha_S}{2\pi} P(x) \frac{1}{\epsilon}\right] q(y) \delta(z - xy) \tag{217}$$

This is almost the complete answer for q. The full result requires the inclusion of virtual radiation, specifically the inclusion of self energy insertions on the legs of the ladder. The treatment of these graphs in the light cone gauge is somewhat delicate. In the light cone gauge with a principal part regularization the self energy contains ultraviolet divergences in the terms proportional to $\not{p}$ as well in the terms proportional to $\not{n}$. These latter divergences require a counterterm proportional to $\not{n}$ which is not present in the original lagrangian. We shall finesse these problems by noting that these graphs can only contribute at $x = 1$ and determine the endpoint contribution by a physical argument. In physical predictions of the QCD parton model Γ is factored into the physical parton distribution. In order to preseve the conservation of quark number we must have.

$$\int_0^1 dx \, \Gamma_{qq}(x,\epsilon) = 1 \tag{218}$$

The full answer for Γ_{qq} can hence be written as

$$\Gamma_{qq}(x,\epsilon) = \delta(1-x) - \frac{\alpha_S}{2\pi} C_F \frac{1}{\epsilon}\Big[\frac{1+x^2}{(1-x)_+} + \frac{3}{2}\delta(1-x)\Big] \tag{219}$$

where the 'plus' distribution is defined so that its integral with any sufficiently smooth distribution f is

$$\int_0^1 dx \frac{f(x)}{(1-x)_+} = \int_0^1 dx \frac{f(x)-f(1)}{(1-x)} \tag{220}$$

The function P_{qq} is the lowest order term of the qq entry in the Altarelli-Parisi matrix

$$P_{qq} = C_F \Big[\frac{1+x^2}{(1-x)_+} + \frac{3}{2}\delta(1-x) \Big] \tag{221}$$

2.5 Deep inelastic scattering in the laboratory frame

To conclude this lecture we shall consider deep inelastic scattering in the laboratory frame. This is a slight digression from the main topic of the lectures, but it provides a fascinating application of parton dynamics when used to describe deep inelastic scattering off nuclei.

The treatment of deep inelastic scattering in the previous section was performed in a frame in which the target was fast moving. In this frame the deep inelastic photon acts as a probe of the parton structure of the target. However in certain circumstances it may be appropriate to consider DIS in a frame other than the infinite momentum frame. Of course, the predictions of the model should be independent of the frame, although clarity of the physical picture may vary depending on the frame. As a test of our understanding we shall therefore consider deep inelastic scattering in the frame in which the virtual photon is fast moving and the target is at rest. This has the added advantage of being the frame in which most experiments are performed.

In the lab frame the parton structure of deep inelastic photon is important and the target proton acts as an absorber of the constituents of the photon.

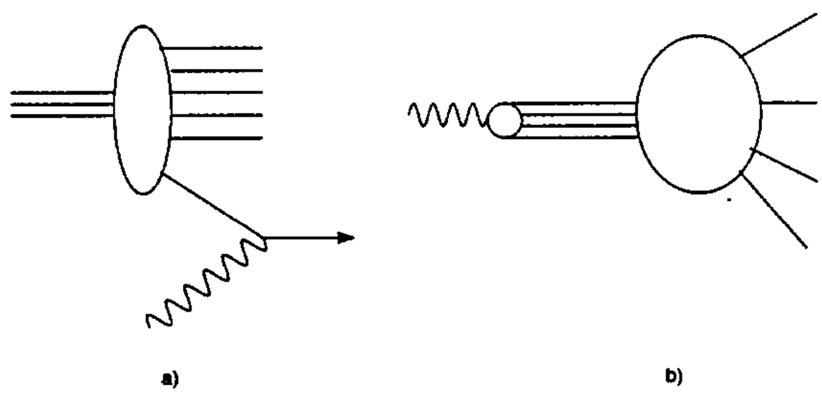

Figure 24: DIS in a) infinite momentum frame, b) laboratory frame at small x.

The kinematics of DIS can be descibed in the rest frame of target of mass m by, $(x = -q^2/(2m\bar{\nu}, \bar{\nu} = P \cdot q/m))$

$$q \approx (\bar{\nu} - mx, 0, 0, \bar{\nu}) \tag{222}$$

$$P = (m, 0, 0, 0) \tag{223}$$

Let us first consider the case when the virtual photon penetrates the nucleus, which occurs when the x of the virtual photon is large. Because the highly virtual photon is very small, (in a sense which I will make clear later) it traverses the nucleus until it encounters a wee parton and transfers all of its momentum $\bar{\nu}$ to it. Immediately after the collision the debris will consist of the original collection of wee partons (minus the struck parton). The struck parton is now separated in rapidity from the remains of the target by a large rapidity $\ln \bar{\nu}$. The struck parton has such a large rapidity and is unable to interact with the wee partons in the time available. Another way of saying of expressing the same concept is to view the event from the point of view of the struck parton. In its rest frame the remainder of the nucleus is Lorentz contracted to a thin disk which flies by in an instant. This describes the scenario which occurs at normal values of x.

There exists another possibility which is important at small values of x. The virtual photon can fluctuate into a hadronic state. Since energy is not conserved in this interaction, the lifetime τ of this fluctuation is finite. It is determined by the standard uncertainty principle argument by calculating the energy difference between the the virtual photon state and the hadronic state of the same momentum (and mass M_n) into which it transforms.

$$\begin{aligned} \Delta E &= \sqrt{\bar{\nu}^2 + M_n^2} - (\bar{\nu} - mx) \\ \tau = \frac{1}{\Delta E} &\approx \frac{1}{mx} \\ \Delta z &\approx \frac{0.2 \text{ fm}}{x} \end{aligned} \tag{224}$$

Thus for sufficiently small x the time for which the fluctuation exists and consequently the distance which the virtual photon travels in its hadronic guise can be bigger than the radius of the target. The fluctuation occurs upstream of the target and the virtual photon arrives at the front surface of the target in the form of a shower of quarks and gluons. If the target is a nucleus this can give rise to the the phenomenon of shadowing.

2.5.1 Shadowing

One context in which it is useful to consider deep inelastic scattering in the laboratory frame is in the discussion of scattering of nuclei in the small x region. We wish to apply the methods of the parton model to deep inelastic scattering off a nuclear target. It is well known that the cross section σ for the scattering of a real photon off a nucleus is not A times bigger than the cross section for scattering off a nucleon, σ_0. We rather find that

$$\sigma = \sigma_0 A^{\alpha} \tag{225}$$

where $\alpha < 1$ implies the existence of a phenomenon known as shadowing.

The important time scale (or equivalently the distance scale) is given by Eq. (224). Thus if $\tau > R$ the virtual photon presents itself at the face of the hadron as a hadronic state. In the naive parton model one therefore expects shadowing for $x < 1/(2Rm)$. If $x < 1/(2Rm)$ hadronic state is formed before the virtual photon reaches the nucleus and the incoming state should interact with the nucleus much as a hadron would. The scattering cross-section goes like πR^2, and the effective value of α is $2/3$.

The nuclear radii are normally parameterised by $R = r_0 A^{1/3}$ with $r_0 = 1.12$ fm. Thus, for example, the nuclear radius of D^2 is $R = 1.4$ fm, for Cu^{64} we have $R = 4.5$ fm and for Xe^{131} we have $R = 5.7$ fm. Thus for a heavy nucleus such as copper or xenon we expect shadowing for $x < 0.02$. Experimental data from E665 and NMC are shown in Fig. 25. The first plot shows the onset of shadowing in the small x region. The second plot shows that the ratio of structure functions in different nuclei is approximately independent of Q^2 in the shadowing region, $x < 0.01$. Experiment seems to indicate that shadowing is a scaling phenomenon.

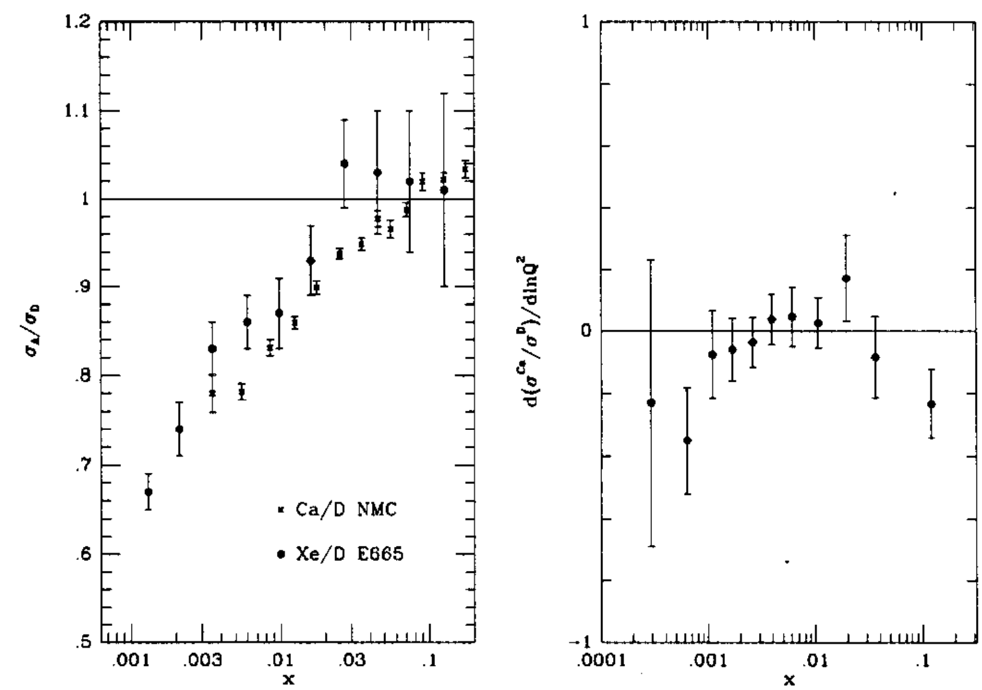

Figure 25: a) Shadowing as a function of x. b) The slope in Q^2 of the dependence cross section ratio as a function of x.

2.5.2 Theory of Shadowing

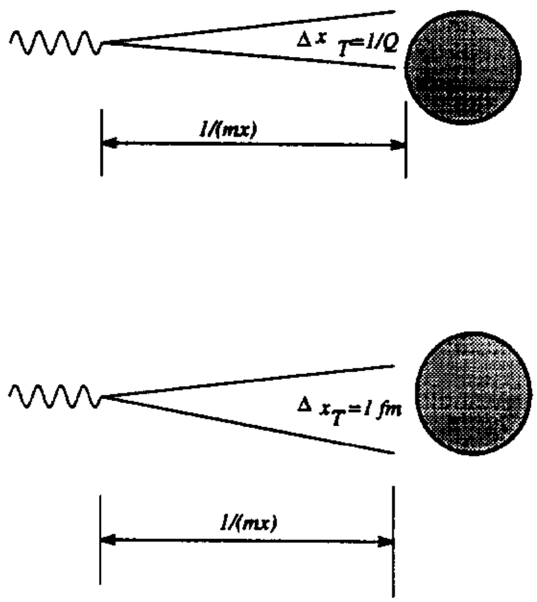

Figure 26: Interaction of virtual photon with a nucleus a) Equipartition of longitudinal momenta b) Unequal partition of longitudinal momenta

We now consider a fluctuation of our deep inelastic photon into a $q\bar{q}$ pair with momenta k_1 and k_2. We are working in the context of the parton model in which all transverse momenta are considered bounded at a hadronic scale which we will denote by m.

$$
\begin{aligned}
q &= (\bar{\nu} - mx, \vec{0}, \bar{\nu}) \qquad (226)\\
k_1 &\approx (k_z + \frac{k_T^2 + m^2}{2k_z}, k_T, k_z) \qquad (227)\\
k_2 &\approx (\bar{\nu} - k_z + \frac{k_T^2 + m^2}{2(\bar{\nu} - k_z)}, -k_T, \bar{\nu} - k_z) \qquad (228)
\end{aligned}
$$

when $k_z > k_T$. Hence the energy denominator corresponding to this fluctuation is

$$\Delta E = \frac{k_T^2 + m^2}{2k_z} + \frac{k_T^2 + m^2}{2(\bar{\nu} - k_z)} - mx \qquad (229)$$

Given the existence of the energy denominator and limited $k_T \sim m$, we can now ask what is the preferred value of k_z. If k_z is very small, $k_z \ll m/x$ the energy deficit will be large and the fluctuation short-lived. If k_z is large, $k_z \gg m/x$ then the transverse spatial extent of the $q\bar{q}$ pair on arrival at the target will be

$$\Delta x_T = \Delta z \theta = \Delta z \frac{k_T}{k_z} \sim \frac{1}{m} \frac{m/x}{k_z} \qquad (230)$$

7) J.D. Bjorken, Lectures given at the International Summer Institute in Theoretical Physics 'Current Induced Reactions', DESY (Hamburg), SLAC-PUB-1756, May 1976.

8) M.R. Adams *et al.*, *Phys. Lett.* **B287** (1992) 375;
T.J. Carroll, University of Illinois Thesis, (1994)

9) P. Amaudruz *et al.*., *Zeit. Phys.* **C51** (1991) 387.

10) SLAC-MIT collaboration: G. Miller et al., *Phys. Rev.* **D5** (1972) 528.

11) BCDMS collaboration: A.C. Benvenuti et al., *Phys. Lett.* **223B** (1989) 485.

12) Yu. L. Dokshitzer, V.A. Khoze, A.H. Mueller and S.I. Troyan 'Basics of Perturbative QCD', Editions Frontières, (1991).

3 Parton distributions and small x physics

3.1 Derivation of GLAP equation

In the last lecture we saw that the property of factorization allows us to separate the low momentum physics from the high momentum physics in a multiplicative way. This separation is performed at a scale μ, which is completely arbitrary and no physical prediction can depend on it. In this section we investigate the constraint provided by this condition. For simplicity, we will consider a non-singlet cross section which can only be initiated by a quark. We therefore have the factorized result,

$$\sigma(Q^2, \mu^2, \alpha_S(\mu^2), \epsilon) = \tilde{\sigma}_q(Q^2, \mu^2, \alpha_S(\mu^2)) \otimes \Gamma_{qq}(\alpha_S(\mu^2), \epsilon) \tag{233}$$

The symbol $\otimes$ indicates a convolution integral over longitudinal momentum fractions of the type given in Eq. (204). If we take moments (*cf.* Eq. (209)) on both sides of Eq. (233) it reduces to a simple product.

$$\sigma(j) = \tilde{\sigma}_q(j, \alpha_S(\mu^2), \mu^2)\Gamma_{qq}(j, \alpha_S(\mu^2), \epsilon) \tag{234}$$

$\tilde{\sigma}$ is the short distance cross section from which all singularities have been factorized. Γ contains the mass singularities which manifest themselves as poles in ϵ. The independence of the full cross section from μ implies that

$$\frac{d}{d\ln\mu}\sigma = 0 \tag{235}$$

and hence that

$$\frac{d}{d\ln\mu}\ln\Gamma(j, \alpha_S(\mu^2), \epsilon) = -\frac{d}{d\ln\mu}\ln\tilde{\sigma}_q(Q^2, \mu^2, \alpha_S(\mu^2)) = \gamma(j, \alpha_S(\mu^2)) \tag{236}$$

The function γ is known as the anomalous dimension, because it measures the deviation of $\tilde{\sigma}$ from its naive scaling dimension. It must be finite and can only depend on $\alpha_S(\mu^2)$ because these are the only variables common to both Γ and $\tilde{\sigma}$. The anomalous dimension is extracted from Eq. (236) by an argument similar to the one given in Section 1.7.1. Because the μ dependence of Γ enter only through the running coupling we have that,

$$\frac{d}{d\ln\mu^2}\ln\Gamma(j, \alpha_S(\mu^2), \epsilon) \equiv \beta(\alpha_S, \epsilon)\frac{d}{d\alpha_S}\ln\Gamma(j, \alpha_S(\mu^2), \epsilon) \tag{237}$$

In the minimal subtraction scheme Γ is given by a series of the form,

$$\Gamma(j, \alpha_S, \epsilon) = 1 + \sum_{i=1}^{\infty}\frac{\Gamma^{(i)}(j, \alpha_S)}{\epsilon^i} \tag{238}$$

and $\beta(\alpha_S, \epsilon)$ is as given by Eq. (84). Comparing the coefficient of the term of order ϵ^0 we find that

$$\gamma(j, \alpha_S) = -\frac{d}{d\ln\alpha_S}\Gamma^{(i)}(j, \alpha_S) \tag{239}$$

The lowest order result for $\gamma_{qq}(j)$ can be derived from Eq. (219).

$$\gamma_{qq}(j, \alpha_S) = \frac{\alpha_S}{2\pi}\int_0^1 dz\ z^{j-1} P_{qq}(z) \tag{240}$$

We therefore find the lowest order non-singlet equation for the 'renormalized' quark distribution function

$$\begin{aligned} \frac{d\tilde{q}(j)}{d\ln\mu^2} &= \gamma_{qq}(j, \alpha_S)\tilde{q}(j) \\ \frac{d\tilde{q}(x)}{d\ln\mu^2} &= \frac{\alpha_S}{2\pi}\int_0^1 dy \int_0^1 dz\ P_{qq}(y)\tilde{q}(z)\ \delta(x - yz) \qquad (241) \\ & \qquad (242) \end{aligned}$$

where

$$\tilde{q}(\tilde{\xi}) = \sum_j \int d\beta d\xi \Gamma_{qq}(\beta) q(\xi)\delta(\tilde{\xi} - \xi\beta) \tag{243}$$

3.2 The GLAP equation

In the 'naive' parton model the structure functions *scale*, i.e. $F(x, Q^2) \to F(x)$ in the asymptotic (Bjorken) limit: $Q^2 \to \infty$, x fixed. In QCD, this scaling is *broken* by logarithms of Q.

Exactly as for the renormalization of the coupling constant, we can regard $q(x)$ as an unmeasureable, *bare* distribution. The collinear singularities are absorbed into this bare distribution at a 'factorization scale' μ_0, which plays a similar role to the renormalization scale. There is therefore no absolute prediction for the 'renormalised' distribution $q(x, \mu)$. What the theory does tell us, however, is how the distribution varies with μ^2.

$$\frac{d}{dt}q(x, t) = \frac{\alpha_S(t)}{2\pi}\int_x^1 \frac{d\xi}{\xi} q(\xi, t) P(\frac{x}{\xi}). \tag{244}$$

This equation – known as the Gribov-Lipatov-Altarelli-Parisi equation – is the analogue of the β function equation describing the variation of $\alpha_S(t)$ with t.

The full prediction of the theory is most easily cast in terms of the *moments* (Mellin transforms) of the distributions:

$$q(j, t) = \int_0^1 dx\ x^{j-1}\ q(x, t). \tag{245}$$

In terms of these moments, the t dependence of the quark distribution function is given by

$$\frac{dq(j, t)}{dt} = \gamma_{qq}(j, \alpha_S(t))\, q(j, t). \tag{246}$$

We next define P_{qq} as the inverse Mellin transform of γ_{qq},

$$\frac{\alpha_S}{2\pi}\,P_{qq}(x,\alpha_S)=\frac{1}{2\pi i}\int_C dj\;x^{-j}\;\gamma_{qq}(j,\alpha_S), \tag{247}$$

where the integration contour C in the complex j plane is parallel to the imaginary axis and to the right of all singularities of the integrand. Taking the inverse Mellin transform of Eq. (246), we obtain in x space,

$$\begin{aligned}\frac{dq(x,t)}{dt} &= \frac{\alpha_S(t)}{2\pi}\int_0^1 d\xi\int_0^1 dz\;\delta(x-\xi z)P_{qq}(z,\alpha_S(t))q(\xi,t)\\ &= \frac{\alpha_S(t)}{2\pi}\int_x^1\frac{d\xi}{\xi}\,P_{qq}\Big(\frac{x}{\xi},\alpha_S(t)\Big)q(\xi,t).\end{aligned} \tag{248}$$

P_{qq} has a perturbative expansion in the running coupling,

$$P_{qq}(z,\alpha_S)=P_{qq}^{(0)}(z)+\frac{\alpha_S}{2\pi}P_{qq}^{(1)}(z)+\dots \tag{249}$$

Retaining only the first term in this expansion gives precisely the result in Eq. (244), with $P\equiv P_{qq}^{(0)}$.

In fact the above derivations are strictly only correct for *differences* between quark distributions, $q=q_i-q_j$. In general, the Altarelli-Parisi (AP) equation is a matrix equation,

$$\frac{d}{dt}\begin{pmatrix}q(x,t)\\ g(x,t)\end{pmatrix}=\frac{\alpha_S(t)}{2\pi}\int_x^1\frac{d\xi}{\xi}\begin{pmatrix}P_{qq}\left(\frac{x}{\xi},\alpha_S(t)\right) & P_{qg}\left(\frac{x}{\xi},\alpha_S(t)\right)\\ P_{gq}\left(\frac{x}{\xi},\alpha_S(t)\right) & P_{gg}\left(\frac{x}{\xi},\alpha_S(t)\right)\end{pmatrix}\begin{pmatrix}q(\xi,t)\\ g(\xi,t)\end{pmatrix}. \tag{250}$$

The AP kernels $P_{ij}^{(0)}(x)$ have an attractive physical interpretation as the probability of finding parton i in a parton of type j with a fraction x of the longitudinal momentum of the parent parton and a transverse momentum much less than μ. The interpretation as probabilities implies that the AP kernels are positive definite for $x<1$. They satisfy the following relations:

$$\begin{aligned}&\int_0^1 dx P_{qq}^{(0)}(x)=0\\ &\int_0^1 dx\;x\Big[P_{qq}^{(0)}(x)+P_{gq}^{(0)}(x)\Big]=0\\ &\int_0^1 dx\;x\Big[2n_f P_{qg}^{(0)}(x)+P_{gg}^{(0)}(x)\Big]=0.\end{aligned} \tag{251}$$

These equations correspond to quark number conservation and momentum conservation in the splittings of quarks and gluons.

The kernels of the AP equations are calculable as a power series in the strong coupling α_S. Both the lowest order terms [2] and the first correction [4] to the evolution kernels have been calculated. The lowest order approximations to the evolution kernels are:

$$\begin{aligned}
P_{qq}^{(0)}(x) &= C_F\left[\frac{1+x^2}{(1-x)_+}+\frac{3}{2}\delta(1-x)\right],\\
P_{qg}^{(0)}(x) &= T_R\left[x^2+(1-x)^2\right], \quad T_R=\frac{n_f}{2},\\
P_{gq}^{(0)}(x) &= C_F\left[\frac{1+(1-x)^2}{x}\right],\\
P_{gg}^{(0)}(x) &= 2N\left[\frac{x}{(1-x)_+}+\frac{1-x}{x}+x(1-x)\right]+\delta(1-x)\frac{(11N-4n_fT_R)}{6}.
\end{aligned} \tag{252}$$

The 'plus prescription' on the singular parts of the kernels is defined as

$$\int_0^1 dx\, f(x)[g(x)]_+ \;=\; \int_0^1 dx\, \left(f(x)-f(1)\right)g(x). \tag{253}$$

The plus prescription is defined under the integral sign, and defines a distribution. In terms of moments these four evolution kernels take the form

$$\begin{aligned}
\gamma_{qq}^{(0)}(j) &= C_F\left[-\frac{1}{2}+\frac{1}{j(j+1)}-2\sum_{k=2}^{j}\frac{1}{k}\right],\\
\gamma_{qg}^{(0)}(j) &= T_R\left[\frac{(2+j+j^2)}{j(j+1)(j+2)}\right],\\
\gamma_{gq}^{(0)}(j) &= C_F\left[\frac{(2+j+j^2)}{j(j^2-1)}\right],\\
\gamma_{gg}^{(0)}(j) &= 2N\left[-\frac{1}{12}+\frac{1}{j(j-1)}+\frac{1}{(j+1)(j+2)}-\sum_{k=2}^{j}\frac{1}{k}\right]-\frac{2}{3}n_fT_R.
\end{aligned} \tag{254}$$

In general the AP equation is a $(2n_f+1)$ dimensional matrix equation in the space of quarks, antiquarks and gluons. However not all of the evolution kernels are distinct so the matrix equation can be considerably simplified. Because of charge conjugation we have that,

$$P_{qq}=P_{\bar{q}\bar{q}}, \quad P_{qg}=P_{\bar{q}g}. \tag{255}$$

At lowest order we have in addition the following relations,

$$P_{\bar{q}q}^{(0)}=0, \quad P_{q_iq_j}^{(0)}=0 \quad (i\neq j). \tag{256}$$

The solution of the AP equation is simplified by considering combinations which are non-singlet (in flavour space) such as $q_i-\bar{q}_i$ or q_i-q_j. In this combination the mixing with the flavour singlet gluons drops out and we have, $(V=q_i-q_j)$,

$$\frac{d}{dt}V(x,t)=\frac{\alpha_S(t)}{2\pi}\left[P_{qq}(\xi)\otimes V(z,t)\right], \tag{257}$$

where $\otimes$ is a shorthand notation for the convolution integral of Eq. (248). Taking moments, this equation becomes

$$\frac{dV(j,t)}{dt} = \frac{\alpha_S(t)}{2\pi}\gamma_{qq}^{(0)}(j)\, V(j,t). \tag{258}$$

Inserting the lowest order form for the running coupling, we find the solution

$$V(j,t) = V(j,0)\left(\frac{\alpha_S(0)}{\alpha_S(t)}\right)^{d_{qq}(j)}, \quad d_{qq}(j) = \frac{\gamma_{qq}^{(0)}(j)}{2\pi b}. \tag{259}$$

It is straightforward to show that $d_{qq}(1) = 0$ and that $d_{qq}(j) < 0$ for $j \geq 2$. This in turn implies that as μ increases the distribution function *decreases* at large x and *increases* at small x. Physically, this can be understood as an increase in the phase space for gluon emission by the quarks as μ increases, with a corresponding degradation in momentum. The trend is clearly visible in the data.

We now turn to the flavour singlet combination of moments. Define the sum over all quark flavours to be given by Σ,

$$\Sigma = \sum_i (q_i + \bar{q}_i). \tag{260}$$

From Eq. (250), which holds for all flavours of quarks, we derive the equation for the flavour singlet combination of parton distributions,

$$\begin{aligned} \frac{d\Sigma}{dt} &= \frac{\alpha_S(t)}{2\pi}\left[P_{qq}^{(0)} \otimes \Sigma + 2n_f P_{qg}^{(0)} \otimes g\right] + O\left(\alpha_S^2(t)\right) \\ \frac{dg}{dt} &= \frac{\alpha_S(t)}{2\pi}\left[P_{gq}^{(0} \otimes \Sigma + P_{gg}^{(0)} \otimes g\right] + O\left(\alpha_S^2(t)\right). \end{aligned} \tag{261}$$

This equation is most easily solved by direct numerical integration in x space starting with an input distribution obtained from data.

We can illustrate some simple properties of the distributions using the moments. Taking the second ($j = 2$) moment of Eq. (261) we find that

$$\frac{d}{dt}\begin{pmatrix} \Sigma(2) \\ g(2) \end{pmatrix} = \frac{\alpha_S(t)}{2\pi}\begin{pmatrix} -C_F\frac{4}{3} & \frac{n_f}{3} \\ C_F\frac{4}{3} & \frac{-n_f}{3} \end{pmatrix}\begin{pmatrix} \Sigma(2) \\ g(2) \end{pmatrix}. \tag{262}$$

The eigenvectors and corresponding eigenvalues of this system of equations are

$$\begin{aligned} O^+(2) &= \Sigma(2) + g(2) \qquad \text{Eigenvalue}: 0 \\ O^-(2) &= \Sigma(2) - \frac{n_f}{4C_F}g(2) \qquad \text{Eigenvalue}: -\left(\frac{4}{3}C_F + \frac{n_f}{3}\right). \end{aligned} \tag{263}$$

Note that the combination O^+, which corresponds to the total momentum carried by the quarks and gluons, is independent of t. The eigenvector O^- vanishes at asymptotic t:

$$O^-(2) = \left(\frac{\alpha_S(0)}{\alpha_S(t)}\right)^{d^-(2)} \to 0, \quad d^-(2) = \frac{-(\frac{4}{3}C_F + \frac{n_f}{3})}{2\pi b} \tag{264}$$

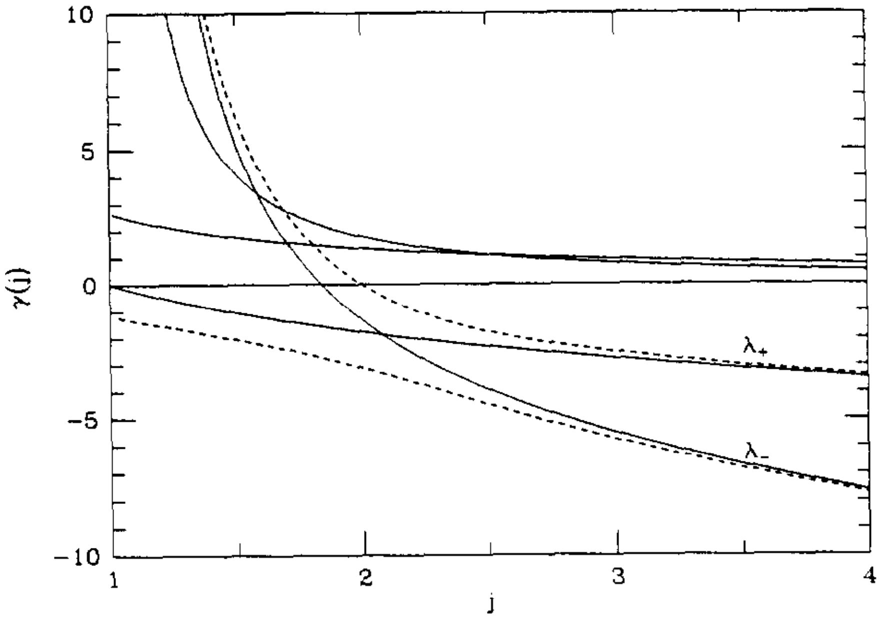

Figure 27: Elements of the anomalous dimension matrix and its eigenvalues vs j

So that asymptotically we have

$$\frac{\Sigma(2)}{g(2)} = \frac{n_f}{4C_F} = \frac{Nn_f}{2(N^2-1)}. \tag{265}$$

The momentum fractions carried by the quarks and gluons in the $\mu \to \infty$ limit are therefore

$$\Sigma(2)\Big|_{t=\infty} = \left(\frac{n_f}{4C_F+n_f}\right), \quad g(2)\Big|_{t=\infty} = \left(\frac{4C_F}{4C_F+n_f}\right). \tag{266}$$

Note, however, that the approach to the asymptotic limit is controlled by $t \sim \ln\mu^2$ and is therefore quite slow. The Q^2 dependence of the momentum fractions are shown in Fig. 28.

For a tabulation of the eigenvectors and eigenvalues of the moments of Eq. (261) we refer the reader to reference [3]. The expected scale dependence of some of the distributions are shown in Figs. 29–32.

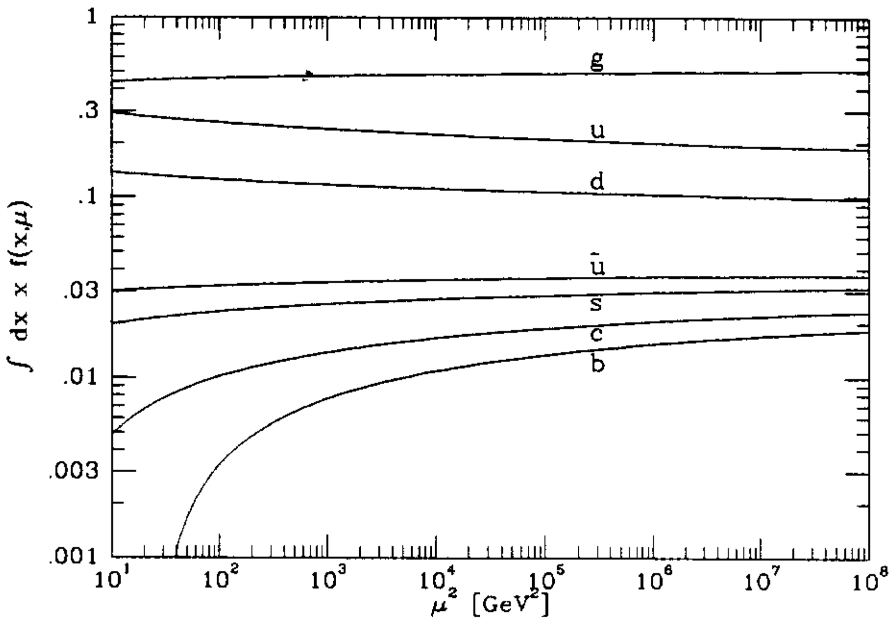

Figure 28: Momentum fractions carried by the quarks and gluons as functions of the scale

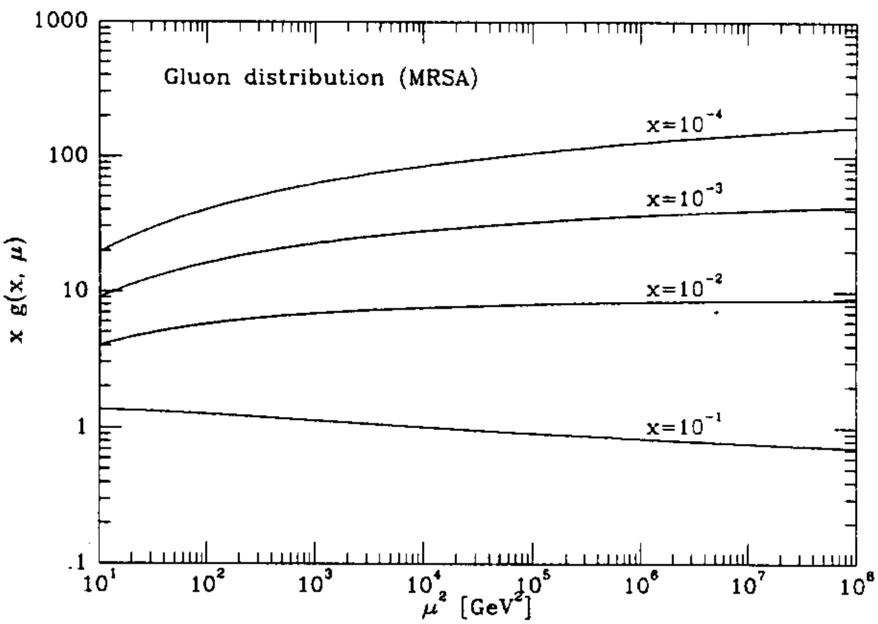

Figure 29: The scale dependence of the gluon distribution

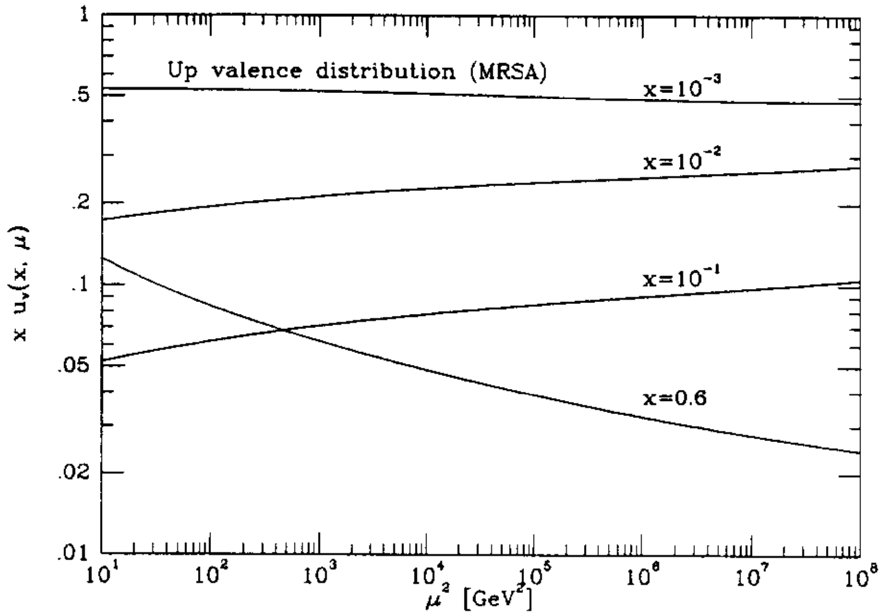

Figure 30: The scale dependence of the valence up distribution

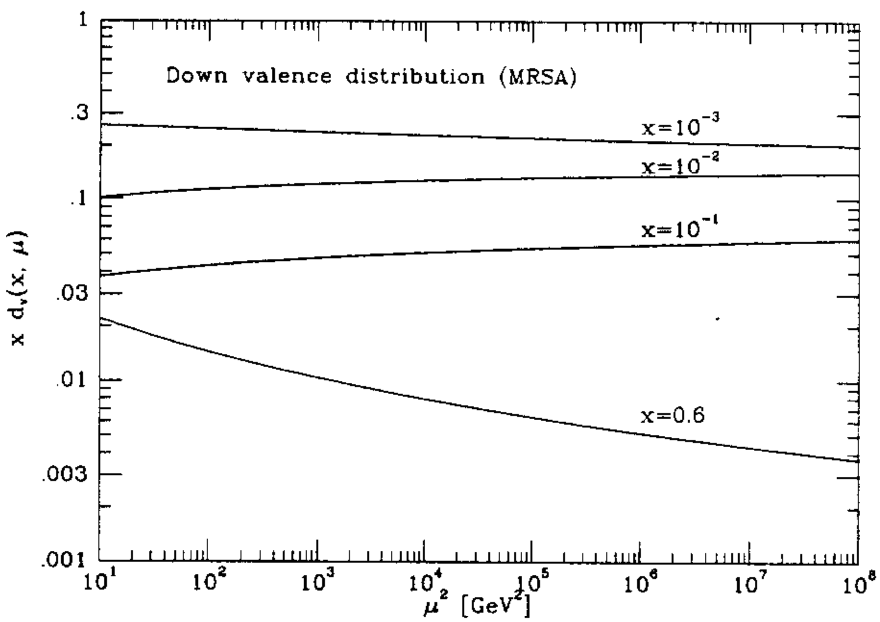

Figure 31: The scale dependence of the valence down distribution

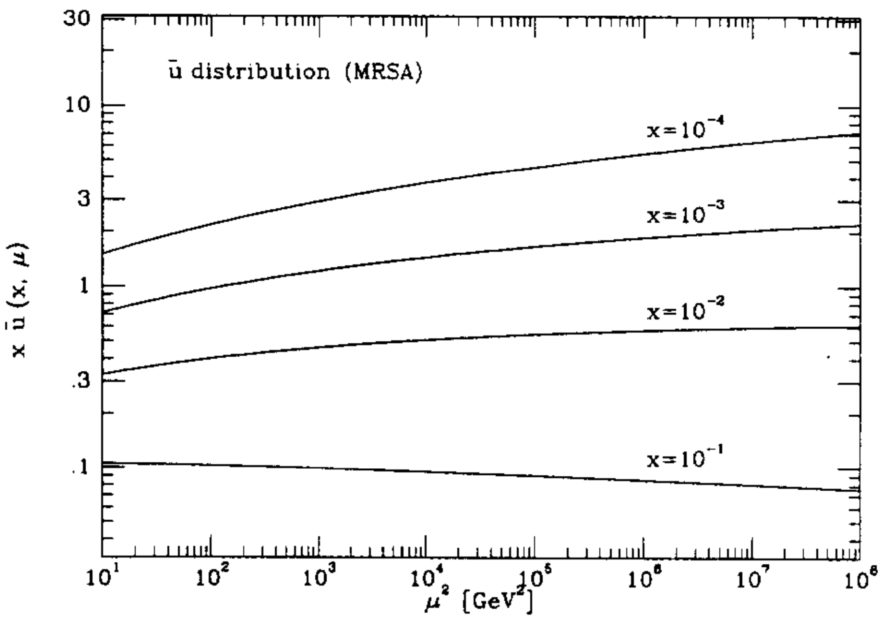

Figure 32: The scale dependence of the anti-up quark distribution

3.3 QCD fits to deep inelastic data

In the the previous section we saw that perturbative QCD predicts the Q^2 *evolution* of the structure functions, rather than the size and shape of the functions themselves. Quantitatively, the variation with Q^2 is controlled by $\alpha_S(Q)$ and hence by the QCD scale parameter Λ. Deep inelastic scattering data provide one of the 'precision' tests of QCD and, arguably, the most accurate determination of $\Lambda_{\overline{MS}}$.

Although the theoretical predictions appear simplest when expressed in terms of structure function moments, it is very difficult to extract such moments from the data. This is because the measurements do not extend to very large and very small x, and some form of *ad hoc* extrapolation is required to construct the moment integrals. A more practical and accurate method is to choose a reference value Q_0 and parametrise the parton distributions at that value, e.g. $q(x, Q_0) = Ax^a(1-x)^b$. These distributions are then evolved numerically, using the Altarelli-Parisi equations, to obtain values for the $F_i(x, Q^2)$ in the kinematic regions where they are measured. Note that in this approach the rate of change with Q^2 of the structure function at a given x depends only on the structure function evaluated at $\xi > x$, *cf.* Eq. (250). Finally, a global numerical fit is performed to determine the 'best' values for the parameters, including Λ. The extent to which the measured value of Λ depends on the other parameters can also be quantified and used to derive a systematic error.

The above procedure is not, however, without problems. The most serious of these are:

- In QCD, the structure functions have 'higher twist' power corrections, which are much more difficult to estimate quantitatively:

$$F(x, Q^2) \; = \; F^{(2)}(x, Q^2) \; + \; \frac{F^{(4)}(x, Q^2)}{Q^2} \; + \; \ldots, \qquad (267)$$

  where the superscripts on the right-hand-side refer to the 'twist' = (dimension − spin) of the contributing operators. To avoid these complications, the analysis must be performed at large Q^2 where the power suppressed terms are negligible.

- The structure function F_2 can be decomposed into singlet and non-singlet ('sea quark' and 'valence quark') parts, which dominate at small and large x respectively. Hence, except at large x, the Q^2 dependence of F_2 is sensitive to the *a priori* unknown gluon distribution and there is potentially a strong Λ-gluon correlation.

- Non-singlet structure functions do not suffer from the gluon correlation problem (see Eq. (257)), but these are only measurable experimentally by constructing differences between cross sections, e.g. $\sigma^{\mu p} - \sigma^{\mu n}$. This inevitably introduces additional systematic and statistical uncertainties.

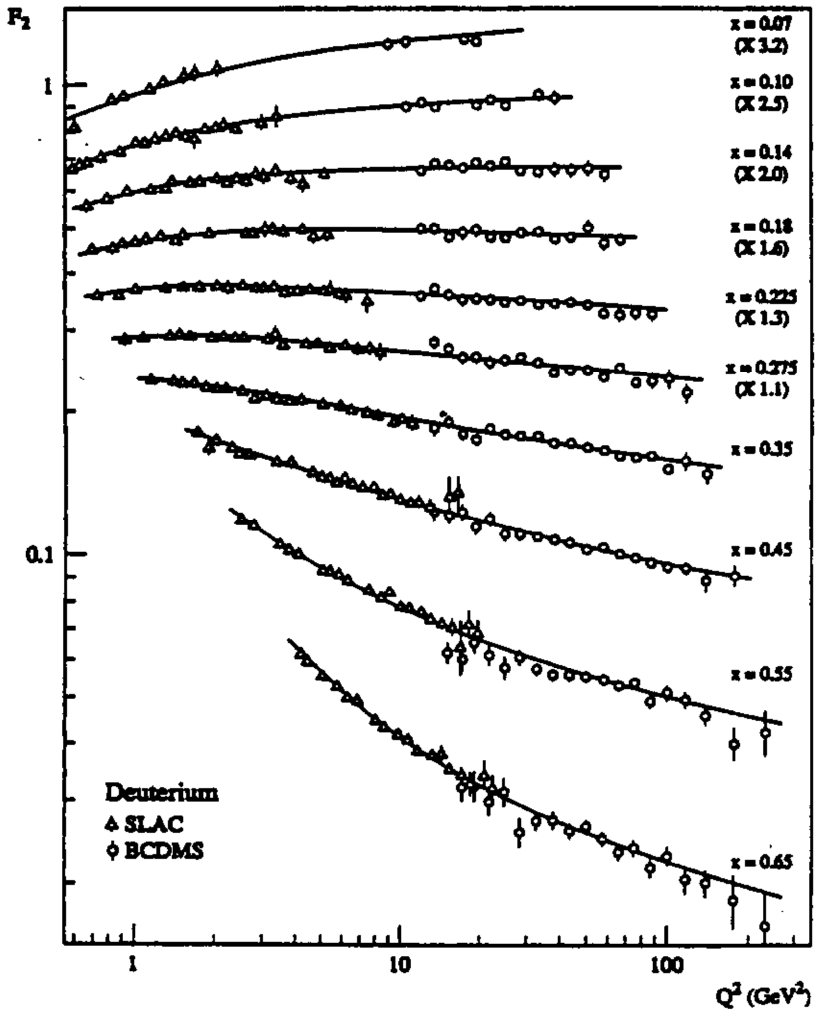

Figure 33: Data on the structure function F_2 in muon-deuterium scattering from Virchaux[7]

The most recent generation of deep inelastic experiments partially solve these problems by collecting high statistics data at large x and Q^2..In fact the precision of contemporary data demands that the next-to-leading order QCD predictions are used in the fits. Beyond leading order a specific renormalization scheme must be chosen, and in practice this is usually the $\overline{MS}$ scheme. For this reason the results quoted in the literature almost always refer to $\Lambda_{\overline{\text{MS}}}$.

Some of the most precise recent data comes from the BCDMS collaboration [6,7,11]. As an example, Fig. 33 shows the structure function F_2 measured in deep inelastic muon-deuterium scattering. The measurements extend up to x values of 0.65 and Q^2 values of several hundred GeV^2. Fig. 34 shows the corresponding logarithmic Q^2 derivative of $\log F_2$ as a function of x. Note that the derivatives in this region are negative, consistent with a structure function which decreases with increasing Q^2.

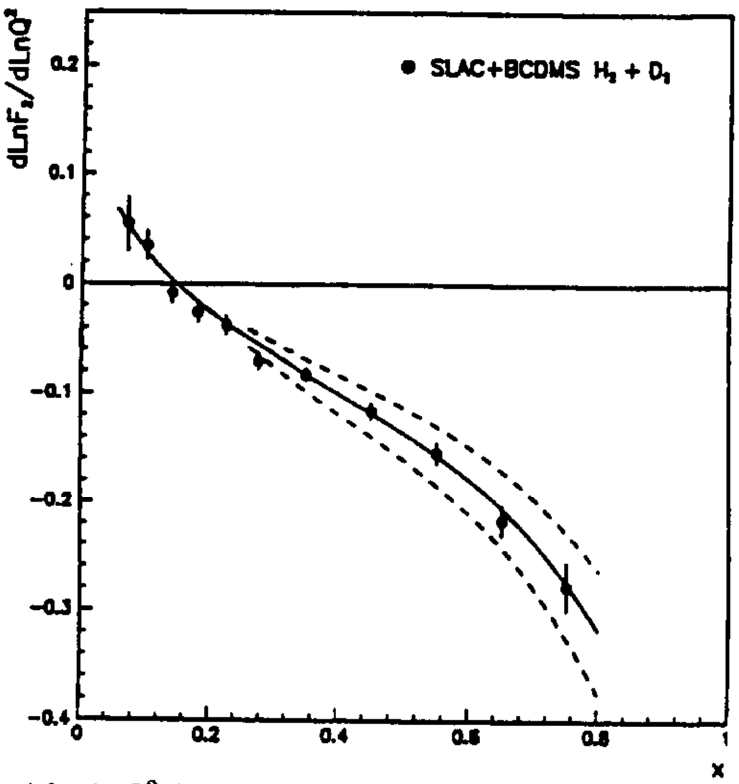

Figure 34: Logarithmic Q^2 derivative of the F_2 structure function with QCD fits from BCDMS

Also shown are the predictions of next-to-leading order QCD for three different values of $\Lambda_{\overline{\rm MS}}$. A detailed fit gives [6]

$$\Lambda^{(4)}_{\overline{\rm MS}} = 220 \pm 15 \pm 50 \text{ MeV} \tag{268}$$

The result for $\alpha_S(M_z)$ derived from Deep Inelastic Scattering is compared with determinations from other processes in Fig. 35 (taken from ref. [8]).

Deep inelastic experiments measure quark densities over a broad range in x up to about $Q = 15$ GeV. Knowing $\Lambda_{\overline{\rm MS}}$, these can then be evolved to higher μ and used for hadron collider phenomenology. Instead of laboriously integrating the Altarelli-Parisi equations each time a parton distribution is required, it is useful to have an analytic approximation, valid to a sufficient accuracy over a prescribed (x, μ) range. Several such parametrizations are available.

The widely used Duke and Owens parametrizations [9], for example, are of the form

$$\begin{aligned} q(x,Q) &= Ax^a(1+cx)(1-x)^b \\ A &= A_0 + A_1 s + A_2 s^2 \qquad \text{etc.} \\ s &= \ln\left(\frac{\ln(Q^2/\Lambda^2)}{\ln(Q_0^2/\Lambda^2)}\right) > 0, \end{aligned} \tag{269}$$

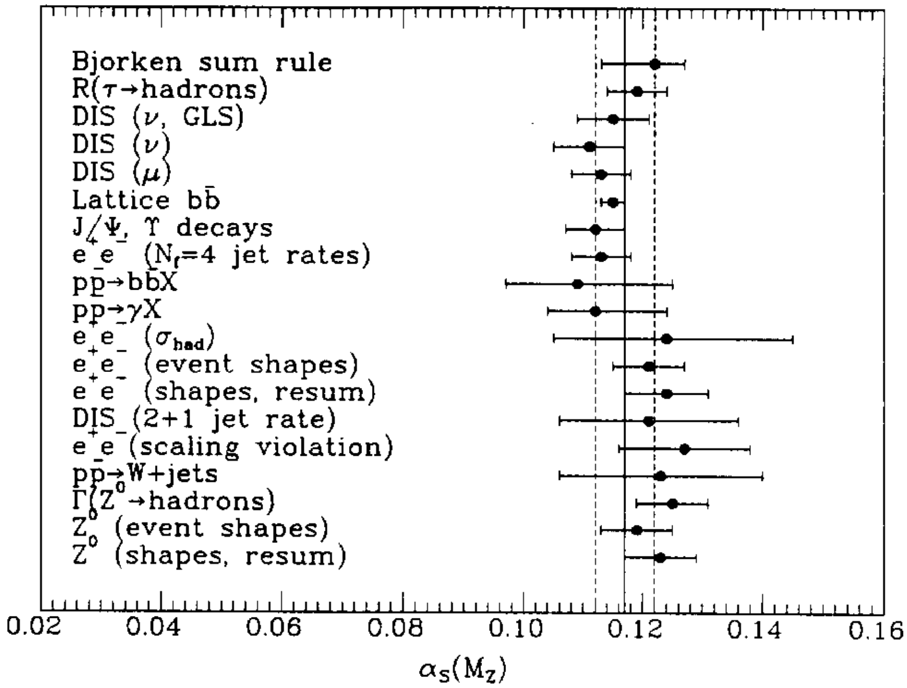

Figure 35: Table of values of $\alpha_S(M_z)$

with the parameters A_0, A_1, ... fitted to an exact leading order evolution to give an accuracy of a few per cent. Because deep inelastic scattering does not significantly constrain the gluon distribution, it was usual – in the past – to include in the parametrizations a choice of gluon distributions, typically a 'hard gluon' and a 'soft gluon', each with its own Λ value. Nowadays, high precision fixed-target prompt photon experiments are able to constrain the gluon, particularly in the medium x range, and 'hard gluon' parametrizations are ruled out [10]. The most recent generation of parton distributions – for example the MRS sets [11] – are obtained from next-to-leading order QCD fits to a wide variety of deep inelastic data, as well as data from prompt photon and lepton pair production. The distributions cover a wide range in x and μ, and are ideal for making quantitative predictions for present and future hadron-hadron and lepton-hadron colliders.

3.3.1 AP equation and small x

From Fig. 29, we see that the gluon distribution grows rapidly at small x. In the asymptotic limit where $x \to 0$ and $\mu \to \infty$ it is possible to determine the behaviour of the distributions directly from the Altarelli-Parisi equations.

The $x \to 0$ limit of the parton distributions is controlled by the behaviour of the anomalous dimensions $\gamma(j)$ near $j = 1$. Considering the gluon only we have

$$\frac{d}{dt}g(j,t) = \frac{\alpha(t)}{2\pi}\gamma_{gg}^{(0)}(j)g(j,t) \tag{270}$$

where from Eq. (254),

$$\gamma_{gg}^{(0)}(j) \approx \frac{2N}{j-1}. \tag{271}$$

In this limit the solution for the moments of the gluon distribution is,

$$g(j,t) = g(j,t_0)\exp\Big(\frac{N\xi}{\pi b(j-1)}\Big), \tag{272}$$

and ξ is defined by,

$$\xi = b\int_{t_0}^{t} dt' \alpha_S(t'). \tag{273}$$

To return to x space we perform the inverse Mellin transform (*cf.* Eq. (247)).

$$\begin{aligned} G(x,t) \equiv xg(x,t) &= \frac{1}{2\pi i}\int dj\; x^{-(j-1)} g(j,t) && (274)\\ &\equiv \frac{1}{2\pi i}\int dj\; g(j,t_0)\exp\big[f(j)\big] && (275)\end{aligned}$$

where the exponent f is,

$$f(j) = \Big[(j-1)\ln(1/x) + \frac{N\xi}{\pi b(j-1)}\Big]. \tag{276}$$

In the limit in which both $\ln(1/x)$ and ξ tend to infinity we can estimate this integral by expanding about the saddle point of the exponential:

$$f(j) = \sqrt{2\xi y} + O(j-j_s)^2,\;\; j_s = 1 + \frac{N}{\pi b}\sqrt{\frac{2\xi}{y}},\;\; y = \frac{2N}{\pi b}\ln(1/x). \tag{277}$$

We therefore find for the asymptotic solution

$$G(x,t) = g(j_s,t_0)\exp\sqrt{2\xi y}, \tag{278}$$

which expressed in the original variables yields

$$g(x) \sim \frac{1}{x}\exp\sqrt{\frac{4N}{\pi b}\ln\frac{\ln\mu^2/\Lambda^2}{\ln\mu_0^2/\Lambda^2}\ln\frac{1}{x}},\;\; N=3,\;\; b = \frac{(33-2n_f)}{12\pi}. \tag{279}$$

Notice that the dependence on the starting distribution enters via the j_sth moment of g. Therefore at fixed ξ/y the initial information enters only as an overall factor.

The derivation of Eq. (279) contains an important technical assumption which we have glossed over. In order that the dominant small x behaviour of the integral, Eq. (274), is given by the saddle point method there must be no singularities to the right of the saddle point in the complex plane. Let us assume that in the small x region the gluon distribution has a behaviour of the form,

$$g(x,t_0) = Ax^{-j_0}. \tag{280}$$

With this form we find that

$$g(j,t_0)=\frac{A}{(j-j_0)} \tag{281}$$

Thus if the distribution at the starting point is steep and $j_0 > j_s$ the above assumption is violated. In this circumstance we expect that the dominant small x behaviour of the integrand is given by closing the contour about the pole in the initial distribution. The estimate of the integral is given by[12],

$$g(x,t)=g(x,t_0)\exp\Big[\frac{N\xi}{\pi b(j_0-1)}\Big]. \tag{282}$$

The x behaviour remains as given by the initial distribution. In either case we expect a rapid growth of the gluon distribution at small x. Measurements of the structure function F_2 from HERA[13,14] indeed show a rapid rise at small x as shown in Fig. 36. This shows that the quark distributions are growing at small x.

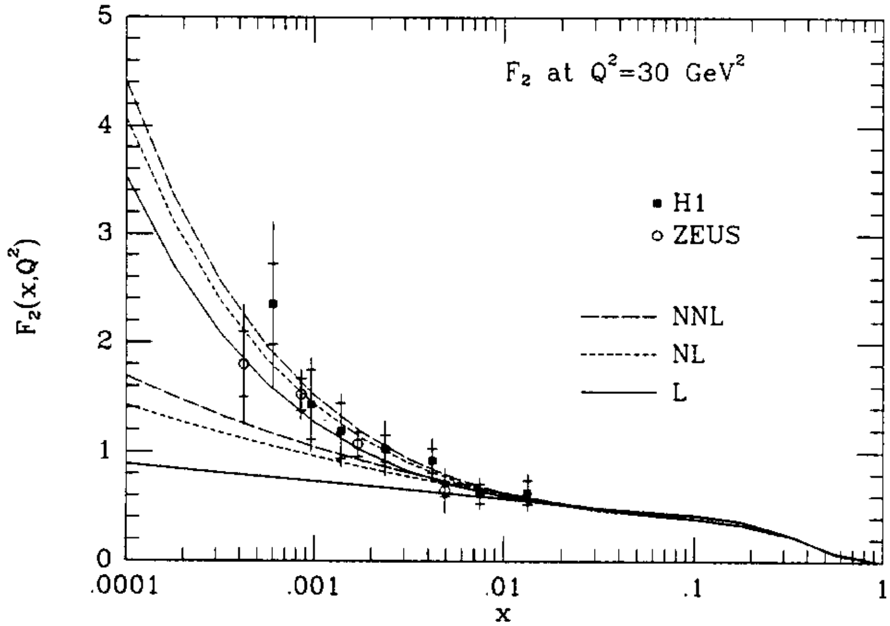

Figure 36: Data on F_2 at small x compared with QCD predictions[12]

A topic which is presently under active investigation [15] is the mechanism which limits the growth of the gluon distribution. In the infinite momentum frame the gluon momentum distribution $G(x,t)$ gives the number of gluons per unit of rapidity with a transverse size greater than $1/\mu$. If the number of gluons grows so large that the partons start to overlap inside the nucleon new effects will come into play. A crude estimate of when this begins to happen is provided by,

$$G(x,t)=\frac{\text{Area of hadron}}{\text{Area of parton}}\sim\mu^2 r^2\sim\mu^2\;25\;\text{GeV}^{-2}, \tag{283}$$

where $r \sim 1/m_\pi$ is the radius of the hadron. At presently attainable values of x the value of $G(x,t)$ does not exceed 3 or 4, so, if the above estimate is correct, the saturation limit is beyond the range of the present colliders.

3.4 BFKL equation

The asymptotic behaviour of high energy scattering is usually discussed in terms of the Balitsky-Fadin-Kuraev-Lipatov (BFKL) equation[17]. In this section we discuss an alternative formulation[18,19] of high energy scattering, which reproduces the BFKL equation, but is simpler to explain. The treatment is expressed in terms of light-cone multiparton wave-functions. The wave function is assumed to be confined in a small transverse distance so that perturbation theory is applicable. In leading order in the number of colours N_c the cross-section is given by the product of the light-cone wave function for a particular Fock state and the interaction cross-section for that state.

Let us consider a colour singlet state which has a non-zero wavefunction to exist as a $q\bar{q}$ state, and let this state be specified by the longitudinal momentum fraction of the quark, z and the transverse momentum k. We want to calculate the wave function of soft gluons emitted from this state. For simplicity, we will consider a $q\bar{q}$ state produced by a charmonium state, so that the quarks are localized in a transverse region of order $1/M$. The first fact to establish is that the transverse separation of the quark-antiquark into which the charmonium fluctuates has a fixed transverse separation during the time of emission of a soft gluon. Calculate the energy difference between the state before and after the emission of the gluon. We are interested in the emission of a gluon such that $z_1 \ll z, (1-z)$ and k_1 of order k in order to get the leading logarithms. The kinematic labelling is shown in Fig.37. The energy denominator of the first diagram is

$$\begin{aligned} \Delta E &= \left((1-z-z_1)P + \frac{(k_1+k)^2}{2(1-z-z_1)P}\right) + \left(z_1 P + \frac{k_1^2}{2z_1 P}\right) \\ &\quad -\left((1-z)P + \frac{(k)^2}{2(1-z)P}\right) \\ &\approx \frac{k_1^2}{2z_1 P} \end{aligned} \tag{284}$$

By the uncertainty principle the lifetime of the intermediate state is of order,

$$\Delta t \approx \frac{2z_1 P}{k_1^2} \tag{285}$$

The transverse velocity of separation of the intermediate $q\bar{q}$ pair is

$$|v_T| \approx \left|\frac{k+k_1}{(1-z-z_1)(z+z_1)P}\right| \tag{286}$$

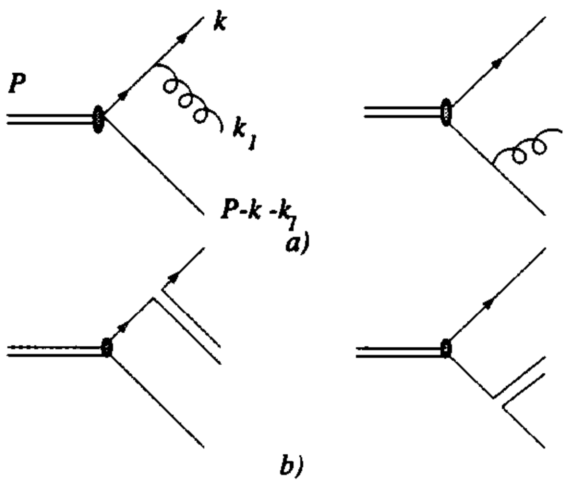

Figure 37: a) Emission of soft gluon. b) Representation as pair of dipoles in large N_c limit

In this time the $q\bar{q}$ state separates a transverse distance, $\Delta b = v_T \Delta t$,

$$\frac{\Delta b}{b} \approx \frac{z_1}{z(1-z)} \ll 1, \quad (k_1 \approx k \sim \frac{1}{b}) \tag{287}$$

Thus at least for the leading logs of z we may consider the transverse separation of the the $q\bar{q}$ pair to be fixed during the time of emission of the soft gluon. So we may write the general cross section for the interaction of the charmonium state with an external probe as the sum over the various Fock states at fixed transverse separation b

$$\Sigma(b;z) = \hat{\sigma}_{q\bar{q}}(b)\Phi_{q\bar{q}}(b;z) + \int dz_1 d^2b_1 \hat{\sigma}_{q\bar{q}g}(b,b_1)\Phi_{q\bar{q}g}(b,b_1;z,z_1) + \ldots \tag{288}$$

The function $\Phi_X(b,\{b_i\};z,\{z_i\})$ is the light cone probability density for the state X with i gluons specified by the transverse coordinates $\{b_i\}$ and longitudinal momentum fractions $\{z_i\}$. In the large N_C limit the cross section $\hat{\sigma}_{q\bar{q}g}(b,b_1)$ simplifies, because the gluon has the colour structure of a $q\bar{q}$ pair. The $q\bar{q}g$ state scatters like the sum of two colour dipoles.

$$\begin{aligned} \hat{\sigma}_{q\bar{q}}(b) &= \hat{\sigma}_d(b) \\ \hat{\sigma}_{q\bar{q}g}(b,b_1) &= \hat{\sigma}_d(b_1) + \hat{\sigma}_d(b_2) \end{aligned} \tag{289}$$

The probability density Φ is calculable for very soft gluons. We will consider first of all the state with one additional gluon. In the soft approximation $\Phi^{[1]}_{q\bar{q}g}(b,b_1;z,z_1)$ is calculable in terms of $\Phi^{[0]}_{q\bar{q}}(b;z)$ which is the zeroth order LC probability density for the $q\bar{q}$ state.

Consider a $q\bar{q}$ state, where the momentum of the antiquark is labelled by k, z. The light cone wave function for the $q\bar{q}$ state may be written as,

$$\Psi^{[0]}_{\alpha\beta}(k; z) \tag{290}$$

The corresponding expression in the fourier conjugate space, (the impact parameter) is

$$\Psi^{[0]}_{\alpha\beta}(b; z) = \int \frac{d^2k}{(2\pi)^2}\Psi^{[0]}_{\alpha\beta}(k; z)e^{ik\cdot b} \tag{291}$$

where the quark is at the origin and the anti-quark is separated from it by a transverse distance b.

The light cone wave function after the gluon emission is,

$$\Psi^{[1]}_{\alpha\beta}(\vec{b}, \vec{b}_1; z, z_1) = \frac{-igt^A}{\pi}\Psi^{[0]}_{\alpha\beta}(\vec{b}; z)\Big[\frac{b_1\cdot\epsilon}{b_1^2} - \frac{b_2\cdot\epsilon}{b_2^2}\Big] \tag{292}$$

where b_1 and b_2 are the transverse separations of the gluon from the quark and anti-quark as shown in Fig. 38.

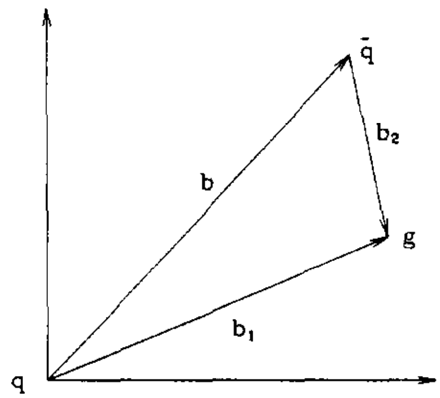

Figure 38: Position in tranverse plane

The corresponding expression in momentum space is more complicated, but can be derived by from the normal covariant amplitude, using the tricks of Lecture 2.

$$\Psi^{[1]}_{\alpha\beta}(k, k_1; z, z_1) = -2igt^A\Big[\Psi^{[0]}_{\alpha\beta}(k; z) - \Psi^{[0]}_{\alpha\beta}(k + k_1; z)\Big]\frac{\epsilon\cdot k_1}{k_1^2} \tag{293}$$

The relationship between the two is demonstrated using

$$\int \frac{d^2k}{(2\pi)^2}\frac{\epsilon\cdot k}{k^2}e^{ik\cdot b} = \frac{i}{2\pi}\frac{\epsilon\cdot b}{b^2} \tag{294}$$

We define the LC probabilities as

$$\begin{aligned}\Phi^{[0]}_{q\bar{q}}(b; z) &= \sum\Big|\Psi^{[0]}_{\alpha\beta}(b; z)\Big|^2 \\ \Phi^{[1]}_{q\bar{q}g}(b, b_1; z, z_1) &= \frac{1}{2\pi}\frac{1}{2z_1}\sum\Big|\Psi^{[1]}_{\alpha\beta}(\vec{b}, \vec{b}_1; z, z_1)\Big|^2\end{aligned} \tag{295}$$

Using Eq. (292) we can show that the LC probability density for the $q\bar{q}g$ state is, ($t^A t^A \approx N_c/2$),

$$\Phi^{[1]}_{q\bar{q}g}(b, b_1; z, z_1) = \frac{\alpha_S N_c}{2\pi^2} \frac{1}{z_1} \Big[\frac{b^2}{b_1^2 b_2^2}\Big] \Phi^{[0]}_{q\bar{q}}(b; z) \tag{296}$$

The change in the $q\bar{q}$ probability density due to the existence of the qqg state is,

$$\Phi^{[1]}_{q\bar{q}g}(b; z) = \int_{z_0}^{z} dz_1 \int d^2 b_1 \Phi^{[1]}_{q\bar{q}g}(b, b_1; z, z_1) \tag{297}$$

The variable z_0 is a cut-off. In order to maintain the normalization of the wave function we must remove this amount from the radiationless $q\bar{q}$ state.

$$\Phi^{[1]}_{q\bar{q}}(b; z) = \Phi^{[0]}_{q\bar{q}}(b, z) - \Phi^{[1]}_{q\bar{q}g}(b, z) \tag{298}$$

Therefore using Eq. (288) we find that the result for the cross section is

$$\Sigma(b, z) = \hat{\sigma}_d(b)\Phi^{[1]}_{q\bar{q}}(b; z) + \int dz_1 d^2 b_1 \Big[\hat{\sigma}_d(b_1) + \hat{\sigma}_d(b_2)\Big] \Phi^{[1]}_{q\bar{q}g}(b, b_1; z, z_1) \tag{299}$$

where the cross section of the $q\bar{q}g$ state is represented as the sum of two dipoles as appropriate in the large N_c limit. Using Eq. (297) we may write this as,

$$\Sigma(b, z) = \hat{\sigma}_d(b)\Phi^{[0]}_{q\bar{q}}(b; z) + \int dz_1 d^2 b_1 \Big[\hat{\sigma}_d(b_1) + \hat{\sigma}_d(b_2) - \hat{\sigma}_{q\bar{q}}(b)\Big] \Phi^{[1]}_{q\bar{q}g}(b, b_1; z, z_1) \tag{300}$$

where $b_2 = b_1 - b$.

We therefore find that the dipole cross section may be written as

$$\Sigma(b, z) = \sigma(b, \xi)\Phi^{[0]}_{q\bar{q}}(b; z) \tag{301}$$

where $\sigma(b, \xi)$ is an effective dipole cross section and $\xi = \ln z/z0$.

$$\sigma(b, \xi) = \hat{\sigma}_d(b) + \frac{\alpha_S N_c}{2\pi^2} \xi d^2 b_1 \Big[\hat{\sigma}_d(b_1) + \hat{\sigma}_d(b_2) - \hat{\sigma}_d(b)\Big] \Big[\frac{b^2}{b_1^2 b_2^2}\Big] \tag{302}$$

The soft gluon emits softer gluons so that in higher orders in α_S we may write this as

$$\frac{d\sigma(\xi, b)}{d\xi} = K \otimes \sigma(\xi, b) \tag{303}$$

where K is the kernel in the transverse plane given by Eq. (302). We have thus derived a differential equation for the z dependence of the cross section for the interaction of the state. The growth of the cross section with energy is due to the growth of the number of dipoles. Eq. (303) is the BFKL equation for the effective dipole cross-section.

3.4.1 Solution of BFKL equation

We seek solutions of this equation which have a power behaviour as a function of b^2. This is most easily accomplished by taking moments.

$$\begin{aligned} S(\gamma,\xi) &= \int_0^\infty \frac{db^2}{b^2}(b^2)^{-\gamma}\sigma(b,\xi) \\ \sigma(b,\xi) &= \frac{1}{2\pi i}\int_C d\gamma\,(b^2)^\gamma S(\gamma,\xi) \end{aligned} \tag{304}$$

The equation becomes

$$\frac{dS(\gamma,\xi)}{d\xi} = \kappa(\gamma)S(\gamma,\xi) \tag{305}$$

leading to a solution of the form

$$S(\gamma,\xi) = S(\gamma,0)\exp[\kappa(\gamma)\xi] \tag{306}$$

The function κ is given by,

$$\begin{aligned} \kappa(\gamma) &= \frac{N_c\alpha_S}{\pi}\chi(\gamma) \\ \chi(\gamma) &= \frac{1}{2\pi}\int d^2b_1\Big[\left(\frac{b_1^2}{b^2}\right)^\gamma + \left(\frac{b_2^2}{b^2}\right)^\gamma - 1\Big]\frac{b^2}{b_1^2b_2^2} \end{aligned} \tag{307}$$

Setting $\left|\vec{b}\right| = b, \vec{b}_1 = b\vec{x}$ and $\vec{b}_2 = b(\vec{x}-\vec{n})$ we find that the expression for χ

$$\chi(\gamma) = \frac{1}{2\pi}\int d^2\vec{x}\,\frac{2(\vec{x}^{\,2})^\gamma - 1}{[\vec{x}^2][(\vec{x}-\vec{n})^2]} \tag{308}$$

The evaluation of the integral in Eq. (308) requires some care and the introduction of a regulator in the intermediate stages, to deal with the ultra-violet divergences which occur in the individual terms at $b_1 = 0$ and $b_2 = 0$. We choose to regulate the integral by continuing to d dimensions.

$$\chi(\gamma) = \lim_{d\to 2}\frac{1}{2\pi}\int d^d\vec{x}\left[\frac{2}{[\vec{x}^2]^{1-\gamma}[(\vec{x}-\vec{n})^2]} - \frac{1}{[\vec{x}^2][(\vec{x}-\vec{n})^2]}\right] \tag{309}$$

We now introduce Feynman parameters using,

$$\frac{1}{a^pb^q} = \frac{\Gamma(p+q)}{\Gamma(p)\Gamma(q)}\int_0^1 dy\frac{y^{p-1}(1-y)^{q-1}}{[ay+b(1-y)]^{p+q}} \tag{310}$$

After performing the shift $\vec{z} = \vec{x} - (1-y)\vec{n}$ we obtain $t = \vec{z}^{\,2}, 2\rho = d-2$

$$\begin{aligned} \chi(\gamma) &= \lim_{d\to 2}\int\frac{d\Omega_d}{4\pi}\int_0^1 dy\int_0^\infty dt\,t^\rho\left[\frac{2(1-\gamma)y^{-\gamma}}{[t+y(1-y)]^{2-\gamma}} - \frac{1}{[t+y(1-y)]^2}\right] \\ \chi(\gamma) &= \lim_{\rho\to 0}\frac{\Gamma^2(1+\rho)}{\rho}\left[\frac{\Gamma(\rho+\gamma)\Gamma(1-\gamma-\rho)}{\Gamma(2\rho+\gamma)\Gamma(1-\gamma)} - \frac{\Gamma(1+\rho)\Gamma(1-\rho)}{\Gamma(1+2\rho)}\right] \end{aligned} \tag{311}$$

The result for χ is,

$$\chi(\gamma) = 2\psi(1) - \psi(\gamma) - \psi(1-\gamma). \tag{312}$$

Here ψ is the digamma function, $\psi(x) = \Gamma'(x)/\Gamma(x)$ for which $\psi(1) = -\gamma_E$. The function χ has a minimum at $\gamma = \frac{1}{2}$ and is plotted in Fig. 39. The function χ has the

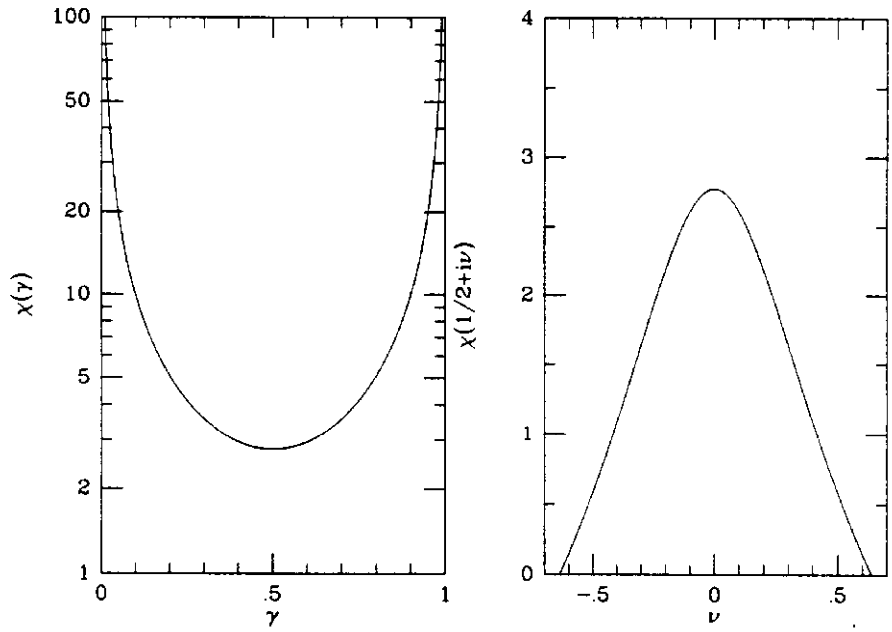

Figure 39: The function $\chi(\gamma)$ (a) on the real axis. (b) parallel to the imaginary axis.

following limiting behaviors:

$$\chi(\gamma) \rightarrow 4\ln 2 + 14\zeta(3)\left(\gamma - \tfrac{1}{2}\right)^2 + O\left(\left(\gamma - \tfrac{1}{2}\right)^4\right), \text{ when } \gamma \rightarrow \tfrac{1}{2}; \tag{313}$$

$$\chi(\gamma) \rightarrow \frac{1}{\gamma} + 2\zeta(3)\gamma^2 + O(\gamma^4), \text{ when } \gamma \rightarrow 0, \tag{314}$$

where $\zeta(3) = 1.20206$.

The growth of the cross section with energy is fixed by taking the inverse Mellin transform of Eq. (306)

$$\sigma(b,\xi) = \frac{1}{2\pi i}\int_C d\gamma \exp[\xi\kappa(\gamma) + \gamma\ln b^2] S(\gamma, 0) \tag{315}$$

The contour is in parallel to the imaginary axis, for $0 < \text{Re } \gamma < 1$. For large ξ this integral may be calculated by saddle point method,

$$\sigma(b,\xi) = (b^2)^{\frac{1}{2}} \frac{\exp[\kappa(\frac{1}{2})\xi]}{\sqrt{\xi\kappa''(\frac{1}{2})}} \exp[-\tfrac{1}{2}\frac{\ln^2 b^2}{\xi\kappa''(\frac{1}{2})}] S(\tfrac{1}{2}, 0) \tag{316}$$

There are two features of this formula which are remarkable. First the behaviour goes like $\sqrt{b^2}$. Second the behaviour with energy goes like s^δ, where

$$\delta = \kappa(\tfrac{1}{2}) = 12\frac{\alpha_S}{\pi}\ln 2 \tag{317}$$

We now should make the connection with the normal gluon distribution function. The gluon distribution function is related to the cross section $\sigma(b,\xi)$. In fact let us define the unintegrated gluon distribution

$$xg(x,Q^2) = \int^{Q^2} dk^2 f(x,k^2) \tag{318}$$

f is the number density of gluon per unit of rapidity with a transverse momentum k^2. We have that

$$f(x,b^2) \sim \frac{\sigma(b,\xi)}{\pi b^2} \tag{319}$$

Hence we derive the asymptotic result that

$$f(x,k^2) \sim \frac{1}{x^\delta}\frac{1}{\sqrt{k^2}} \tag{320}$$

References

1) R.P. Feynman, 'Photon Hadron Interactions', W.A. Benjamin, New York (1972).

2) G. Altarelli and G. Parisi, *Nucl. Phys.* **B126** (1977) 298.

3) G. Altarelli, *Phys. Rep.* **81** (1982) 1.

4) G. Curci, W. Furmanski and R. Petronzio, *Nucl. Phys.* **B175** (1980) 27;
W. Furmanski and R. Petronzio, *Phys. Lett.* **97B** (1980) 437.

5) EMC collaboration: J.J. Aubert et al., *Nucl. Phys.* **B259** (1985) 189.

6) BCDMS collaboration: A.C. Benvenuti et al., *Phys. Lett.* **223B** (1989) 490.

7) M. Virchaux, Proceedings of 'QCD, 20 years later', eds, P.M. Zerwas and H.A. Kastrup, World Scientific, 1993.

8) B.R. Webber, Proc. 27th Int. Conf. on High Energy Physics, Glasgow, Scotland, July 1994.

9) D.W. Duke and J.F. Owens, *Phys. Rev.* **D30** (1984) 49.

10) A.D. Martin, R.G. Roberts and W.J. Stirling, *Phys. Rev.* **D37** (1988) 1161;
Mod. Phys. Lett. **A4** (1989) 1135.

11) A.D. Martin, R.G. Roberts and W.J. Stirling, RAL-preprint RAL 94-055 (1994);
P.N. Harriman, A.D. Martin, R.G. Roberts and W.J. Stirling, *Phys. Rev.* **D42** (1990) 798.

12) R.K. Ellis, Z. Kunszt and E.M. Levin, *Nucl. Phys.* **B420** (1994) 517.

13) I. Abt et al., *Nucl. Phys.* **407** (1993) 515.

14) J. Martin, Proceedings of the XVI Symposium on Lepton-Photon Interactions, Cornell University, Ithaca, NY (August 1993).

15) L.V. Gribov, E.M. Levin and M.G. Ryskin, *Phys. Rep.* **100** (1982) 1.

16) J.C. Collins and D.E. Soper, *Ann. Rev. Nucl. Part. Sci.* **37** (1987) 383.

17) Ya. Ya. Balitsky and L. N. Lipatov, *Sov. J. Nucl. Phys.* **28** (1978) 822;
E. A. Kuraev, L. N. Lipatov, and V. S. Fadin, *Sov. Phys. JETP* **45** (1977) 199.

18) A. H. Mueller, *Nucl. Phys.* **B415** (1994) 373;
A. H. Mueller and B. Patel, *Nucl. Phys.* **B425** (1994) 471.

19) N. N Nikolaev, B. G. Zakharov and V. R. Zoller, Jülich preprint, KFA-IKP(TH)-1994-01.

4 Applications of perturbative QCD

4.1 Fragmentation functions

The methods of the QCD improved parton model can also be applied to the decay of a parton. In this case it is appropriate to define a decay function D_i^H which describes the fragmentation of a parton i into a hadron H which carries a fraction z of the longitudinal momentum of the incoming parton. These fragmentation functions are most easily extracted from e^+e^- annihilation. If q is the timelike four momentum of the virtual photon, $q^2 = Q^2$, the pion inclusive cross-section may be written as

$$\frac{d\sigma}{dz} = 3\sigma_0 \sum_f e_f^2 \left[D_q^\pi(z,t) + D_{\bar{q}}^\pi(z,t)\right], \tag{321}$$

$$z = \frac{2p \cdot q}{Q^2}, \quad t = \ln\frac{Q^2}{\Lambda^2}. \tag{322}$$

σ_0 is the cross-section for the production of a single colour of quark-antiquark pair. In magnitude it is equal to the muon pair production cross section weighted by the square of the charge, Eq. (99). Because of the effects of collinear radiation the fragmentation functions satisfy the timelike modification of the Gribov-Lipatov-Altarelli-Parisi equation,

$$\begin{aligned} \frac{d}{dt}D_q(z,t) &= \frac{\alpha_S(Q^2)}{2\pi}\left[D_q^\pi \otimes P_{qq} + D_g^\pi \otimes P_{gq}\right] \\ \frac{d}{dt}D_g(z,t) &= \frac{\alpha_S(Q^2)}{2\pi}\left[\left(D_q^\pi + D_{\bar{q}}^\pi\right) \otimes P_{qg} + D_g^\pi \otimes P_{gg}\right]. \end{aligned} \tag{323}$$

In the leading logarithmic approximation, (lowest order in α_S), the GLAP kernels are the same as for the space-like parton distribution case. The first perturbative corrections to the timelike GLAP kernels are given in Ref. [1]. Corrections to the short-distance cross-section are discussed in Ref. [2].

Note that the multiplicity of hadrons in the final state is given by,

$$\sum_H \int dz \frac{d\sigma}{dz} = < n^H > \sigma_{tot} \tag{324}$$

The total multiplicity is related to the first moment of the fragmentation function.

4.1.1 Multiplicities in jets

An important problem for the design of experimental detectors is the multiplicity of hadrons to be expected in a high energy jet. A high energy jet can be thought of as a highly virtual timelike parton which decreases its virtuality by parton bremsstrahlung leading to a parton shower. At some low virtuality the methods of perturbation theory cease to be valid and the partons fragment into hadrons. In QCD the hadron multiplicity of a gluon jet is not perturbatively calculable because this last phase of jet evolution is not described by perturbation theory. However the growth of the multiplicity with the energy of the jet is determined by the parton shower and is a reliable prediction of perturbative QCD. We take as our starting point the GLAP evolution equation for the gluon fragmentation function. We work in the moment representation where N is the moment variable.

$$\frac{d}{dt}D_g(N,t) = \frac{\alpha_S(Q^2)}{2\pi}\Big[D_g(N)\gamma_{gg}(N) + \ldots\Big]. \tag{325}$$

The driving term is the growth of the multiplicity of the gluons so we neglect the effects of mixing with quarks. From Eq. (254) the anomalous dimension corresponding to the gluon splitting function contains a singularity for $N = 1$. Retaining only this most singular term we see that,

$$\frac{dD_g(N,t)}{dt} \sim \frac{\alpha_S}{2\pi}\frac{2N_c}{(N-1)}D_g(N,t). \tag{326}$$

The singularity at $N = 1$ is due to the emission of soft gluons. Because of this singularity it would appear at first sight that the growth of the multiplicity is not calculable in QCD.

This is not correct. The energy dependence of the multiplicity is calculable because of an interplay of kinematic and dynamic effects as we shall now demonstrate. Remember that the GLAP equation in lowest order corresponds to a summation of ladder diagrams with each rung containing a single gluon exchange.

In x space we may write the GLAP equation as,

$$\frac{dD_g(Q^2,\mu^2,x)}{d\ln Q^2} = \frac{\alpha_S(Q^2)}{2\pi}\int_x^1 \frac{dz}{z}P(z)D_g\left(Q^2,\mu^2,\frac{x}{z}\right) \tag{327}$$

where $D_g(Q^2,\mu^2,x)$ is the fragmentation function of a gluon of all virtualities up to scale Q^2. μ^2 is some lower cut-off at which the fragmentation becomes non-perturbative. Let us introduce the unintegrated fragmentation function $d(r^2,\mu^2,x)$ which describes the fragmentation of gluons of virtuality r^2.

$$D_g\left(Q^2,\mu^2,x\right) = \int_{\mu^2}^{Q^2}\frac{dr^2}{r^2}d\left(r^2,\mu^2,x\right) \tag{328}$$

In terms of d, the GLAP equation can be rewritten as,

$$d\left(k^2,\mu^2,x\right) \sim \int_x^1 \frac{dz}{z}P(z)\int_{\mu^2}^{k^2}\frac{dr^2}{r^2}\frac{\alpha_S(r^2)}{2\pi}d\left(r^2,\mu^2,\frac{x}{z}\right) \tag{329}$$

In Eq. (329) we have dropped a homogeneous term which vanishes for $k^2 \gg \mu^2$. In

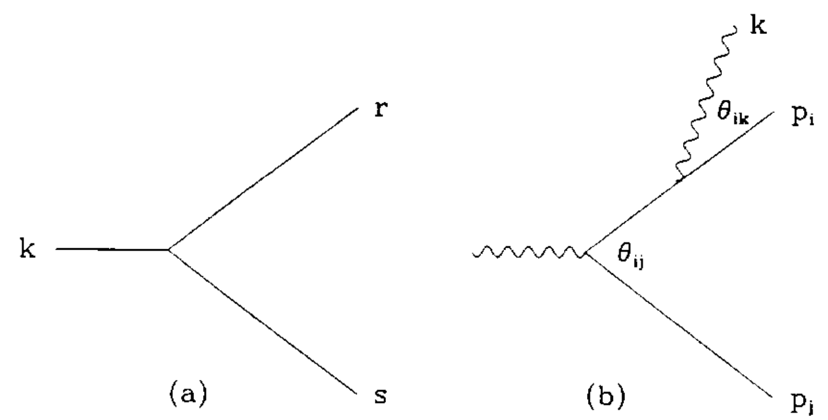

Figure 40: (a) Kinematics of parton cascade. (b) Angular ordering in QED

this form the ladder structure of the equation is manifest. Since we are interested in the emission of very soft gluons it is important to consider the kinematics of the gluon splitting in detail. A gluon of momentum k splits into two gluons of momenta r and s as shown in Fig. 40(a). We now introduce the Sudakov decompositions for k, r and s.

$$k^\mu = p^\mu + \frac{k^2}{2} n^\mu, \quad r^\mu = z p^\mu + \frac{r^2 + r_T^2}{2z} n^\mu + r_T^\mu, \quad s^\mu = (1-z) p^\mu + \frac{s^2 + r_T^2}{2(1-z)} n^\mu - r_T^\mu \quad (330)$$

The maximum value of r^2 comes from the region $r_T^2 = s^2 = 0$ and is limited by

$$z k^2 > r^2 \quad (331)$$

Correctly including this kinematic constraint Eq. (329) becomes,

$$d\left(k^2, \mu^2, x\right) \sim \int_x^1 \frac{dz}{z} P(z) \int_{\mu^2}^{k^2 z} \frac{dr^2}{r^2} \frac{\alpha_S(r^2)}{2\pi} d\left(r^2, \mu^2, \frac{x}{z}\right) \quad (332)$$

In terms of the original fragmentation function D_g this can be written as,

$$k^2 \frac{\partial}{\partial k^2} D_g\left(k^2, x\right) \sim \frac{\alpha(\ln k^2)}{2\pi} \int_x^1 \frac{dz}{z} \frac{2N_c}{z} D_g\left(k^2 z, \frac{x}{z}\right) \quad (333)$$

Note that the rescaling of $k^2 \to k^2 z$ would be non-leading were it not for the singularity of P_{gg} at $z = 0$. For simplicity we first consider the case of a fixed coupling constant, defined as $\bar{\alpha} = N_c \alpha_S / \pi$. Taking moments of Eq. (333) we obtain,

$$\frac{d}{d \ln k^2} D_g(N, k^2) = \bar{\alpha} \int_0^1 \frac{dz}{z} z^{N-1} D_g(N, z k^2). \quad (334)$$

If D_g has the anomalous dimension $\gamma(N)$, then $D_g(N) \sim (k^2)^{\gamma(N)}$. With this ansatz D_g satisfies,

$$\left[\frac{d}{d\ln k^2} - \gamma(N)\right] D_g(N) = 0 \tag{335}$$

and from Eq. (334) γ is given by,

$$\gamma(N) = \frac{\bar{\alpha}}{N-1+\gamma(N)}. \tag{336}$$

Solving the quadratic equation we obtain the following answer for γ.

$$\gamma(N) = -\frac{(N-1)}{2} \pm \sqrt{\left(\frac{(N-1)^2}{4} + \bar{\alpha}\right)} = \frac{\bar{\alpha}}{(N-1)} - \frac{\bar{\alpha}^2}{(N-1)^3} + \dots \tag{337}$$

Note that the resummed $\gamma(N)$ is finite for $N = 1$ although every term in the power series expansion is infinite. The emission of very soft gluons has been inhibited by kinematics and the divergence at $N = 1$ has been tamed.

Eq. (337) is still the wrong answer for the anomalous dimension in QCD, because for very soft gluons it is not sufficient to consider only the ladder graphs which are included in the GLAP equation. The GLAP equation treats correctly all logarithms of Q^2 but not all logs of $1/x$. Interference graphs are as important as ladder graphs. Remarkably it turns out in explicit calculation[3] that the net effect of the interference graphs is to remove all the contributions of the ladder graphs in all regions in which the emission angles are not ordered down the cascade.

The correct answer in QCD is given by the ladder graphs with a dynamical constraint that the gluons are emitted at ever decreasing angles as we proceed to lower virtualities. The result for $\gamma(N)$ is,

$$\gamma(N) = -\frac{(N-1)}{4} + \sqrt{\frac{(N-1)^2}{16} + \frac{\bar{\alpha}}{2}} = \frac{\bar{\alpha}}{(N-1)} - \frac{2\bar{\alpha}^2}{(N-1)^3} + \dots \tag{338}$$

Solving Eq. (325) we obtain,

$$D_g(Q^2, N) \sim \exp \int^{\ln Q^2} \gamma_N\left(\bar{\alpha}_S\left(t\right)\right) dt \tag{339}$$

which for the first moment gives,

$$D_g(Q^2, N=1) \sim \exp \int^{\ln Q^2} \sqrt{\frac{N_c}{2\pi b t}} dt \sim \exp\, 2\sqrt{\frac{N_c}{2\pi b} \ln Q^2/\mu^2} \tag{340}$$

A heuristic explanation of the reason for angular ordering can be obtained[4] by using an analogy from QED. Consider an incoming virtual photon which decays into an electron-positron pair as shown in Fig. 40(b). An additional soft photon of momentum k is subsequently radiated from the electron-positron pair. In old-fashioned perturbation theory the virtual state consisting of an electron and a positron differs in energy from the final state containing an electron, a positron and a soft photon by an energy ΔE,

$$\begin{aligned}\Delta E &= (E_i + E_j + E_k) - (E_{i+k} + E_j) \\ &= \sqrt{|\vec{p}_i|^2 + m^2} + |\vec{k}| - \sqrt{\left(\vec{p}_i + \vec{k}\right)^2 + m^2}.\end{aligned} \tag{341}$$

In the limit of very large $\vec{p}_i$ and small θ_{ik} this becomes,

$$\Delta E \sim |\vec{k}|\theta_{ik}^2. \tag{342}$$

By the uncertainty principle the virtual electron state lives for a time Δt which is approximately given by

$$\Delta t \sim \frac{1}{|\vec{k}|\theta_{ik}^2} \sim \frac{\lambda_T}{\theta_{ik}}, \tag{343}$$

where $\lambda_T \sim 1/k_T \sim 1/(k\theta_{ik})$ is the transverse wavelength of the emitted soft photon. In this interval of time Δt the electron and positron separate a transverse distance given by

$$\Delta d = \Delta t \theta_{ij} = \frac{\lambda_T \theta_{ij}}{\theta_{ik}}. \tag{344}$$

If $\theta_{ik} > \theta_{ij}$, the separation of the electron and positron is less than the transverse wavelength of the emitted soft photon. The emitted soft photon perceives the electron-positron pair as an unresolved charge neutral object and no radiation occurs. If, on the other hand, the emitted photon lies within the cone described by the electron positron pair, $\theta_{ik} > \theta_{ij}$, the radiation is uninhibited.

This example indicates the reason for angular ordering in QED. The generalisation of this argument to QCD is complicated by the fact that the gluons themselves carry colour charge, but the angular ordering result persists.

4.1.2 Colour coherence

For the case of three jet events in e^+e^- annihilation the coherence of the radiation from the hard partons leads to the *string effect* [5,6]. In the language of perturbative QCD, the string effect is a result of constructive and destructive interference. Of course, it is entirely unremarkable that such interference effects should be observed in quantum field theory. However, it is interesting to note that the experimental evidence indicates that such interference effects survive the hadronisation process, a phenomenon which the authors of ref.[6] call *local parton-hadron duality.*

At sufficiently high energy, the colour structure of the hard final state partons will determine the pattern of associated radiation. Because the distribution of this radiation is not significantly altered by hadronisation, the observed pattern of the hadrons which lie between the jets will depend on the colour of the partons participating in the hard scatter.

We illustrate the derivation of the angle ordered approximation in the process $e^+e^- \to q\bar{q}g$. Soft gluons are emitted only inside certain angular regions around the directions of the hard partons q, $\bar{q}$ and g. We introduce the angular variables $\zeta_i = 1 - \cos\theta_i$, where θ_i is the angle between the soft gluon and the hard parton i, and $\zeta_{ij} = 1 - \cos\theta_{ij}$ where θ_{ij} is the angle between hard partons i and j. In terms of these variables the eikonal factor which describes the emission of soft radiation may be written,

$$[ij] = g^2 \frac{p_i.p_j}{p_i.kk.p_j} = \frac{g^2}{|k|^2} \frac{\zeta_{ij}}{\zeta_i\zeta_j} = \Big(\frac{g^2}{2\,|k|^2} \Big\{\frac{\zeta_{ij}}{\zeta_i\zeta_j} + \frac{1}{\zeta_i} - \frac{1}{\zeta_j}\Big\}\Big) + \big(i \leftrightarrow j\big) \tag{345}$$

where $|k|$ represents the energy of the soft gluon. The lines i and j are colour connected. The eikonal factor in Eq. (345) is the same as the factor obtained in the soft photon approximation in QED[7]. The expression in braces contains the collinear pole at $\zeta_i = 0$ but not that at $\zeta_j = 0$. Furthermore, when averaged over the azimuthal angle ϕ_i around the direction of hard parton i, it vanishes outside the cone $\zeta_i = \zeta_{ij}$. In fact [3,6],

$$\int \frac{d\phi_i}{2\pi} \left\{\frac{\zeta_{ij}}{\zeta_i\zeta_j} + \frac{1}{\zeta_i} - \frac{1}{\zeta_j}\right\} = \frac{2}{\zeta_i}\Theta(\zeta_{ij} - \zeta_i). \tag{346}$$

Hence, averaging each term with respect to azimuth around its direction of singularity, we may write,

$$[ij] = \frac{g^2}{|k|^2\,\zeta_i}\Theta(\zeta_{ij} - \zeta_i) + \frac{g^2}{|k|^2\,\zeta_j}\Theta(\zeta_{ij} - \zeta_j). \tag{347}$$

Eq. (347) has the same form as the incoherent radiation emission result but with a dynamically imposed angular constraint on the phase space.

An elegant way to examine the pattern of soft radiation associated with a hard scattering event is to compare e^+e^- annihilation into three jets with annihilation into two jets and a photon. The parton final states are $q\bar{q}g$ and $q\bar{q}\gamma$. From Eq. (347) we deduce that the soft radiation (and hence the particle flow) is dynamically constrained by angular ordering to lie between the colour connected lines. For the purposes of this argument the colour degrees of freedom of the gluon can be approximately regarded as a $q\bar{q}$ system, with the quark part connected to the outgoing antiquark line and the antiquark part connected to the outgoing quark line as shown in Fig. 41(a). The soft radiation in the $q\bar{q}g$ event is then expected to lie predominantly between the gluon and the quark and the gluon and the antiquark. In contrast for the $q\bar{q}\gamma$ event the radiation occurs predominantly between the quark and the antiquark. Data from the TPC collaboration[8] are shown in Fig. (42). The jets are ordered in energy $E_1 > E_2 > E_3$ and the third jet is assumed to be the gluon. In the angular regions near the cores of jets 1 and 2, the distributions of the $q\bar{q}g$ and $q\bar{q}\gamma$ events agree very well. In the region between jets 1 and 2, opposite the gluon jet or the photon, the data show a depletion in particle production in $q\bar{q}g$ compared to $q\bar{q}\gamma$.

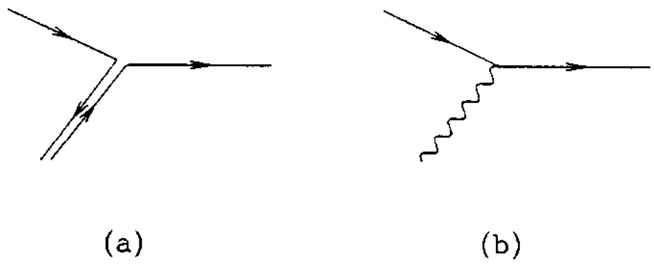

Figure 41: Colour structure of (a) $q\bar{q}g$ event (b) $q\bar{q}\gamma$ event

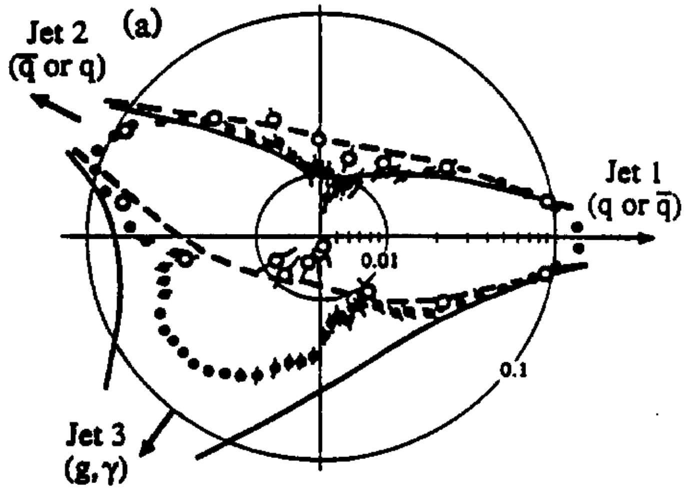

Figure 42: Particle flow on a logarithmic scale as a function of angle in the plane of the event for $q\bar{q}\gamma$, (open points) and $q\bar{q}g$, (closed points).

It is an interesting property of the theory that the emission of gluons in the final state can, to a good approximation, be represented by a semi-classical parton 'branching' or 'cascade' picture, i.e. the quarks emit gluons which in turn emit more gluons etc. This property is evident, for example, in Eq. (347) where it is shown that the eikonal factor obtained from the interference of Feynman diagrams can be approximately represented as a sum of probabilities. The quarks produced at the photon vertex after an e^+e^- annihilation have 'virtuality' (i.e. are off mass shell) of the order of the total centre-of-mass energy. Parton branching then takes place, reducing the virtualities, until all the final state partons have virtualities of the order of the hadronic mass scale ($O(1$ GeV$)$). This first stage of the fragmentation can be described in terms of QCD perturbation theory. Finally, the partons 'hadronise' to give final states made up of pions, kaons and other hadrons. The hadronisation of the partons cannot be described perturbatively, but instead can be *modelled*, the parameters being determined by fitting to the data. In this way jet fragmentation Monte Carlos are constructed. Different ways of performing the non-perturbative hadronisation lead to different models [9] which can be compared with experimental data.

4.2 Factorization in hadron-hadron collisions

We now turn from processes involving hadrons in the final state to processes with hadrons in the initial state. The property of factorization allows us to use the QCD parton model to describe inelastic processes involving hadrons. In this section we shall present a simple classical model that illustrates why the factorization property holds and when it should fail. As an example of a hard process we consider the production of a massive vector boson V – in practice a massive photon, W or Z – in the collision of two hadrons,

$$H_1(P_1) + H_2(P_2) \to V + X. \tag{348}$$

This is in many respects the simplest hard process involving two hadrons, since the observed vector boson in the final state carries no colour and its leptonic decay products are observed directly. It is therefore the easiest to analyse and consequently has received the most theoretical attention.

A very important theoretical issue in this process is whether the partons in hadron H_1, through the influence of their colour fields, change the distribution of partons in hadron H_2 before the hard scattering occurs, thus spoiling the simple parton picture. Soft gluons which are created long before the collision are potentially troublesome in this respect.

We shall argue that soft gluons do not in fact spoil the parton picture, using a simple model [10] from classical electrodynamics. The vector potential due to a current density J is given by [11]

$$A^\mu(t,\vec{x}) = \int dt' d\vec{x}' \, \frac{J^\mu(t',\vec{x}')}{|\vec{x}-\vec{x}'|} \, \delta(t' + |\vec{x}-\vec{x}'| - t), \quad c = 1, \tag{349}$$

where the delta function provides the retarded behaviour required by causality. Consider a particle with charge e travelling in the positive z direction with constant velocity β. The non-zero components of the current density are

$$\begin{aligned} J^t(t,\vec{x}) &= e\delta(\vec{x} - \vec{r}(t)) \\ J^z(t,\vec{x}) &= e\beta\delta(\vec{x} - \vec{r}(t)), \quad \vec{r}(t) = \beta t\hat{z}, \end{aligned} \tag{350}$$

where $\hat{z}$ is a unit vector in the z direction. The charge passes through the origin at time $t = 0$. At an observation point (the position of hadron H_2) described by coordinates x, y and z, the vector potential at time t due to the passage of the fast moving charge is obtained by performing the integrations in Eq. (349) using the current density of Eq. (350). The result is

$$A^t(t,\vec{x}) = \frac{e\gamma}{\sqrt{[x^2 + y^2 + \gamma^2(\beta t - z)^2]}}$$

$$
\begin{aligned}
A^x(t,\vec{x}) &= 0 \\
A^y(t,\vec{x}) &= 0 \\
A^z(t,\vec{x}) &= \frac{e\gamma\beta}{\sqrt{[x^2+y^2+\gamma^2(\beta t-z)^2]}},
\end{aligned}
\tag{351}
$$

where $\gamma^2 = 1/(1-\beta^2)$. The observation point can be taken to be the target hadron H_2 which is at rest near the origin, so that $\gamma \approx s/m^2$. Note that for large γ and fixed non-zero $(\beta t - z)$ some components of the potential tend to a constant independent of γ, suggesting that there will be non-zero fields which are not in coincidence with the arrival of the particle, even at high energy. However at large γ the potential is a pure gauge piece and hence does not lead to E or B fields. The implication of this result is that a covariant formulation which uses the vector potential A will not be the most efficient method to handle this problem, since we will have large fields which ultimately have no physical effect.

To show that these large terms in the vector potential have no effect we compute the field strengths from Eq. (351). The leading terms in γ cancel and the field strengths are of order $1/\gamma^2$ and hence of order m^4/s^2. For example, the electric field along the z direction is

$$
E^z(t,\vec{x}) = F^{tz} \equiv \frac{\partial A^z}{\partial t} + \frac{\partial A^t}{\partial z} = \frac{e\gamma(\beta t - z)}{[x^2+y^2+\gamma^2(\beta t-z)^2]^{\frac{3}{2}}}. \tag{352}
$$

Thus the force experienced by a charge in the hadron H_2, at any fixed time before the arrival of the quark, decreases as m^4/s^2. There are residual interactions which distort the distribution of quarks in hadron H_2, but their effects vanish at high energies. A breakdown of factorization at order $1/s^2$ is therefore to be expected in perturbation theory and has been demonstrated explicitly in ref. [12]. Note that these effects are due to the long range nature of the vector field. In the realistic case of an incoming colour neutral hadron there are no long-range colour fields. It is therefore possible that the factorization property is even better in the full theory than in perturbation theory.

4.3 Jet Physics

4.3.1 Kinematics and jet definition

The scattering of two hadrons provides two broad band beams of incoming partons. These incoming beams have a spectrum of longitudinal momenta determined by the parton distribution functions. The centre of mass of the parton-parton scattering is normally boosted with respect to the centre of mass of the two incoming hadrons. It is therefore useful to classify the final state in terms of variables which transform simply under longitudinal boosts. For this purpose we introduce the rapidity y, the transverse momentum p_T and the azimuthal angle ϕ. In terms of these variables, the four components of momenta of a particle of mass m may be written as

$$p^\mu = \left(\sqrt{p_T^2 + m^2}\cosh(y), p_T \sin\phi, p_T \cos\phi, \sqrt{p_T^2 + m^2}\sinh(y)\right). \tag{353}$$

The rapidity y is therefore defined by

$$y = \frac{1}{2}\ln\left(\frac{E + p_z}{E - p_z}\right), \tag{354}$$

and is additive under the restrictive class of Lorentz transformations corresponding to a boost along the z direction. Rapidity differences are boost invariant.

In practice the rapidity is normally replaced by the pseudorapidity η,

$$\eta = -\ln\tan(\frac{\theta}{2}), \tag{355}$$

which coincides with the rapidity in the $m \to 0$ limit. It is a more convenient variable experimentally, since the angle θ from the beam direction is measured directly in the detector. It is also standard to use the transverse *energy* rather than the transverse *momentum* for similar reasons. Many methods can be used to define what is meant by a jet. There is no best definition, but one must be sure that both theoretical and experimental analyses use the same definition. A commonly used definition of a jet is a cluster of transverse energy E_T in a cone of size ΔR, where

$$\Delta R = \sqrt{[(\Delta y)^2 + (\Delta\phi)^2]}. \tag{356}$$

In the two-dimensional y, ϕ plane, lines of constant ΔR describe a circle around the axis of the jet. The cone size can be chosen at the experimentalist's convenience, and the measured jet cross-section will depend on the value chosen.

4.3.2 Two-jet cross sections

In QCD, two-jet events result when an incoming parton from one hadron scatters off an incoming parton from the other hadron to produce two high transverse momentum partons which are observed as jets. From momentum conservation the two final state partons are produced with equal and opposite momenta in the subprocess centre-of-mass frame. If only two partons are produced, and the relatively small intrinsic transverse momentum of the incoming partons is neglected, then the two jets will be back-to-back in azimuth and balanced in transverse momentum in the laboratory frame.

For a $2 \to 2$ parton scattering process

$$\text{parton}_i(p_1) + \text{parton}_j(p_2) \to \text{parton}_k(p_3) + \text{parton}_l(p_4), \tag{357}$$

described by a matrix element M, the parton cross section is

$$\frac{E_3 E_4 d^6\hat{\sigma}}{d^3p_3 d^3p_4} = \frac{1}{2\hat{s}}\frac{1}{16\pi^2}\overline{\sum}|M|^2\,\delta^4(p_1 + p_2 - p_3 - p_4), \tag{358}$$

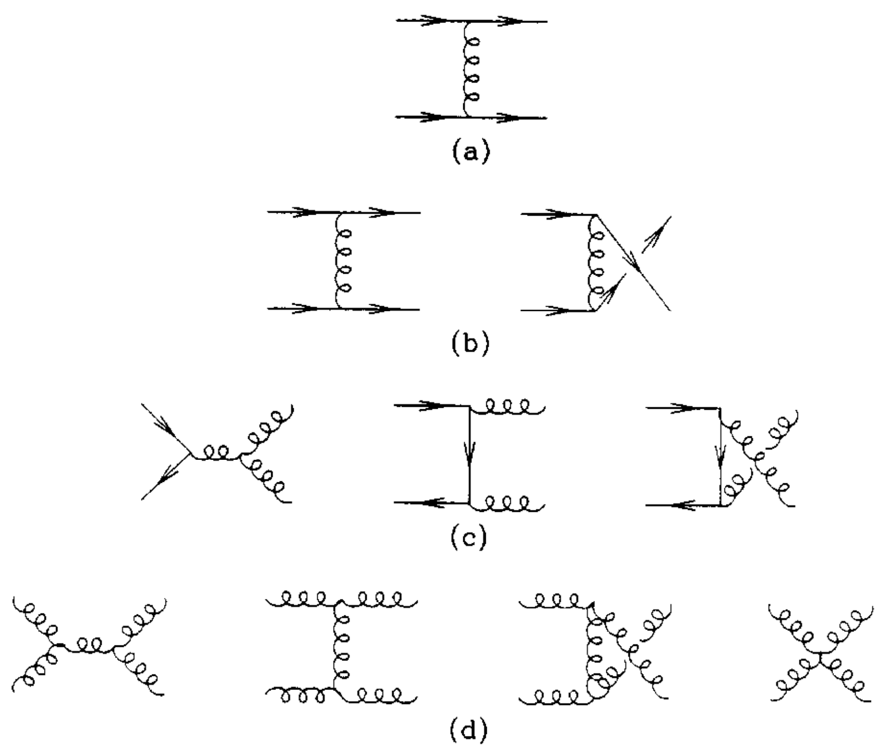

Figure 43: Diagrams for jet production

All parton processes which contribute in lowest order can be derived from the diagrams shown in Fig. 43 by including other diagrams which are related by crossing. Expressions for the leading order matrix elements squared $\overline{\sum}|M|^2$, averaged and summed over initial and final state spins and colours are given in Table 5 in the notation $\hat{s} = (p_1 + p_2)^2$, $\hat{t} = (p_1 - p_3)^2$ and $\hat{u} = (p_2 - p_3)^2$. The value of these matrix elements at 90 degrees, also shown in Table 5, gives an idea of the importance of the subprocesses.

The two-jet cross section may be written as a sum of terms each representing the contribution to the cross section due to a particular combination of incoming (i, j) and outgoing (k, l) partons. Using Eq. (358) the result for the two jet inclusive cross section is,

$$\frac{d^3\sigma}{dy_3 dy_4 dp_T^2} = \frac{1}{16\pi s^2} \sum_{i,j} \sum_{k,l} (\frac{f_i(x_1, \mu)}{x_1})(\frac{f_j(x_2, \mu)}{x_2}) \overline{\sum} |M(ij \to kl)|^2 \frac{1}{1 + \delta_{kl}} \quad (359)$$

where the $f_i(x, \mu)$ represent the number distributions for partons of type i ($i = u, \bar{u}, d, \bar{d}, g, \ldots$ etc.), evaluated at momentum scale μ, and y_3 and y_4 represent the laboratory rapidities of the outgoing partons. For massless partons the rapidities and pseudorapidities may be used interchangeably. The Kronecker delta function introduces the statistical factor necessary for identical final state partons. If we

Process	$\sum\lvert M\rvert^2/g^4$	$\theta^* = \pi/2$
$q\,q' \to q\,q'$	$\frac{4}{9}\,\frac{\hat{s}^2+\hat{u}^2}{\hat{t}^2}$	2.22
$q\,q \to q\,q$	$\frac{4}{9}\,(\frac{\hat{s}^2+\hat{u}^2}{\hat{t}^2}+\frac{\hat{s}^2+\hat{t}^2}{\hat{u}^2})-\frac{8}{27}\,\frac{\hat{s}^2}{\hat{u}\hat{t}}$	3.26
$q\,\overline{q} \to q'\,\overline{q'}$	$\frac{4}{9}\,\frac{\hat{t}^2+\hat{u}^2}{\hat{s}^2}$	0.22
$q\,\overline{q} \to q\,\overline{q}$	$\frac{4}{9}\,(\frac{\hat{s}^2+\hat{u}^2}{\hat{t}^2}+\frac{\hat{t}^2+\hat{u}^2}{\hat{s}^2})-\frac{8}{27}\,\frac{\hat{u}^2}{\hat{s}\hat{t}}$	2.59
$q\,\overline{q} \to g\,g$	$\frac{32}{27}\,\frac{\hat{t}^2+\hat{u}^2}{\hat{t}\hat{u}}-\frac{8}{3}\frac{\hat{t}^2+\hat{u}^2}{\hat{s}^2}$	1.04
$g\,g \to q\,\overline{q}$	$\frac{1}{6}\,\frac{\hat{t}^2+\hat{u}^2}{\hat{t}\hat{u}}-\frac{3}{8}\frac{\hat{t}^2+\hat{u}^2}{\hat{s}^2}$	0.15
$g\,q \to g\,q$	$-\frac{4}{9}\,\frac{\hat{s}^2+\hat{u}^2}{\hat{s}\hat{u}}+\frac{\hat{u}^2+\hat{s}^2}{\hat{t}^2}$	6.11
$g\,g \to g\,g$	$\frac{9}{2}\,(3-\frac{\hat{t}\hat{u}}{\hat{s}^2}-\frac{\hat{s}\hat{u}}{\hat{t}^2}-\frac{\hat{s}\hat{t}}{\hat{u}^2})$	30.4

Table 5: The invariant matrix elements squared $\sum\lvert M\rvert^2$ for two-to-two parton subprocesses with massless partons. The colour and spin indices are averaged (summed) over initial (final) states.

assume that the detector and jet algorithm are 100% efficient, the rapidities and p_T of the outgoing jets may be identified with those of the outgoing partons.

We now consider the kinematics of the two produced jets in detail. The laboratory rapidity (y_{boost}) of the two-parton system and the equal and opposite rapidities ($\pm y^*$) of the two jets in the parton-parton centre-of-mass system are given in terms of the observed rapidities by:

$$y_{\text{boost}} = (y_3 + y_4)/2, \quad y^* = (y_3 - y_4)/2. \tag{360}$$

For a massless parton the centre of mass scattering angle θ^* is given by,

$$\cos\theta^* = \frac{p_z^*}{E^*} = \frac{\sinh(y^*)}{\cosh(y^*)} = \tanh(\frac{y_3 - y_4}{2}), \tag{361}$$

where $y^* = y_3 - y_{\text{boost}}$. The measurement of the rapidity difference of the two jets in the laboratory frame determines the subprocess centre of mass scattering angle θ^*.

The longitudinal momentum fractions of the incoming partons x_1 and x_2 in Eq. (359) are given in terms of p_T, y_3 and y_4 by momentum conservation:

$$x_1 = x_T e^{y_{\text{boost}}} \cosh(y^*), \quad x_2 = x_T e^{-y_{\text{boost}}} \cosh(y^*), \quad y_{\text{boost}} = \frac{1}{2} \ln \frac{x_1}{x_2}, \tag{362}$$

where $x_T = 2p_T/\sqrt{s}$. Lastly, the invariant mass of the jet-jet system can be written as,

$$M_{JJ}^2 = \hat{s} = 4p_T^2 \cosh^2(y^*). \tag{363}$$

Given a knowledge of the parton distributions from deep inelastic scattering experiments, Eq. (359) may be used to make leading order QCD predictions for jet production in hadron-hadron collisions. For example, the inclusive jet cross section at the parton level may be obtained by integrating Eq. (358) over the momentum of one of the jets.

$$\frac{Ed^3\hat{\sigma}}{d^3p} \equiv \frac{d^3\hat{\sigma}}{dyd^2p_T} = \frac{1}{2\hat{s}} \frac{1}{8\pi^2} \overline{\sum} |M|^2 \, \delta(\hat{s} + \hat{t} + \hat{u}), \tag{364}$$

where $\hat{t}$ and $\hat{u}$ are fixed by $\hat{s}$ and the centre of mass scattering angle,

$$\begin{aligned} \hat{t} &= -\frac{\hat{s}}{2}\,(1 - \cos\theta^*) \\ \hat{u} &= -\frac{\hat{s}}{2}\,(1 + \cos\theta^*). \end{aligned} \tag{365}$$

Again assuming that the detector and jet algorithm are 100% efficient, so that $p^\mu_{\text{jet}} = p^\mu_{\text{parton}}$, the single jet inclusive cross section is obtained from Eq. (364) by folding in the parton distribution functions:

$$\begin{aligned} \frac{E_J d^3\hat{\sigma}}{d^3p_J} &= \frac{1}{16\pi^2 s} \sum_{i,j,k,l=q,g} \int_0^1 \frac{dx_1}{x_1} \frac{dx_2}{x_2} \, f_i(x_1,\mu) f_j(x_2,\mu) \\ &\quad \overline{\sum} |M(ij \to kl)|^2 \, \frac{1}{1+\delta_{kl}} \delta(\hat{s} + \hat{t} + \hat{u}). \end{aligned} \tag{366}$$

Note that this result corresponds to massless quarks and gluons and that no distinction is made between quark and gluon jets.

4.3.3 Comparison with experiment

Although large p_T jet production has been studied at different machines over a period of many years, the definitive data are from the high energy $p\bar{p}$ colliders, i.e. from the UA1 and UA2 collaborations at the CERN $p\bar{p}$ collider ($\sqrt{s}$ = 546 GeV and 630 GeV) and from the CDF and D0 collaborations at the FNAL Tevatron collider ($\sqrt{s}$ = 1.8 TeV). It appears that only at these very high collision energies does the identification and measurement of large p_T jets become relatively unambiguous. At

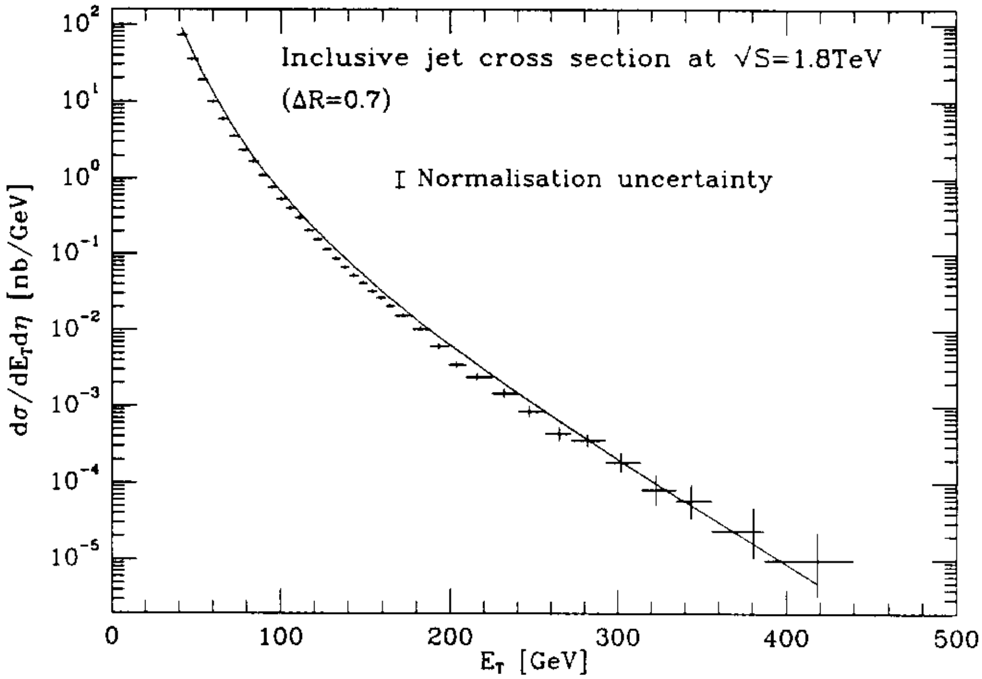

Figure 44: Jet E_T distribution from the CDF collaboration, compared with a next-to-leading order QCD prediction from [13].

lower energies it is difficult to separate the jets from the other 'underlying' hadrons in the event.

Two quantities are particularly useful for comparing theory with experiment. The first is the jet p_T distribution, obtained from the inclusive cross section by

$$\frac{Ed^3\sigma}{d^3p} \equiv \frac{d^3\sigma}{d^2p_T dy} \longrightarrow \frac{1}{2\pi E_T}\frac{d^2\sigma}{dE_T d\eta} \tag{367}$$

where the third term follows if we assume that the jets are approximately massless.

Fig. 44 shows the jet E_T distribution in $p\bar{p}$ collisions at $\sqrt{s} = 1.8$ TeV, from the CDF collaboration. The curve is the QCD prediction, calculated in next-to-leading order (i.e. $O(\alpha_S^3)$) by S. D. Ellis et al. [13] and using the HMRSB parton distributions from reference [14]. The next-to-leading order contributions considerably reduce the dependence on the scale parameter μ, and allow a more precise treatment of effects due to the finite width of the jet. The agreement is excellent, especially considering that there are essentially no free parameters in the theoretical prediction. Note that at this energy about half the cross section comes from quark-gluon scattering, the other half coming from gluon-gluon scattering at the lower E_T end, and quark-(anti)quark scattering at the high E_T end.

The second quantity of interest is the jet angular distribution. In the parton-parton centre of mass, the angular distribution is sensitive to the form of the $2 \rightarrow 2$

matrix elements. The differential cross section for a jet pair of mass M_{JJ} produced at an angle θ^* to the beam direction in the jet-jet centre of mass can readily be obtained from Eq. (359) using the transformation

$$dp_T^2 dy_3 dy_4 \equiv \frac{s}{2} dx_1 dx_2 d\cos\theta^* \tag{368}$$

to give

$$\begin{aligned} \frac{d^2\sigma}{dM_{JJ}^2 d\cos\theta^*} &= \sum_{i,j=q,g} \int_0^1 dx_1 dx_2\, f_i(x_1,\mu) f_j(x_2,\mu)\, \delta(x_1 x_2 s - M_{JJ}^2)\, \frac{d\hat{\sigma}^{ij}}{d\cos\theta^*} \\ &= \sum_{\{ij\}} \frac{\tau_J}{s} \frac{dL_{ij}(\tau_J,\mu)}{d\tau_J} \frac{d\hat{\sigma}^{ij}}{d\cos\theta^*}, \end{aligned} \tag{369}$$

with $\tau_J = M_{JJ}^2/s$ and

$$\frac{d\hat{\sigma}^{ij}}{d\cos\theta^*} = \sum_{k,l} \frac{1}{32\pi M_{JJ}^2} \overline{\sum} |M(ij \to kl)|^2 \frac{1}{1+\delta_{kl}} \tag{370}$$

Note that for each subprocess the $d\hat{\sigma}/d\cos\theta^*$ is symmetrised in $\hat{t}$ and $\hat{u}$ (unless $k \equiv l$). Thus, for example,

$$\frac{d\hat{\sigma}^{u\bar{d}}}{d\cos\theta^*} = \frac{\pi\alpha_S^2}{2M_{JJ}^2} \frac{4}{9} \left[\frac{4+(1+\cos\theta^*)^2}{(1-\cos\theta^*)^2} + \frac{4+(1-\cos\theta^*)^2}{(1+\cos\theta^*)^2} \right]. \tag{371}$$

Numerically the most important subprocesses are $gg \to gg$, $gq \to gq$ and $q\bar{q} \to q\bar{q}$. For each of these, the θ^* distributions have the familiar Rutherford scattering behaviour at small angle, characteristic of the exchange of a vector boson in the t-channel:

$$\frac{d\hat{\sigma}}{d\cos\theta^*} \sim \frac{1}{\sin^4(\frac{\theta^*}{2})}. \tag{372}$$

It is convenient to plot the data in terms of the variable χ, which removes the Rutherford singularity [15],

$$\chi = \frac{1+\cos\theta^*}{1-\cos\theta^*}. \tag{373}$$

In the small angle limit ($\chi \to \infty$) the cross section differential in χ is then

$$\frac{d\hat{\sigma}}{d\chi} \sim \text{constant}. \tag{374}$$

Data on the angular distribution from the CDF collaboration are shown in Fig. 45, with the leading order QCD prediction. Again, there is excellent agreement. Note that these data automatically rule out certain other quark scattering mechanisms.

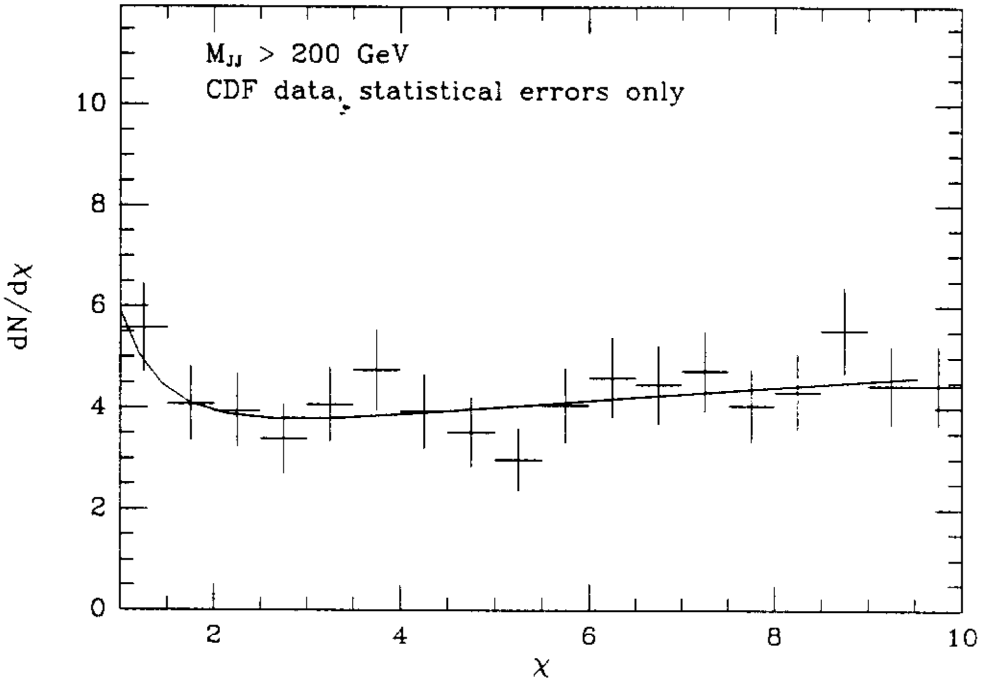

Figure 45: χ distribution from the CDF collaboration compared with the leading order QCD prediction

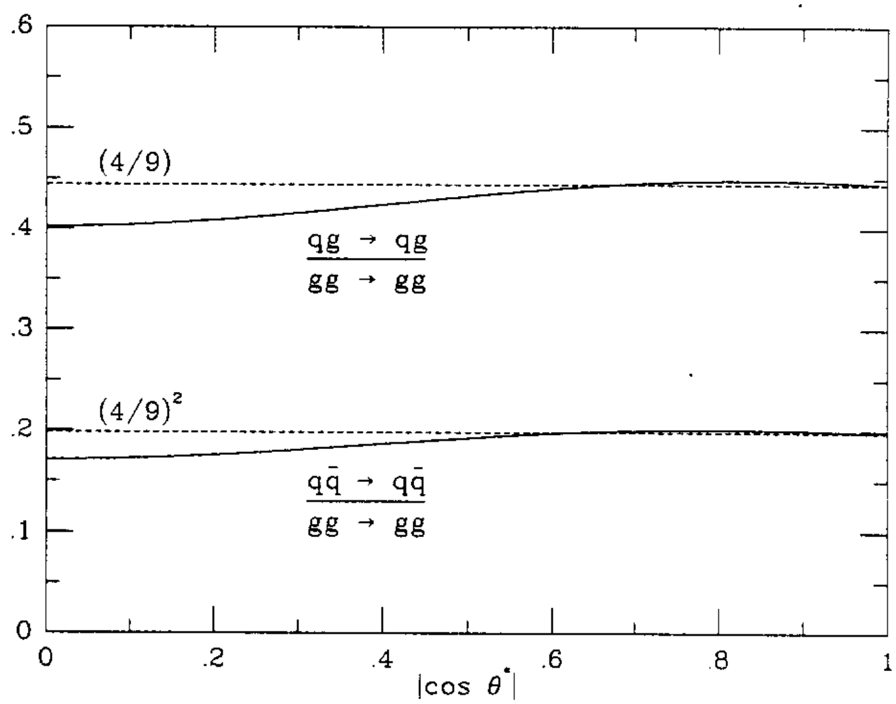

Figure 46: Quark-antiquark and quark-gluon angular distributions, normalised to that for $gg \to gg$

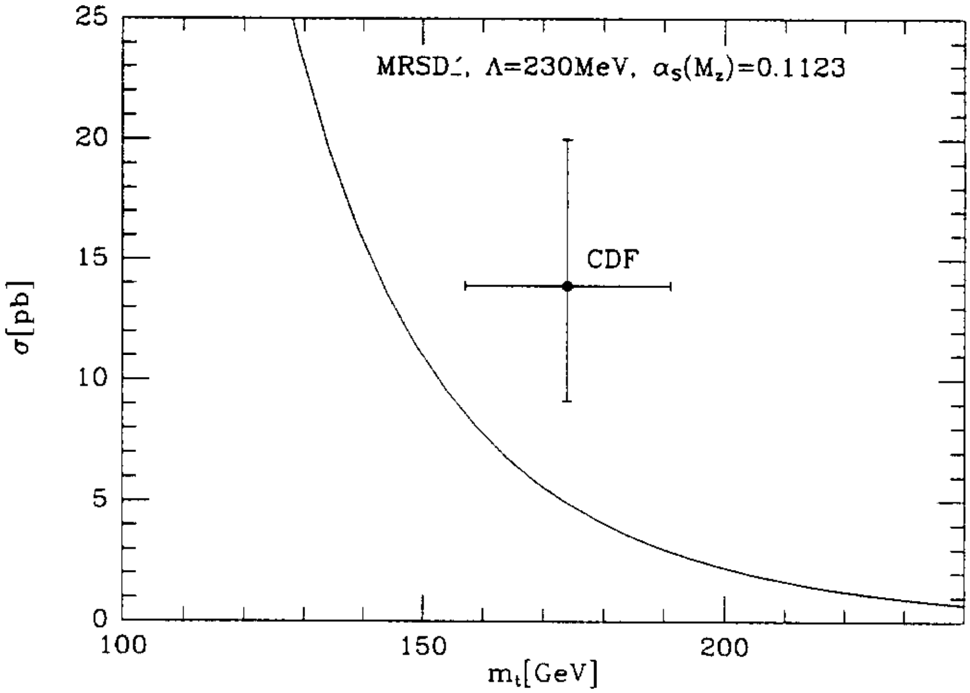

Figure 47: Comparison of the CDF point with the theory.

Fermi constant. In the limit in which $m_t \gg M_W$ the total t width is given by,

$$\Gamma(t \to bW) = \frac{G_F m_t^3}{8\pi\sqrt{2}} |V_{tb}|^2 \approx 1.73 \text{ GeV} \left(\frac{m_t}{174 \text{ GeV}}\right)^3 . \tag{377}$$

When the top quark is so heavy that the width becomes bigger than a typical hadronic scale the top quark decays before it hadronises. Hadrons containing the top quark do not have time to form. Gluon radiation associated with the top and bottom quarks is considered in ref. [19].

Although not strictly related to my topic, I would like to insert here a parenthetical remark on the relative size of the errors in the measurement of m_W and m_t. One way of estimating the importance of the errors in these measurements is the role which they play in constraining the mass of the standard model Higgs. This is shown in Fig. 48, kindly provided for me by Takeuchi. Fig. 48 shows that in the 'metric' provided by the sensitivity to the standard model Higgs boson, we may already consider the top quark mass to well measured relative to the mass of the W.

4.4.2 Bottom quark production

Results for bottom quark production at CDF[20] are shown in Fig. 49. Results on bottom quark production have also been presented by D0[21]. The first thing to notice about the bottom quark cross-section is that it is large at collider energies. Roughly

For example, a model in which quarks scatter by exchanging a *scalar* gluon would give a less singular behaviour ($\sin^{-2}(\theta^*/2)$) at small angle.

It is also interesting to note that the angular dependences of the dominant subprocesses are very similar. Fig. 46 shows the $\cos\theta^*$ dependence of the $qg \to qg$ and $q\bar{q} \to q\bar{q}$ subprocesses normalised to $gg \to gg$. These ratios are evidently rather constant at the numerical values 4/9 and $(4/9)^2$ respectively. This can be understood in terms of the colour structure of the Feynman diagrams. Thus to a good approximation the $gg \to gg$ subprocess can be used as the 'universal' subprocess in the result given in Eq. (369), i.e. the angular dependence effectively factors out leaving a convolution of parton distributions. This is called the *single effective subprocess approximation* [15].

4.4 Experiments on heavy quark production

4.4.1 Top quark production

The CDF collaboration working at the Fermilab collider at $\sqrt{S} = 1.8$ TeV has presented evidence for production of the top quark[16]. Although the observed events present many of the features expected of the top quark there are a number of aspects of the data which are not yet understood by the top quark hypothesis. The D0 collaboration (as of July 1994) observes no significant signal above background[17].

On the assumption that the events observed by CDF are due to the production of the top quark, the value found for the top quark mass is[16]

$$m_t = 174 \pm 10^{+13}_{-12}\ \text{GeV} \tag{375}$$

Using this value of the mass, CDF find that the value of the top quark cross section is

$$\sigma_{t\bar{t}}(m_t = 174\ \text{GeV}) = 13.9^{+6.1}_{-4.8}\ \text{pb} \tag{376}$$

The theoretical expectation for this cross section, calculated in second order QCD, is shown in Fig. 47 as a function of m_t. The measured cross section is somewhat above theoretical expectation. In the remainder of this lecture I will review the calculation of theoretical cross section in order to assess its reliability. Of course it would be especially interesting if the experimental cross section were significantly bigger than the theoretical expectation. We know very little about the top quark and phenomena not foreseen in the standard model could be occurring. Candidates for such phenomena are described in refs. [18].

For the rest of this lecture I shall consider the top quark to be described by the minimum standard model and to decay to a W and a b-quark. When the mass of the top is much larger than the mass of the W it decays to an on-shell W boson and a b quark. This process has a semi-weak decay rate involving only one power of the

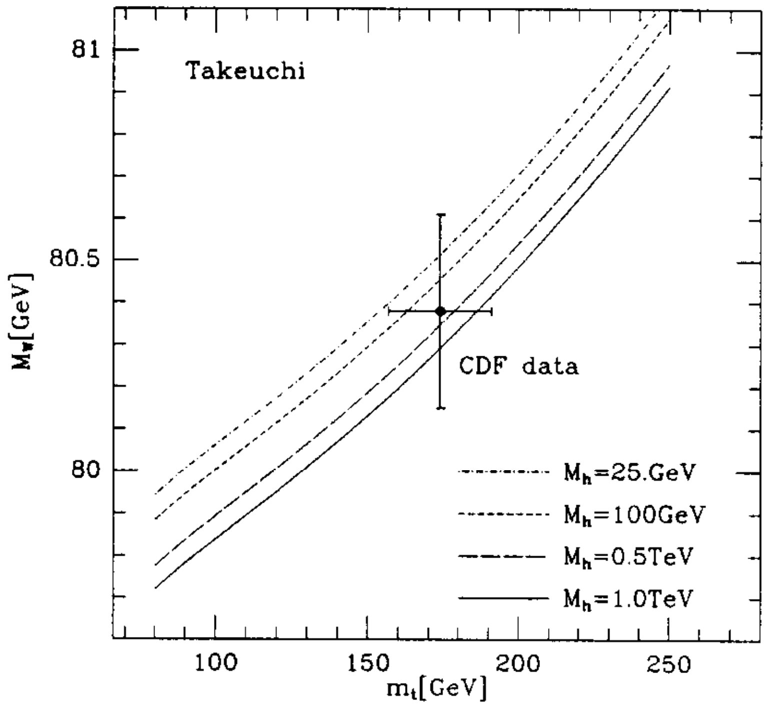

Figure 48: M_W vs. m_t compared to the standard model

one event in a thousand contains a bottom quark. At a luminosity of 10^{31} cm^{-2}s^{-1}, the rate of production of b quarks with a p_T greater than 5 GeV is 100 Hz. This enormous flux of b quarks offers the possibility to do much b physics at a hadron collider. It is important to emphasize that hadron machines produce many types of hadrons containing b quarks. The physics topics which they can observe are complementary to the physics at a dedicated e^+e^- collider.

From Fig. 49 we see that the cross section for bottom quark production as measured by CDF lies somewhat above the theoretical prediction. The D0 data (not shown) lies closer to the theoretical prediction[21]. Fig. 49 also gives some idea of the time evolution of the measurement. The major reason for the change in the measured cross-section has been the measurement by CDF of the fraction of J/ψ's coming from b quarks. In the analysis of the earlier data this fraction was assumed to be 63%. The number measured with the help of the Silicon Vertex detector is close to 30%. The Silicon Vertex (SVX) detector performs a precise measurement of tracks and can determine whether or not vertices are displaced from the primary interaction point. The prompt production of J/ψ's (*i.e.*the production not coming from the decay of a B-meson) is an interesting theoretical and experimental topic in its own right, but it will not be be discussed further[22].

Since both the production of top and bottom seem to lie above the theoretical prediction it is interesting to go back and review the theoretical status of these processes. We shall see that, despite the superficial similarity, they are in fact rather

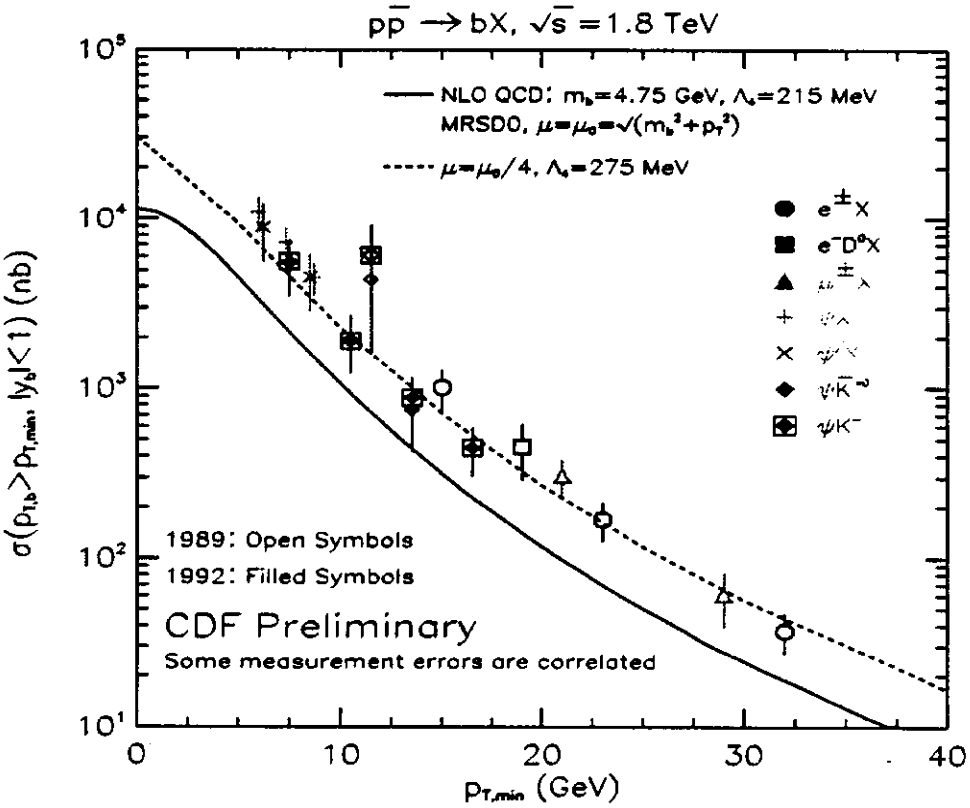

Figure 49: Bottom cross section from CDF

different processes with completely different theoretical errors.

4.5 The theory of heavy quark production

The leading order processes for the production of a heavy quark Q of mass m are,

$$\begin{array}{ll} (a) & q(p_1) + \overline{q}(p_2) \to Q(p_3) + \overline{Q}(p_4) \\ (b) & g(p_1) + g(p_2) \to Q(p_3) + \overline{Q}(p_4) \;, \end{array} \tag{378}$$

where the four momenta of the partons are given in brackets. The Feynman diagrams which contribute to the matrix elements squared in $O(g^4)$ are shown in Fig. 50. The invariant matrix elements squared [23,24] which result from the diagrams in Fig. 50 are given in Table 6. The matrix elements squared have been averaged (summed) over initial (final) colours and spins, (as indicated by $\overline{\sum}$). In order to express the matrix elements in a compact form, we have introduced the following notation for the ratios of scalar products,

$$\tau_1 = \frac{2p_1.p_3}{\hat{s}}, \quad \tau_2 = \frac{2p_2.p_3}{\hat{s}}, \quad \rho = \frac{4m^2}{\hat{s}}, \quad \hat{s} = (p_1 + p_2)^2. \tag{379}$$

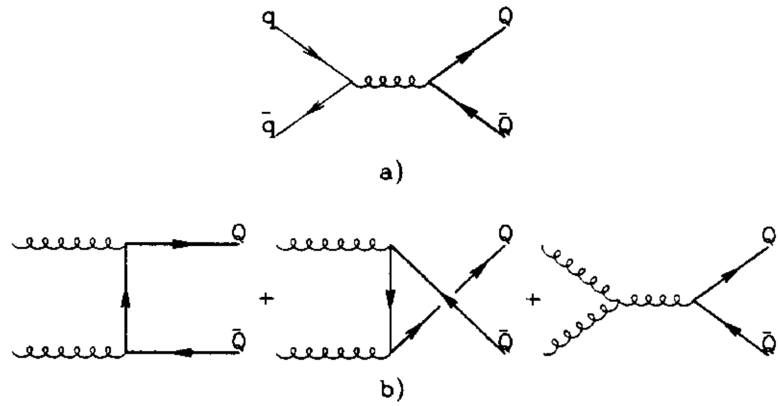

Figure 50: Lowest order Feynman diagrams for heavy quark production

Process	$\overline{\sum}\|M\|^2/g^4$
$q\,\overline{q} \to Q\,\overline{Q}$	$\frac{4}{9}\left(\tau_1^2+\tau_2^2+\frac{\rho}{2}\right)$
$g\,g \to Q\,\overline{Q}$	$\left(\frac{1}{6\tau_1\tau_2}-\frac{3}{8}\right)\left(\tau_1^2+\tau_2^2+\rho-\frac{\rho^2}{4\tau_1\tau_2}\right)$

Table 6: Lowest order processes for heavy quark production. $\overline{\sum}|M|^2$ is the invariant matrix element squared. The colour and spin indices are averaged (summed) over initial (final) states.

In leading order the short distance cross section is obtained from the invariant matrix element in the normal fashion [7]:

$$d\hat{\sigma}_{ij} = \frac{1}{2\hat{s}}\frac{d^3p_3}{(2\pi)^3 2E_3}\frac{d^3p_4}{(2\pi)^3 2E_4}(2\pi)^4\delta^4(p_1+p_2-p_3-p_4)\overline{\sum}|M_{ij}|^2 . \tag{380}$$

The first factor is the flux factor for massless incoming particles. The other terms come from the phase space for two-to-two scattering.

Consider first the differential cross section. Let us denote the momenta of the incoming hadrons, which are moving in the z direction, by P_1 and P_2 and the square of the total centre of mass energy by s where $s=(P_1+P_2)^2$.

$$d\sigma(P_1,P_2) = \sum_{i,j}\int dx_1 dx_2\, F_i(x_1,\mu)F_j(x_2,\mu)\, d\hat{\sigma}_{ij}(\alpha_S(\mu), x_1P_1, x_2P_2) \tag{381}$$

The functions F_i are the number densities of light partons (gluons, light quarks and antiquarks) evaluated at a scale μ. The short distance cross section in Eq. (381) is to be evaluated for parton momenta $p_1 = x_1 P_1$, $p_2 = x_2 P_2$ and hence the square of the total parton centre of mass energy is $\hat{s} = x_1 x_2 s$, if we ignore the masses of the incoming particles. The rapidity variable for the two final state partons is defined in terms of their energies and longitudinal momenta as,

$$y = \tfrac{1}{2}\ln\left[\frac{E+p_z}{E-p_z}\right]. \tag{382}$$

Using Eqs. (380) and (381) the result for the invariant cross section may be written as,

$$\frac{d\sigma}{dy_3 dy_4 d^2 p_T} = \frac{1}{16\pi^2\hat{s}^2}\sum_{ij} x_1 F_i(x_1,\mu) x_2 F_j(x_2,\mu) \overline{\sum} |M_{ij}|^2. \tag{383}$$

The energy momentum delta function in Eq. (380) fixes the values of x_1 and x_2 if we know the value of the p_T and rapidity of the outgoing heavy quarks. In the centre of mass system of the incoming hadrons we may write the components of the parton four momenta as (E, p_x, p_y, p_z)

$$\begin{aligned} p_1 &= \tfrac{1}{2}\sqrt{s}(x_1, 0, 0, x_1) \\ p_2 &= \tfrac{1}{2}\sqrt{s}(x_2, 0, 0, -x_2) \\ p_3 &= (m_T\cosh y_3, p_T, 0, m_T\sinh y_3) \\ p_4 &= (m_T\cosh y_4, -p_T, 0, m_T\sinh y_4). \end{aligned} \tag{384}$$

Applying energy and momentum conservation we obtain,

$$x_1 = \frac{m_T}{\sqrt{s}}(e^{y_3}+e^{y_4}), \quad x_2 = \frac{m_T}{\sqrt{s}}(e^{-y_3}+e^{-y_4}), \quad \hat{s} = 2m_T^2(1+\cosh\Delta y). \tag{385}$$

The transverse mass of the heavy quarks is denoted by $m_T = \sqrt{(m^2 + p_T^2)}$ and $\Delta y = y_3 - y_4$ is the rapidity difference between the two heavy quarks.

Using Eqs. (383) and (385), we may write the cross section for the production of two massive quarks calculated in lowest order perturbation theory as,

$$\frac{d\sigma}{dy_3 dy_4 d^2 p_T} = \frac{1}{64\pi^2 m_T^4(1+\cosh(\Delta y))^2}\sum_{ij} x_1 F_i(x_1,\mu)\, x_2 F_j(x_2,\mu)\, \overline{\sum} |M_{ij}|^2. \tag{386}$$

Expressed in terms of m, m_T and Δy the matrix elements for the two processes in Table 6 are,

$$\overline{\sum} |M_{q\bar{q}}|^2 = \frac{4g^4}{9}\Big(\frac{1}{1+\cosh(\Delta y)}\Big)\Big(\cosh(\Delta y) + \frac{m^2}{m_T^2}\Big) \tag{387}$$

$$\overline{\sum} |M_{gg}|^2 = \frac{g^4}{24}\Big(\frac{8\cosh(\Delta y) - 1}{1+\cosh(\Delta y)}\Big)\Big(\cosh(\Delta y) + 2\frac{m^2}{m_T^2} - 2\frac{m^4}{m_T^4}\Big). \tag{388}$$

Note that, because of the specific form of the matrix elements squared, the cross section, Eq. (386), is damped as the rapidity separation Δy between the two heavy quarks becomes large. It is therefore to be expected that the dominant contribution to the total cross section comes from the region $\Delta y \leq 1$. Heavy quarks produced by $q\bar{q}$ annihilation are more closely correlated in rapidity than those produced by gluon-gluon fusion.

We shall now illustrate why it is plausible that heavy quark production is described by perturbation theory [25]. We consider the propagators in the diagrams shown in Fig. 50. In terms of the above variables they can be written as,

$$\begin{aligned} (p_1+p_2)^2 &= 2p_1.p_2 &&= 2m_T^2(1+\cosh\Delta y) \\ (p_1-p_3)^2-m^2 &= -2p_1.p_3 &&= -m_T^2(1+e^{-\Delta y}) \\ (p_2-p_3)^2-m^2 &= -2p_2.p_3 &&= -m_T^2(1+e^{\Delta y}). \end{aligned} \tag{389}$$

Note that the denominators are all off-shell by a quantity of least of order m^2. It is this fact which distinguishes the production of a light quark from the production of a heavy quark. When a light quark is produced by these diagrams the lower cut-off on the virtuality of the propagators is provided by the light quark mass, which is less than the QCD scale Λ. Since propagators with small virtualities give the dominant contribution, the production of a light quark will not be calculable in perturbative QCD. In the production of a heavy quark, the lower cut-off is provided by the mass m. It is therefore plausible that heavy quark production is controlled by α_S evaluated at the heavy quark scale.

Note also that the contribution to the cross section from values of p_T which are much greater than the quark mass is also suppressed. The differential cross section falls like $1/m_T^4$ and as m_T increases, the parton flux decreases because of the increase of x_1 and x_2 according to Eq. (385). Since all dependence on the transverse momentum appears in the transverse mass combination, the dominant contribution to the cross section comes from transverse momenta of the order of the mass of the heavy quark.

Thus for a sufficiently heavy quark we expect the methods of perturbation theory to be applicable. It is the mass of the heavy quark which provides the large scale in heavy quark production. The heavy quarks have transverse momenta of the order of the heavy quark mass and are produced close in rapidity. The production is predominantly central, because of the rapidly falling parton fluxes. Final state interactions which transform the heavy quarks into the observed hadrons will not change the size of the cross section. A possible mechanism which might spoil this simple picture would be the interaction of the produced heavy quark with the debris of the incoming hadrons. However these interactions with spectator partons are suppressed by powers of the heavy quark mass [26]. For a sufficiently heavy quark they can be ignored.

4.6 Higher order corrections

The results of a next-to-leading calculation are also available [27,28]. The standard perturbative QCD formula for the inclusive production of a heavy quark Q of momentum p and energy E,

$$H_A(P_1) + H_B(P_2) \to Q(p) + X \tag{390}$$

determines the invariant cross-section as follows,

$$\frac{E\, d^3\sigma}{d^3p} = \sum_{i,j} \int dx_1\, dx_2 \left[\frac{E\, d^3\hat{\sigma}_{ij}(x_1P_1, x_2P_2, p, m, \mu)}{d^3p}\right] F_i^A(x_1, \mu)\, F_j^B(x_2, \mu). \tag{391}$$

The symbol $\hat{\sigma}$ denotes the short distance cross-section from which the mass singularities have been factored. Since the sensitivity to momentum scales below the heavy quark mass has been removed, $\hat{\sigma}$ is calculable as a perturbation series in $\alpha_S(\mu^2)$. The scale μ is *a priori* only determined to be of the order of the mass m of the produced heavy quark. The corrections to Eq. (391) are suppressed by powers of the heavy quark mass.

At this point we list the parton sub-processes which contribute to the inclusive cross-sections.

$$\begin{array}{lll}
q+\overline{q} \to & Q+\overline{Q}, & \alpha_S^2, \alpha_S^3 \\
g+g \to & Q+\overline{Q}, & \alpha_S^2, \alpha_S^3 \\
q+\overline{q} \to & Q+\overline{Q}+g, & \alpha_S^3 \\
g+g \to & Q+\overline{Q}+g, & \alpha_S^3 \\
g+q \to & Q+\overline{Q}+q, & \alpha_S^3 \\
g+\overline{q} \to & Q+\overline{Q}+\overline{q}, & \alpha_S^3.
\end{array} \tag{392}$$

Note the necessity of including both real and virtual gluon emission diagrams in order to calculate the full $O(\alpha_S^3)$ cross-section. Examples of diagrams required for a full $O(\alpha_S^3)$ calculation are shown in Fig. 51.

Integrating Eq. (391) over the momentum p we obtain the total cross section for the production of a heavy quark pair,

$$\sigma(S) = \sum_{i,j} \int dx_1 dx_2\, \hat{\sigma}_{ij}(x_1x_2S, m^2, \mu^2)\, F_i^A(x_1, \mu) F_j^B(x_2, \mu) \tag{393}$$

where S is the square of the centre of mass energy of the colliding hadrons A and B.

The total short distance cross section $\hat{\sigma}$ for the inclusive production of a heavy quark from partons i, j can be written as,

$$\hat{\sigma}_{ij}(s, m^2, \mu^2) = \frac{\alpha_S^2(\mu^2)}{m^2} f_{ij}\Big(\rho, \frac{\mu^2}{m^2}\Big) \tag{394}$$

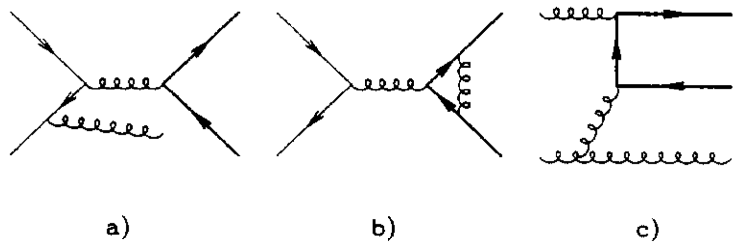

Figure 51: Examples of diagrams contributing beyond the leading order

with $\rho = 4m^2/s$, and s the square of the partonic centre of mass energy. μ is the renormalisation and factorisation scale. In ref. [27] a complete description of the functions f_{ij} including the first non-leading correction is provided. These may be used to calculate heavy quark production at any energy and heavy quark mass.

Eq. (394) completely describes the short distance cross-section for the production of a heavy quark of mass m in terms of the functions f_{ij}, where the indices i and j specify the types of the annihilating partons. The dimensionless functions f_{ij} have the following perturbative expansion,

$$f_{ij}\big(\rho, \frac{\mu^2}{m^2}\big) = f_{ij}^{(0)}(\rho) + g^2(\mu^2)\big[f_{ij}^{(1)}(\rho) + \overline{f}_{ij}^{(1)}(\rho)\ln(\frac{\mu^2}{m^2})\big] + O(g^4) \qquad (395)$$

In order to calculate the f_{ij} in perturbation theory we must perform both renormalisation and factorisation of mass singularities. The subtractions required for renormalisation and factorisation are done at mass scale μ. The dependence on μ is shown explicitly in Eq. (395). The energy dependence of the cross-section is given in terms of the ratio ρ,

$$\rho = \frac{4m^2}{s}, \quad \beta = \sqrt{1-\rho}. \qquad (396)$$

The running of the coupling constant α_S is determined by the renormalisation group,

$$\begin{aligned} \frac{d\alpha_S(\mu^2)}{d\ln\mu^2} &= -b_0\alpha_S^2 - b_1\alpha_S^3 + O(\alpha_S^4), \quad \alpha_S = \frac{g^2}{4\pi} \\ b_0 &= \frac{(33-2n_f)}{12\pi}, \quad b_1 = \frac{(153-19n_f)}{24\pi^2} \end{aligned} \qquad (397)$$

where n_f is the number of light flavours.

The quantities $f^{(1)}$ depend on the scheme used for renormalisation and factorisation. The results of ref. [27] are obtained in an extension of the $\overline{MS}$ renormalisation and factorisation scheme. They display interesting features which control the size of the $O(\alpha_S^3)$ corrections.

The functions $f_{ij}^{(0)}$ defined in Eqs. (394,395) are,

$$f_{q\bar{q}}^{(0)}(\rho) = \frac{\pi\beta\rho}{27}\Big[2+\rho\Big] \tag{398}$$

$$f_{gg}^{(0)}(\rho) = \frac{\pi\beta\rho}{192}\Big[\frac{1}{\beta}(\rho^2+16\rho+16)\ln\Big(\frac{1+\beta}{1-\beta}\Big) - 28 - 31\rho\Big] \tag{399}$$

$$f_{gq}^{(0)}(\rho) = f_{g\bar{q}}^{(0)}(\rho) = 0 \tag{400}$$

We now turn to the higher order corrections in Eq. (395) which are separated into two terms. The $\overline{f}^{(1)}(\rho)$ terms are the coefficients of $\ln(\mu^2/m^2)$ and are determined by renormalisation group arguments from the lowest order cross-sections,

$$\overline{f}_{ij}^{(1)}(\rho) = \frac{1}{8\pi^2}\Big[4\pi\, b_0\, f_{ij}^{(0)}(\rho) - \int_\rho^1 dz_1 f_{kj}^{(0)}(\frac{\rho}{z_1})P_{ki}(z_1) - \int_\rho^1 dz_2 f_{ik}^{(0)}(\frac{\rho}{z_2})P_{kj}(z_2)\Big]. \tag{401}$$

The quantities $f^{(1)}$ in Eq. (395) can only be obtained by performing a complete $O(\alpha_S^3)$ calculation. The functions $f^{(0)}, f^{(1)}$ and $\overline{f}^{(1)}$ are shown plotted in

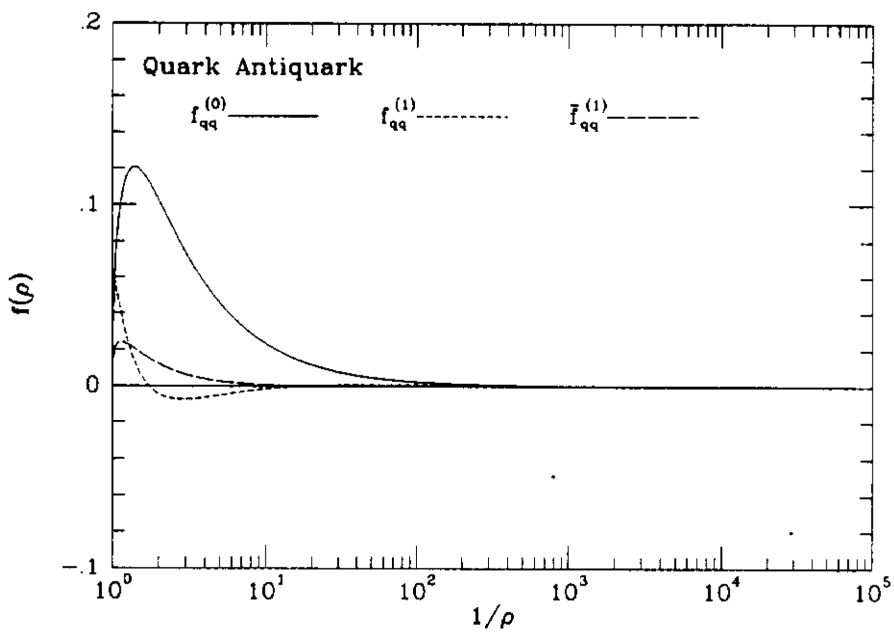

Figure 52: Quark antiquark contributions to short distance cross-section

Figs. 52,53,54 for the cases of quark-antiquark, gluon-gluon and gluon-quark fusion respectively. Notice the strikingly different behaviour of the gluon-gluon and gluon-quark higher order terms in the high energy limit, $\rho \to 0$. These latter processes allow the exchange of a spin one gluon in the t-channel and are therefore dominant in the high energy limit.

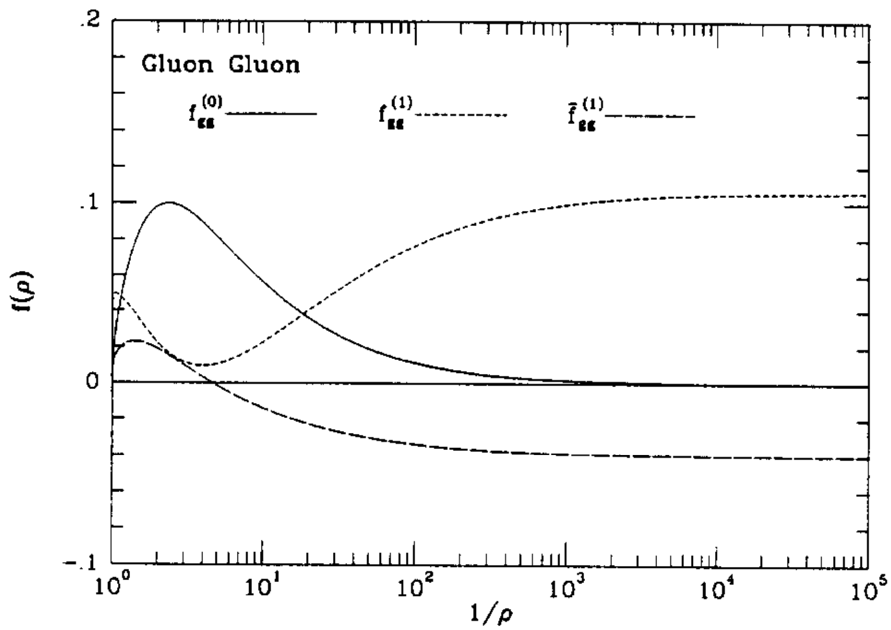

Figure 53: Gluon gluon contributions to short distance cross-section

A preliminary idea of the size of the corrections can be obtained from Figs. 52, 53 and 54 even before folding with the parton distribution functions. Taking a typical value for $g^2 \approx 2$, we see that the radiative corrections are large, particularly in the vicinity of the threshold. The significance of the constant cross-section region (gg, gq) at high energy will depend on the rate of fall-off of the structure functions with which the partonic cross-section must be convoluted. We now describe the analytic structures responsible for the behaviour of the higher order terms.

4.6.1 Behaviour near threshold

Near threshold,($\beta \to 0$), the analytic structure of the higher order terms is given by,

$$\begin{aligned}
f^{(1)}_{q\bar{q}} &\to \mathcal{N}_{q\bar{q}}\Big[-\frac{\pi^2}{6}+\beta\Big(\frac{16}{3}\ln^2(8\beta^2)-\frac{82}{3}\ln(8\beta^2)\Big)+O(\beta)\Big] \\
f^{(1)}_{gg} &\to \mathcal{N}_{gg}\Big[\frac{11\pi^2}{42}+\beta\Big(12\ln^2(8\beta^2)-\frac{366}{7}\ln(8\beta^2)\Big)+O(\beta)\Big] \\
f^{(1)}_{gq} &\to O(\beta).
\end{aligned} \tag{402}$$

The normalisation, $\mathcal{N}_{ij}$ of the expressions in Eq. (402) is determined as follows,

$$\mathcal{N}_{ij}=\frac{1}{8\pi^2}\frac{f^{(0)}_{ij}(\rho)}{\beta}\bigg|_{\beta=0},\quad \mathcal{N}_{q\bar{q}}=\frac{1}{72\pi},\quad \mathcal{N}_{gg}=\frac{7}{1536\pi}. \tag{403}$$

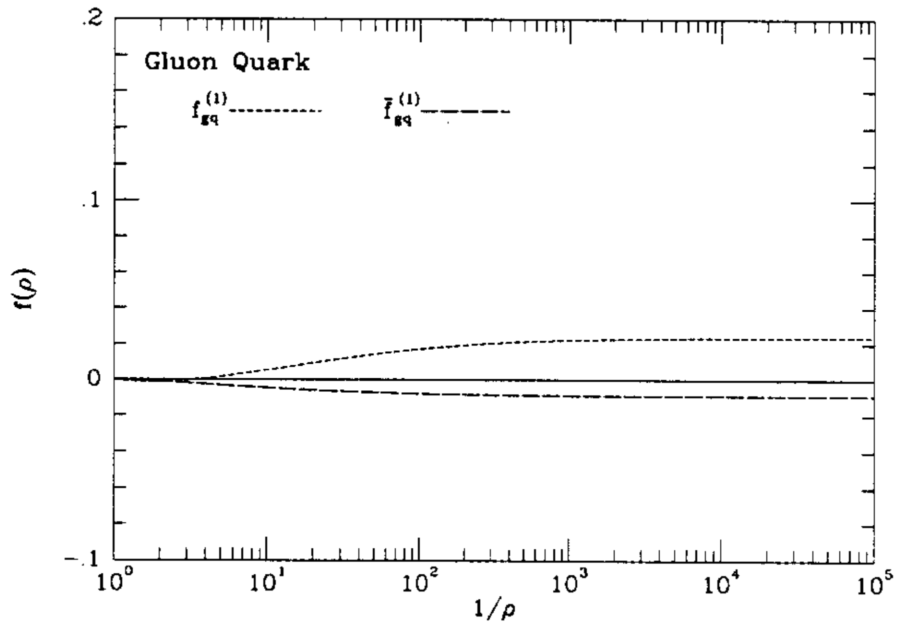

Figure 54: Gluon-quark contributions to the parton cross section

Notice that in this order in perturbation theory the cross-section is finite at threshold. This is due to the $1/\beta$ singularity which is responsible for the binding in a coulomb system. The coulomb attraction tends to increase the cross-section when the incoming partons are in a singlet state (gg), and decrease the cross-section when the incoming partons are in an octet state ($gg, q\bar{q}$). This results in a net positive term for the gg case. For top production at $m_t = 174$ GeV the overall correction due to this effect even after resummation is small[29] (of order a few %), because of cancellation between gg and $q\bar{q}$.

4.6.2 Behaviour at high energy

As shown in Figs. 53 and 54 the gg and qg cross sections tend to a constant at high energy. The lowest order cross section for gg involves fermion t-channel exchange and therefore falls off at large s as can be seen from Fig. 53. For the higher order terms a constant behaviour is found,

$$
\begin{aligned}
f^{(1)}_{gg} &\to 6k + O(\rho \ln^2 \rho) \\
f^{(1)}_{gq} &\to \frac{4}{3}k + O(\rho \ln^2 \rho)
\end{aligned}
\tag{404}
$$

The constant behaviour leads to large corrections especially in b production. Attempts have been made to resum the large effects by including the effects of Lipatov ladders in [30].

4.7 Estimates of rates

In this section we examine the effect of the radiative corrections on the production of heavy quarks at the energies of current $p\bar{p}$ colliders. The total cross section is obtained by integrating the product of the short distance cross sections and the parton fluxes. We use the parton distribution functions of MRS[31].

To assess the significance of the radiative corrections and the relative importance of the various kinematic regions we must know the flux of incoming partons. We define the parton flux function Φ,

$$\Phi_{ij}(\tau,\mu) = \tau \int_0^1 dx_1 \int_0^1 dx_2\, F_i^A(x_1,\mu) F_j^B(x_2,\mu)\delta(x_1 x_2 - \tau). \qquad (405)$$

In terms of these parton fluxes the hadronic cross-section is given by,

$$\frac{d\sigma(S,m^2)}{\ln\tau} = \frac{\alpha_S^2(\mu^2)}{m^2}\sum_{i,j}\Phi_{ij}(\tau,\mu) f_{ij}(\frac{\rho^H}{\tau},\frac{\mu^2}{m^2}), \quad \rho^H = \frac{4m^2}{S} \quad . \qquad (406)$$

The cross section calculated in Eq. (406) is shown in Figs. 55 and 56 for the case

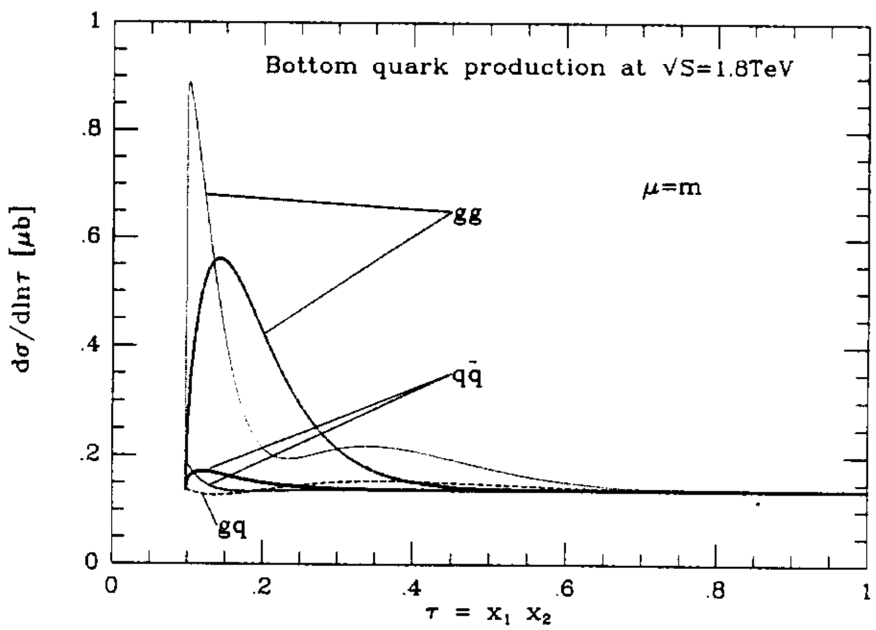

Figure 55: Contributions to bottom cross-section

of bottom and top production at 1.8 TeV. The heavy curves are the $O(\alpha_S^2)$ contributions and the lighter curves are the $O(\alpha_S^3)$ contributions. Note that bottom quark production at collider energies is predominantly due to gluons with quite small values of x. By contrast top quark production is due to quark-antiquark annihilation. The

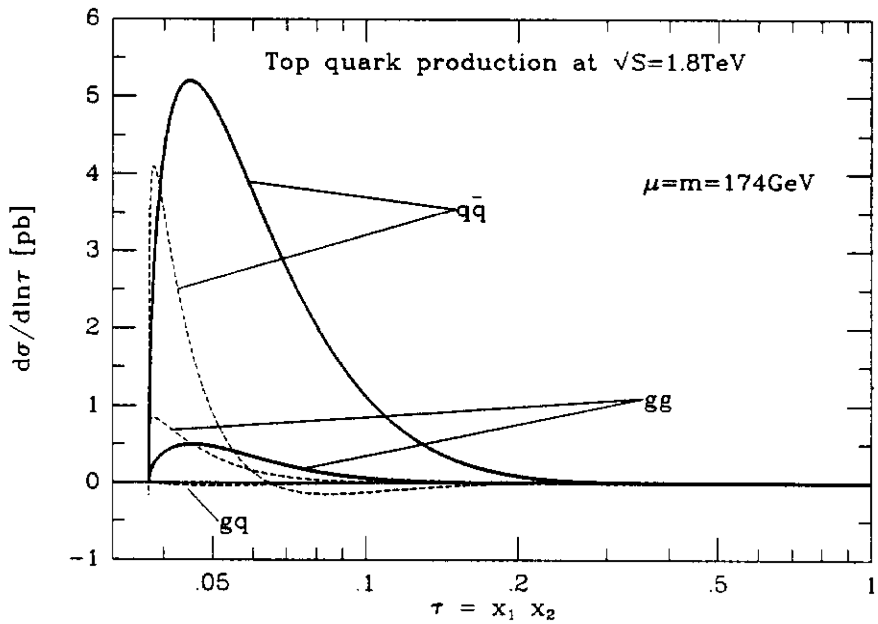

Figure 56: Contributions to top cross-section

horizontal scales are logarithmic, so that the areas in the figures are proportional to the size of a given contribution to the total cross section, (see Eq. (406)). The higher order corrections are found to be moderate in the case of top, but very large for the bottom quark.

The rapid rise of the cross section near threshold is due to the logarithmic terms displayed in Eq. (402). These corrections are more important for smaller top quark mass, when gluon-gluon processes which have inherently larger corrections are more important. The resummation of these large logarithmic corrections has been performed in ref. [36]. The resummation is hard to control without treatment of order $1/m$ effects.

We now turn to numerical estimates. Recent predictions for charm and bottom production are given in ref. [32]. Turning to top quark production, earlier estimates are given in [33,34,35]. The sensitivity of the prediction for the total top cross section to the shape of the parton distribution functions is quite small. For the $MRS(D_0')$ distribution the result for $m = 174$ GeV is $\sigma(\mu = m) = 4.93$ pb; the corresponding result for the $MRS(D_-')$ distribution is 4.91 pb. The effect of α_S uncertainty is more important. Increasing α_S by 10%, $\alpha_S(M_Z) \rightarrow 0.124$ the cross section changes by 23% to 6.04 pb. This may be an overestimate since it does not take into account the increased shrinkage of the quark distribution functions for larger α_s in the evolution from lower energy. The scale dependence uncertainty is small as shown in Fig. 57. For $m/2 < \mu < 2m$ we find that $5.1 > \sigma > 4.4$ pb for $m = 174$ GeV. I find that, at a fixed top mass, the cross section is unlikely to be uncertain by more than 30%. For

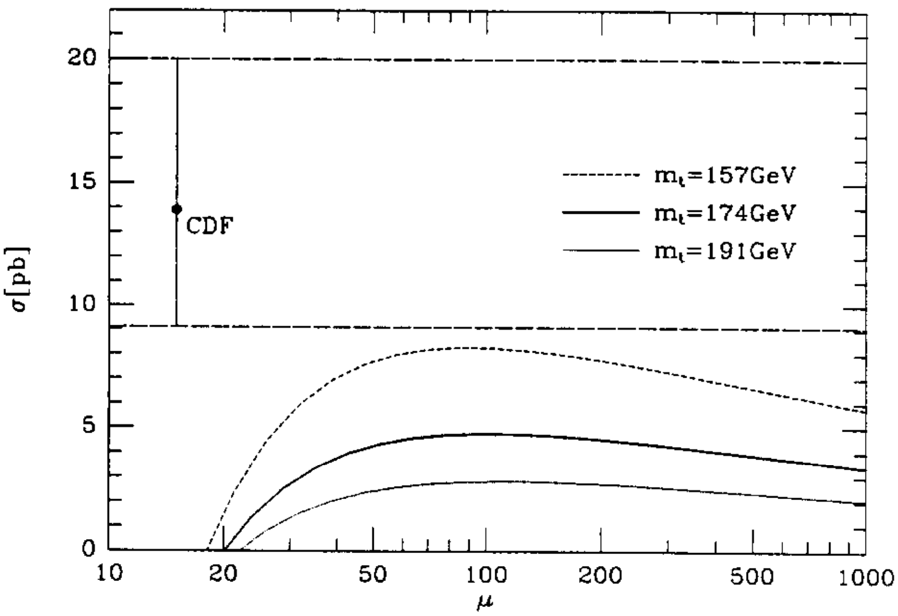

Figure 57: The μ dependence of the theoretical top cross section

m_t = 174 GeV the top cross section is 35% bigger at $\sqrt{S}$ = 2 TeV and more than 100 times bigger at LHC as shown in Fig. 58.

The result for the bottom cross section is shown in Fig. (59). As anticipated above, the $O(\alpha_S^3)$ corrections are large and lead to a doubling of the prediction for the cross section. The matching of the finite order calculation shown in Fig. (59) with a resummed cross cross section with better control of the high energy behaviour remains an open question in bottom production.

In conclusion, we have seen that bottom and top quark production are governed by rather different mechanisms. The top cross section is expected to be rather reliable. The bottom cross section is still rather uncertain.

Acknowledgement

I am most grateful to W.J. Stirling and B.R. Webber for their help in preparing the written version of these lectures.

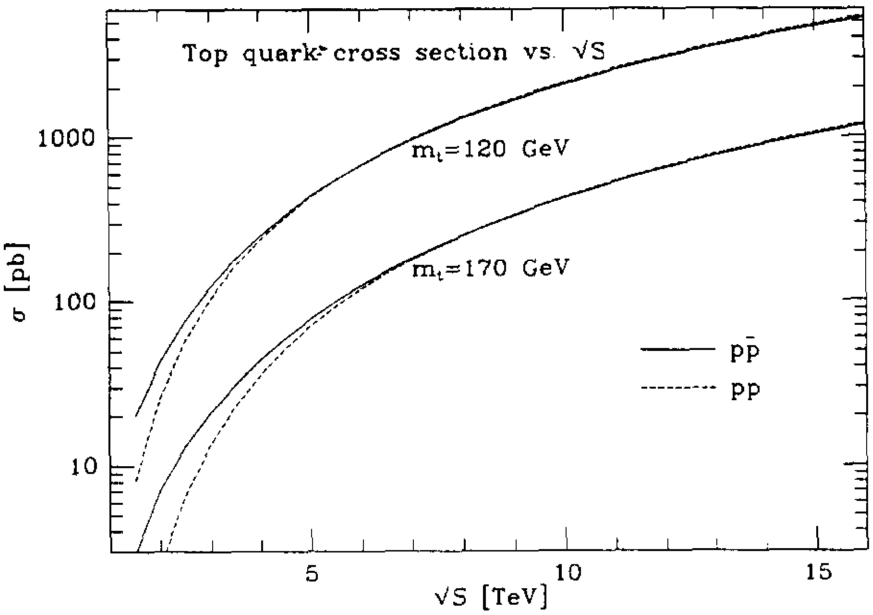

Figure 58: Energy dependence of the top cross-section.

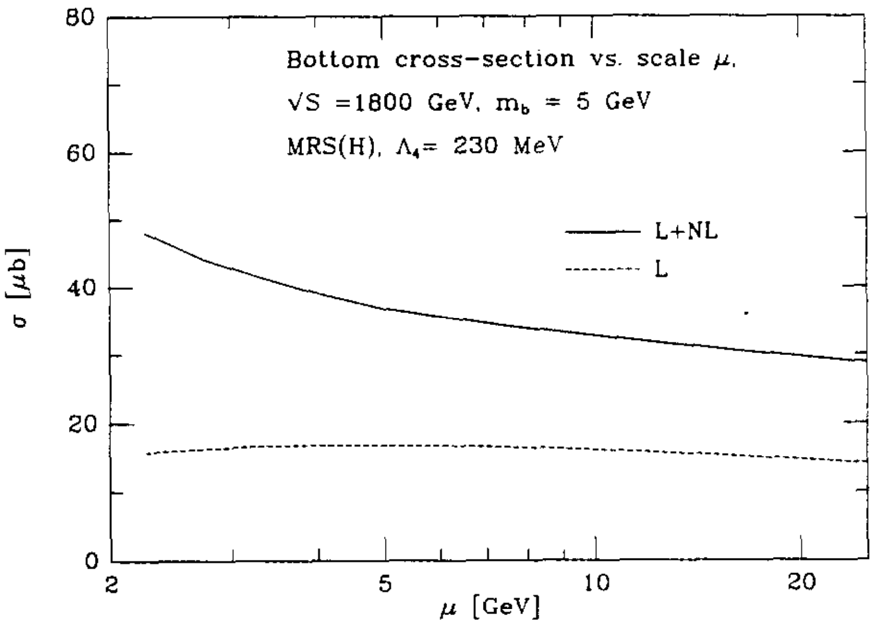

Figure 59: μ dependence of the bottom cross section

References

1) G. Curci, W. Furmanski and R. Petronzio, *Nucl. Phys.* **B175** (1980) 27;
W. Furmanski and R. Petronzio, *Phys. Lett.* **97B** (1980) 437.

2) G. Altarelli *et al.*, *Nucl. Phys.* **B160** (1979) 301.

3) A. Bassetto *et al.*, *Nucl. Phys.* **B207** (1982) 189.

4) Yu.L. Dokshitzer *et al.*, *Rev. Mod. Phys.* **60** (1988) 373.

5) B. Andersson *et al.*, *Phys. Rep.* **97** (1983) 33.

6) Ya.L. Azimov *et al.*, *Phys. Lett.* **165B** (1985) 147.

7) see, for example, J.D. Bjorken and S.D. Drell, 'Relativistic Quantum Fields', McGraw Hill, New York (1964).

8) TPC Collaboration: H. Aihara *et al.*, *Phys. Rev. Lett.* **57** (1986) 945.

9) B.R. Webber, *Ann. Rev. Nucl. Part. Sci.* **36** (1986) 253.

10) R. Basu *et al.*, *Nucl. Phys.* **B244** (1984) 221.

11) J. D. Jackson, 'Classical Electrodynamics', John Wiley (1962).

12) R. Doria, J. Frenkel and J.C. Taylor, *Nucl. Phys.* **B168** (1980) 93.

13) S.D. Ellis, Z. Kunszt and D.E. Soper, *Phys. Rev. Lett.* **64** (1990) 2121.

14) P.N. Harriman, A.D. Martin, R.G. Roberts and W.J. Stirling, preprint RAL-90-007 (1990), to be published in Physical Review D.

15) B. Combridge and C.J. Maxwell, *Nucl. Phys.* **B239** (1984) 429.

16) CDF Collaboration: F. Abe *et al.*, *Phys. Rev.* **D50** (1994) 2966.

17) D0 collaboration: P. Grannis, Proc. 27th Int. Conf. on High Energy Physics, Glasgow, Scotland, July 1994. S. Abachi *et al.*, *Phys. Rev. Lett.* **72** (1994) 2138.

18) E.J. Eichten and K.D. Lane, *Phys. Lett.* **B327** (1994) 129;
C.T. Hill and S.J. Parke, *Phys. Rev.* **D49** (1994) 4454.

19) V.A. Khoze, J. Ohnemus and W.J. Stirling, *Phys. Rev.* **D49** (1994) 1237.

20) F. Abe *et al.*, Fermilab-Conf-94/136-E and references therein.

21) K. Bazizi, Talk presented at the 29th rencontre de Moriond, Fermilab-Conf-94-300-E (1994).

22) E. Braaten *et al.*, Fermilab-PUB-94/135-T, (May 1994);
G. Bodwin *et al.*, Fermilab-PUB-94/073-T (1994).

23) M. Gluck, J.F. Owens and E. Reya, *Phys. Rev.* **D17** (1978) 2324;
B. Combridge, *Nucl. Phys.* **151** (1979) 429.

24) R.K. Ellis, *Strong Interactions and Gauge Theories,* edited by J. Tran Thanh Van, Editions Frontières, Gif-sur-Yvette, 1986, p. 339;
R.K. Ellis, Proceedings of the 17th SLAC summer institute on particle physics, SLAC-REPORT-361, p.45 (1989).

25) J.C. Collins, D.E. Soper and G. Sterman, *Nucl. Phys.* **B263** (1986) 37

26) S.J. Brodsky, J.C. Collins, S.D. Ellis, J.F. Gunion and A.H. Mueller, in *Proc. 1984 Summer Study on the Design and Utilization of the Superconducting Super Collider*, Fermilab, Batavia, Illinois, 1984, p. 227;
S.J. Brodsky, J.F. Gunion and D.E. Soper, *Phys. Rev.* **D36** (1987) 2710.

27) P. Nason, S. Dawson and R. K. Ellis, *Nucl. Phys.* **B303** (1988) 607;
Nucl. Phys. **B327** (1989) 49; E. *Nucl. Phys.* **B335** (1990) 260.

28) W. Beenakker, H. Kuijf, W. van Neerven, J. Smith, *Phys. Rev.* **D40** (1954) 89.

29) V. Fadin, V. Khoze and T. Sjöstrand, *Zeit. Phys.* **C48** (19613) 90.

30) J. C. Collins and R. K. Ellis, *Nucl. Phys.* **B360** (1991) 3.

31) A. Martin, R. Roberts and W.J. Stirling, *Phys. Lett.* **306** (1993) 145, (Erratum *Phys. Lett.* **309** (1993) 492).

32) S. Frixione *et al.*, CERN-TH.7292/94 (1994).

33) R. K. Ellis, *Phys. Lett.* **B259** (1991) 492

34) E. Laenen, J. Smith and W. van Neerven, *Phys. Lett.* **B321** (19254) 94.

35) G. Altarelli *et al.*, *Nucl. Phys.* **B308** (1988) 724.

36) E. Laenen, J. Smith and W. van Neerven, *Nucl. Phys.* **B369** (19543) 92.